

2015

DNA-binding interactions of nickel Schiff base complexes

Nawal Masoud O Assadawi
University of Wollongong

Follow this and additional works at: <https://ro.uow.edu.au/theses>

University of Wollongong

Copyright Warning

You may print or download ONE copy of this document for the purpose of your own research or study. The University does not authorise you to copy, communicate or otherwise make available electronically to any other person any copyright material contained on this site.

You are reminded of the following: This work is copyright. Apart from any use permitted under the Copyright Act 1968, no part of this work may be reproduced by any process, nor may any other exclusive right be exercised, without the permission of the author. Copyright owners are entitled to take legal action against persons who infringe their copyright. A reproduction of material that is protected by copyright may be a copyright infringement. A court may impose penalties and award damages in relation to offences and infringements relating to copyright material.

Higher penalties may apply, and higher damages may be awarded, for offences and infringements involving the conversion of material into digital or electronic form.

Unless otherwise indicated, the views expressed in this thesis are those of the author and do not necessarily represent the views of the University of Wollongong.

Recommended Citation

Assadawi, Nawal Masoud O, DNA-binding interactions of nickel Schiff base complexes, Master of Philosophy thesis, School of Chemistry, University of Wollongong, 2015. <https://ro.uow.edu.au/theses/4662>

Research Online is the open access institutional repository for the University of Wollongong. For further information contact the UOW Library: research-pubs@uow.edu.au



DNA-Binding Interactions of Nickel Schiff
Base Complexes

Nawal Masoud O Assadawi

Master of Science

This thesis is presented as part of the requirement for the award
of the Degree of

Master of Philosophy

of the

University of Wollongong

School of Chemistry

November 2015

Declaration

I, Nawal Assadawi, declare that this thesis, submitted in partial fulfilment of the requirements for the award of Master of Philosophy, in the School of Chemistry, University of Wollongong, is wholly my own work unless otherwise referenced or acknowledged. This work has not been submitted for qualification at any other academic institution.

Nawal Assadawi

23rd November 2015

Abstract

A series of eleven different nickel Schiff base complexes was synthesized by a two-step procedure. Initially ethylenediamine, phenylenediamine or *meso*-1,2-diphenylethylenediamine was reacted with either 2,3- or 2,5-dihydroxybenzaldehyde in the presence of Ni(II) to afford six novel dihydroxylated nickel Schiff base complexes. Five of these complexes were then successfully reacted with 1-(2-chloroethyl) piperidine hydrochloride to form a series of derivatives featuring two appended ethyl piperidine moieties. All new complexes were characterised using 1D and 2D nuclear magnetic resonance (NMR) spectroscopy, elemental microanalysis and in some instances electrospray ionisation mass spectrometry (ESI-MS). The solid-state structures of three nickel complexes (**5**), (**8**) and (**10**) were determined by single crystal X-ray crystallography, and revealed that the coordination geometry around the nickel ion was square planar in each case.

The ability of the nickel complexes containing appended ethyl piperidine groups to bind to a double-stranded 16mer DNA molecule, and a tetramolecular DNA quadruplex, was investigated using ESI-MS and circular dichroism (CD) spectroscopy. The results of these studies, as well as those performed simultaneously using a series of previously reported analogues prepared by the same synthetic pathway, but with 2,4-dihydroxybenzaldehyde as one of the initial reactants, enabled the effect of varying the position of the ethyl piperidine groups on DNA-binding properties to be explored. Generally, it was found that changing the position of the ethyl

piperidine groups had only a small effect on binding affinity towards either type of DNA molecule. In most cases there was good agreement between orders of relative binding affinity towards a given DNA molecule determined using the two spectroscopic techniques. On some occasions, however, the results of binding studies conducted using ESI-MS and CD spectroscopy diverged significantly. This may have been the result of the two methods showing different sensitivities towards different aspects of the metal complex/DNA interaction, and the varying stabilities of the non-covalent complexes formed in these systems, to the gas phase environment of the ESI mass spectrometer or to the solution phase used in CD experiments.

Acknowledgements

Foremost, I would like to express my deepest gratitude to my supervisor Assoc. Prof. Stephen Ralph for his continuous support, patience, motivation, and immense knowledge. His guidance helped me through all the time spent in writing of this thesis. Thank you Steve for taking time out from your busy schedule to read, correct and revise my thesis, especially in the latter stages.

Besides my supervisor, I would like to thank my co-supervisor Dr. Chris Richardson. Thank you for your input and expertise with the synthesis, purification and crystallisation of my complexes, as well as your help with NMR characterisations and crystallography.

To Prof. Jenny Beck, thank you for your guidance, expertise, support and patiently revising and correcting my thesis.

Special thanks go to Dr. Kimberley Davis who was always willing to help and give her best suggestions. Thank you for reading and correcting my writing before anyone else did.

Thank you all for your contribution to the development of my research, I would never have been able to finish writing on time without your guidance and help.

Additionally, I would like to thank Dr. Céline Kelso for her help in the mass spec lab, especially with the instrumental issues.

Last but not the least; I would like to thank my husband for always supporting me and encouraging me. He was always there cheering me up and stood by me through the good times and bad. I would also like to thank my parents for the support they provided me through my entire life.

Table of Contents

Declaration.....	ii
Abstract.....	iii
Acknowledgements.....	v
Table of Contents.....	vii
List of Figures.....	ix
List of tables.....	xvi
Abbreviations.....	xviii
Chapter 1 Introduction.....	1
1.1 Historical overview of anticancer drugs.....	1
1.2 Duplex DNA.....	6
1.3 Quadruplex DNA and telomeres.....	12
1.4 Metal complexes that bind to DNA.....	19
1.4.1 Metal complexes that bind to dsDNA.....	20
1.4.2 Metal complexes that bind to quadruplex DNA.....	27
1.5 Aims.....	36
Chapter 2 Materials and methods.....	39
2.1 Chemicals.....	39
2.2 Characterisation of nickel Schiff base complexes.....	40
2.2.1 Physical measurements.....	40
2.2.2 Crystallography.....	41
2.3 Oligonucleotides.....	42
2.3.1 Purification of single-stranded oligonucleotides.....	42
2.3.2 Preparation of dsDNA (D2).....	43
2.3.3 Preparation of qDNA (Q4).....	44

2.4	Reactions of oligonucleotides with nickel Schiff base complexes.....	44
2.4.1	ESI-MS experiments.....	44
2.4.2	CD Experiments.....	46
Chapter 3	Synthesis and characterisation of nickel Schiff base complexes.....	47
3.1	Synthesis of hydroxylated nickel Schiff base complexes.....	47
3.2	Synthesis of alkylated nickel Schiff base complexes.....	53
3.3	Discussion of Synthetic methods.....	61
3.3.1	Hydroxylated nickel Schiff base complexes.....	61
3.3.2	Alkylated nickel Schiff base complexes.....	73
3.4	Crystallographic Data.....	87
Chapter 4	DNA binding experiments.....	97
4.1	Introduction.....	97
4.2	Results and discussion.....	98
4.2.1	DNA binding experiments performed using nickel complexes containing the 1,2-phenylenediamine moiety.....	98
4.2.2	DNA binding experiments performed using nickel complexes containing the 1,2-ethylenediamine moiety.....	115
4.2.3	DNA binding experiments performed using nickel complexes containing the <i>meso</i> -1,2-diphenylethylene-diamine moiety.....	129
Chapter 5	Conclusions.....	137
Chapter 6	References.....	146

List of Figures

Figure 1.1: The structure of nitrogen mustard and some derivatives; a) nitrogen mustard (mechlorethamine); b) chlorambucil, and c) melphalan.	3
Figure 1.2: Structure of some folic acid analogues used clinically as anticancer agents: a) aminopterin, and b) methotrexate.	4
Figure 1.3: Structure of some platinum anticancer complexes: a) cisplatin; b) carboplatin, and c) oxaliplatin.....	5
Figure 1.4: The chemical structures of the nitrogenous bases present in DNA.	7
Figure 1.5: a) Schematic illustration of the structure of double-stranded DNA. b) Structures of the two types of Watson-Crick base pairs present in B-form DNA.	8
Figure 1.6: The structures of A-DNA, B-DNA and Z-DNA. Adapted from various references. ^{53,54}	9
Figure 1.7: Structure of some DNA minor groove binders: a) distamycin, and b) netropsin.	11
Figure 1.8: Structure of some organic intercalators: a) ethidium bromide, and b) daunomycin.....	12
Figure 1.9: a) a schematic structure of a G-quadruplex formed by stacking of G-tetrads from four parallel DNA strands; b) structure of a G-tetrad featuring the Hoogsteen hydrogen bonding. ($M^+ = Na^+$ or K^+).	15
Figure 1.10: Schematic illustration of some different qDNA topologies: a) Intermolecular parallel tetramolecular G-quadruplex; b) intermolecular	

antiparallel bimolecular G-quadruplex; c) intramolecular antiparallel unimolecular G-quadruplex. Adapted from various references. ^{89,90}	16
Figure 1.11: Structures of some compounds that bind to qDNA: a) 2,6-diamidoanthraquinone; b) TMPyP4; c) BRACO19, and d) telomestatin.....	18
Figure 1.12: Examples of mononuclear metal complexes that bind to dsDNA: a) [Cu(phen) ₂] ⁺ ; b) [Pt(en) ₂] ²⁺ ; c) Ni(II)*Lys-Gly-His; d) [Co(NH ₃) ₆] ³⁺ , and e) [Co(en) ₃] ³⁺	21
Figure 1.13: Examples of platinum metallointercalators: a) [Pt(terpy)-(SCH ₂ CH ₂ OH)] ⁺ ; b) [Pt(bipy)(en)] ²⁺ ; c) [Pt(phen)(en)] ²⁺	22
Figure 1.14: Examples of some octahedral metallointercalators: a) [Ru(DIP) ₃] ²⁺ , and b) [Ru(phen) ₂ (dppz)] ²⁺	24
Figure 1.15: Structures of dsDNA-binding Ru(II) complexes studied by Urathamakul and co-workers: a) [Ru(phen) ₃] ²⁺ ; b) [Ru(phen) ₂ (dpq)] ²⁺ ; c) [Ru(phen) ₂ (dppz)] ²⁺ ; d) [Ru(phen) ₂ (dpqC)] ²⁺ ; e) [Ru(phen) ₂ (dpqMe ₂)] ²⁺ ; f) [Ru(phen) ₂ (pda)] ²⁺ . ¹⁴³	26
Figure 1.16: Structure of some metal porphyrin complexes that have been shown to bind to and stabilise quadruplex DNA: a) a manganese(III) porphyrin complex, and b) Mn-TMPyP4.....	29
Figure 1.17: Structure of some platinum(II) complexes shown to bind to quadruplex DNA by Reed and co-workers. ¹⁵³	30
Figure 1.18: Structure of some nickel(II) salphen complexes shown to bind to quadruplex DNA by Reed and co-workers. ¹⁵⁴	31
Figure 1.19: Structure of some of the metal Schiff base complexes whose qDNA-binding properties were studied by Arola-Arnal and co-workers. ¹⁵⁵	32

Figure 1.20: Structure of some of the metal Schiff base complexes whose qDNA-binding properties were studied by Davis and co-workers. ^{156,157}	34
Figure 1.21: Structures of the hydroxylated nickel Schiff base complexes synthesized in this study.	37
Figure 1.22: Structures of the alkylated nickel Schiff base complexes under study.	38
Figure 3.1: Reaction scheme for the synthesis of nickel Schiff base complex (2).	62
Figure 3.2: ¹ H NMR spectrum of complex (2).	64
Figure 3.3: a) COSY spectrum of complex (2); b) NOESY spectrum of complex (2). Selected key correlations are highlighted.	66
Figure 3.4: a) ¹³ C NMR spectrum of complex (2); b) HSQC spectrum of complex (2), with C-H correlations highlighted.	68
Figure 3.5: a) ¹ H NMR spectrum of complex (4); b) COSY spectrum of complex (4). Key correlations are highlighted.	69
Figure 3.6: NOESY spectrum of complex (4). Key correlations are highlighted.	70
Figure 3.7: a) ¹³ C spectrum of complex (4); b) HSQC spectrum of complex (4); and c) HMBC spectrum of complex (4), with C-H correlations highlighted. Two artefacts in the HMBC spectrum are highlighted with arrows.	71
Figure 3.8: Reaction scheme for the synthesis of nickel Schiff base complex (8).	74
Figure 3.9: ¹ H NMR spectrum of complex (8).	76
Figure 3.10: a) Expanded view of the aromatic region of the COSY spectrum of complex (8); b) Expanded view of the aliphatic portion of the COSY spectrum of complex (8) selected key correlations are highlighted.	77
Figure 3.11: NOESY spectrum of complex (8), with key correlations highlighted. .	78

Figure 3.12: a) ^{13}C NMR spectrum of complex (8); b) HSQC spectrum of complex (8); c) HMBC spectrum of complex (8), with C-H correlations highlighted. ...	80
Figure 3.13: ^1H NMR spectrum of complex (10).	82
Figure 3.14: COSY spectrum of complex (10). Key correlations are highlighted. ...	83
Figure 3.15: NOESY spectrum of complex (10). Key correlations are highlighted.	84
Figure 3.16: a) The ^{13}C NMR spectrum of complex (10); b) HSQC spectrum of complex (10); c) HMBC spectrum of complex (10). Key correlations are highlighted.	86
Figure 3.17: ORTEPs for the molecular structures of complexes (5), (8) and (10).	88
Figure 3.18: Different perspectives of the stacking of the three nickel complexes in the lattice of complex (5): a) all three nickel complexes in the crystal lattice; b) the short contacts between complexes (5A) and (5B); c) the short contacts between (5B) and (5C). Some hydrogen atoms were omitted for clarity.....	92
Figure 3.19: Perspective view of the stacking of pairs of complexes in the lattice of complex (8).	94
Figure 3.20: View of complex (10) highlighting the non co-planar arrangement of the six membered chelate rings around the nickel ion. The ethyl piperidine moieties were omitted for clarity.....	95
Figure 3.21: Perspective view of the stacking of pairs of complexes in the lattice of complex (10).	96
Figure 4.1: Structures of nickel Schiff base complexes containing the 1,2-phenylenediamine moiety, with ethyl piperidine pendant groups attached at different locations on the Schiff base.	99
Figure 4.2: Negative ion ESI mass spectra of solutions containing D2 and different ratios of (8). (a) Free D2; (b) D2:(8) = 1:1; (c) D2:(8) = 1:3; (d) D2:(8) = 1:6;	

(e) D2:(**8**) = 1:9. ● = free D2; ▲ = [D2 + (**8**)]; ■ = [D2 + 2(**8**)]; ◆ = [D2 + 3(**8**)]; ✕ = [D2 + 4(**8**)]; ○ = [D2 + 5(**8**)]; □ = [D2 + 6(**8**)]. 100

Figure 4.3: Negative ion ESI mass spectra of solutions containing D2 and different nickel Schiff base complexes at a 1:6 ratio. (a) Free D2; (b) D2 + (**8**); (c) D2 + (**11**); (d) D2 + (**14**). ● = free D2; ▲ = [D2 + (Ni)]; ■ = [D2 + 2(Ni)]; ◆ = [D2 + 3(Ni)]; ✕ = [D2 + 4(Ni)]; ○ = [D2 + 5(Ni)]. 103

Figure 4.4: Relative abundances of ions in spectra of solutions containing D2 and different nickel Schiff base complexes at a 1:6 ratio. 105

Figure 4.5: Circular dichroism spectra (200-400 nm) of solutions containing D2 and different ratios of nickel Schiff base complexes. (a) D2 + (**8**); (b) D2 + (**11**); (c) D2 + (**14**). 107

Figure 4.6: Negative ion ESI mass spectra of solutions containing Q4 and different nickel Schiff base complexes at a 1:6 ratio. (a) Free Q4; (b) Q4 + (**8**); (c) Q4 + (**11**); (d) Q4 + (**14**). ● = free Q4; ▲ = [Q4 + (Ni)]; ■ = [Q4 + 2(Ni)]; ◆ = [Q4 + 3(Ni)]; ✕ = [Q4 + 4(Ni)]; ○ = [Q4 + 5(Ni)]. 109

Figure 4.7: Relative abundances of ions in ESI mass spectra of solutions containing Q4 and different nickel Schiff base complexes at a 1:6 ratio. 111

Figure 4.8: Circular dichroism spectra (200-400 nm) of solutions containing Q4 and different ratios of nickel Schiff base complexes. (a) Q4 + (**8**); (b) Q4 + (**11**); (c) Q4 + (**14**). 113

Figure 4.9: Structures of nickel Schiff base complexes containing the 1,2-ethylenediamine moiety, whose binding to dsDNA and qDNA are explored in this section. 116

Figure 4.10: Negative ion ESI mass spectra of solutions containing D2 and different nickel Schiff base complexes at a 1:6 ratio. (a) Free D2; (b) D2 + (**7**); (c) D2 +

(10); (d) D2 + (13). ● = free D2; ▲ = [D2 + (Ni)]; ■ = [D2 + 2(Ni)]; ◆ = [D2 + 3(Ni)]; ✕ = [D2 + 4(Ni)]. 118

Figure 4.11: Relative abundances of ions from free DNA and different non-covalent complexes in spectra of solutions containing D2 and different nickel Schiff base complexes at a 1:6 ratio. 119

Figure 4.12: Circular dichroism spectra (200-400 nm) of solutions containing D2 and different ratios of nickel Schiff base complexes. (a) D2 + (7); (b) D2 + (10); (c) D2 + (13). 121

Figure 4.13: Negative ion ESI mass spectra of solutions containing Q4 and different nickel Schiff base complexes at a 1:6 ratio. (a) Free Q4; (b) Q4 + (7); (c) Q4 + (10); (d) Q4 + (13). ● = free Q4; ▲ = [Q4 + (Ni)]; ■ = [Q4 + 2(Ni)]; ◆ = [Q4 + 3(Ni)]; ✕ = [Q4 + 4(Ni)]. 124

Figure 4.14: Relative abundances of ions in ESI mass spectra of solutions containing Q4 and different nickel Schiff base complexes at a 1:6 ratio. ... 125

Figure 4.15: Circular dichroism spectra (200-400 nm) of solutions containing Q4 and different ratios of nickel Schiff base complexes. (a) Q4 + (7); (b) Q4 + (10); (c) Q4 + (13). 127

Figure 4.16: Structures of nickel Schiff base complexes containing the meso-1,2-diphenylethylenediamine moiety, whose binding to dsDNA and qDNA are explored in this section. 130

Figure 4.17: Negative ion ESI mass spectra of solutions containing D2 and different nickel Schiff base complexes at a 1:6 ratio. (a) Free D2; (b) D2 + (12); (c) D2 + (15). ● = free D2; ▲ = [D2 + (Ni)]; ■ = [D2 + 2(Ni)]. 131

Figure 4.18: Circular dichroism spectra (200-400 nm) of solutions containing D2 and different ratios of nickel Schiff base complexes. (a) D2 + (12); (b) D2 + (15). 132

Figure 4.19: Negative ion ESI mass spectra of solutions containing Q4 and different nickel Schiff base complexes at a 1:6 ratio. (a) Free Q4; (b) Q4 + (12); (c) Q4 + (15). ● = free Q4; ▲ = [Q4 + (Ni)]; ■ = [Q4 + 2(Ni)]; ◆ = [Q4 + 3(Ni)]. .. 134

Figure 4.20: Circular dichroism spectra (200-400 nm) of solutions containing different ratios of Q4 and nickel Schiff base complexes. (a) Q4 + (12); (b) Q4 + (15). 135

List of tables

Table 2.1: Properties of the DNA molecules used in this study.....	43
Table 2.2: Volume of stock solutions used to prepare nickel/DNA samples for analysis by ESI-MS.....	45
Table 2.3: ESI-MS conditions used for the analysis of DNA/metal complex solutions.....	45
Table 2.4: Instrument parameters used to acquire all CD spectra of nickel/ DNA samples.	46
Table 2.5: Volumes of the DNA/metal complex stock required for CD samples.....	46
Table 3.1: Yields of hydroxylated nickel Schiff base complexes.	63
Table 3.2: Yields of alkylated nickel Schiff base complexes.	75
Table 3.3: Summary of crystallographic data for complexes (5), (8) and (10).....	89
Table 3.4: Selected bond lengths (Å) and angles (°) for nickel Schiff base complexes.....	90
Table 4.1: Effect of addition of nickel Schiff base complexes on the CD spectrum of D2.*	107
Table 4.2: Effect of addition of nickel Schiff base complexes on the CD spectrum of Q4.*	114
Table 4.3: Effect of addition of nickel Schiff base complexes on the CD spectrum of D2.*	122
Table 4.4: Effect of addition of nickel Schiff base complexes on the CD spectrum of Q4.*	128

Table 4.5: Effect of addition of nickel Schiff base complexes on the CD spectrum of
D2.* 132

Table 4.6: Effect of addition of nickel Schiff base complexes on the CD spectrum of
Q4.* 135

Abbreviations

A	adenine
bipy	2,2'-bipyridine
BRACO19	N-[9-[4-(dimethylamino)anilino]-6-(3-pyrrolidin-1-ylpropanoylamino)acridin-3-yl]-3-pyrrolidin-1-ylpropanamide
C	cytosine
CD	circular dichroism
CDCl ₃	chloroform-D
COSY	correlation spectroscopy
cisplatin	cis-(diamminodichloro)platinum (II)
CT-DNA	calf thymus DNA
DCM	dichloromethane
DIP	4,7-diphenyl-1,10-phenanthroline
DMSO	dimethyl sulfoxide
DNA	deoxyribonucleic acid
dppz	dipyrido[3,2-a:2,3-c]phenazine
dpq	dipyrido[3,2-d:2'3'-f]quinoxaline

dpqMe ₂	6,7-dimethyl-2,3-di(pyridin-2-yl)quinoxaline
dpqc	dipyrido[3,2-a:2'3'-c](6,7,8,9-tetrahydro)phenazine
dsDNA	double-stranded DNA
eilatin	dibenzo[b,j]dipyrido[4,3,2-de:2,3,4-gh][1,10]phenanthroline
en	1,2-diaminoethane
ESI	electrospray ionization
EtBr	ethidium bromide
FRET	fluorescence resonance energy transfer
FID	fluorescent intercalator displacement
G	guanine
HMBC	heteronuclear single-quantum correlation
HSQC	heteronuclear single-quantum correlation
IC ₅₀	inhibitory concentration required to cause death of 50% of the cell population
MeOH	methanol
MS	mass spectrometry
NH ₄ OAc	ammonium acetate
NMR	nuclear magnetic resonance

NOESY	nuclear overhauser effect spectroscopy
qDNA	quadruplex DNA
salen	N,N'-bis(salicylidene)ethylenediamine
salphen	N,N'-bis(salicylidene)phenylenediamine
ssDNA	single-stranded DNA
T	thymine
T _m	melting temperature
TMPyP	tetra(N-methyl-4-pyridyl-porphine
terpy	2,2':6'2"-terpyridine
pda	9,10-diaminophenanthrene
phen	phenanthroline
phi	9,10-phenanthrenequinone
phzi	benzo[a]phenazin-5,6-quinone diimine

CHAPTER 1 INTRODUCTION

1.1 Historical overview of anticancer drugs

Over the years, several treatment options for cancer have been developed. These comprise surgery, radiotherapy and chemotherapy, as well as combinations of all three approaches. Cancer treatment based on surgery or radiotherapy cures only about half of the cancer cases, and then may only prolong the lives of patients. The aim of most chemotherapeutic treatments is to kill tumour cells through inhibition of cell division. Accordingly, many cytotoxic anticancer drugs have been developed through this approach. Deoxyribonucleic acid (DNA) is well known as the intracellular target for a wide range of compounds which exhibit antibacterial, antiviral and anticancer properties.¹ The interaction of anticancer drugs with DNA molecules, enzymes and also some proteins may cause inhibition of cellular division mechanisms, eventually leading to cancer cell death. Cytotoxic agents can damage DNA either directly or indirectly. Direct damage is caused through disruption of DNA replication, while indirect damage is caused through inhibiting the synthesis of the building blocks of DNA, such as folic acid, the four heterocyclic bases, or the corresponding nucleotides. Nitrogen mustards are examples of anticancer drugs that damage DNA directly, while folic acid analogues are examples of anticancer drugs that damage DNA indirectly.²⁻⁶ During the last few decades numerous compounds with anticancer activity have been investigated, however many of them cannot be used clinically due to their toxic side effects and lack of specificity. In order to be potentially

useful as an anticancer agent, a chemical compound must exhibit a high degree of selective cytotoxicity towards cancer cells, as well as produce few side effects when administered to patients.

Initially, the discovery of most anticancer drugs was based on the experimental observation of the biological effects of large numbers of chemical compounds or serendipitous discoveries, rather than knowledge of their mechanisms of biological action. Despite this, some chemical compounds have been successful in curing or prolonging the survival of many cancer patients.⁷ Nitrogen mustard derivatives, folic acid analogues and platinum complexes are just some examples of a wide range of chemical compounds that have been used successfully as anticancer drugs in recent decades, and continue to be used in the clinic.

The anticancer activity of the mustards was first discovered in 1935, when the ability of mustard gas to inhibit the transplantation of tumours in animal models was reported.⁸ This anticancer activity attracted more attention when soldiers died as a result of their exposure to sulfur mustard during the Second World War. It was observed that sulfur mustard caused massive damage to bone marrow and lymph nodes in gas-exposed persons.⁹⁻¹¹ The toxic effect on the lymphatic system suggested a possible use of mustards as anticancer drugs for treatment of lymphomas and leukaemias. Although sulfur mustard was highly toxic when used in cancer therapy, it led to the development of a series of analogues known as the nitrogen mustards. In the early 1940s, Goodman and Gilman examined the potential therapeutic effects of nitrogen mustard (mechlorethamine, Figure 1.1a) on a transplanted

lymphoid tumour. After using it in clinical trials on patients with non-Hodgkin's lymphoma and severe airway obstruction, marked regression was observed.^{9,12,13} Unfortunately, treatment with mechlorethamine resulted in severe side effects. This led to the development of chlorambucil and melphalan (Figure 1.1b and c, respectively) which are widely used for the treatment of lymphoma, leukaemia and ovarian carcinoma.¹⁴

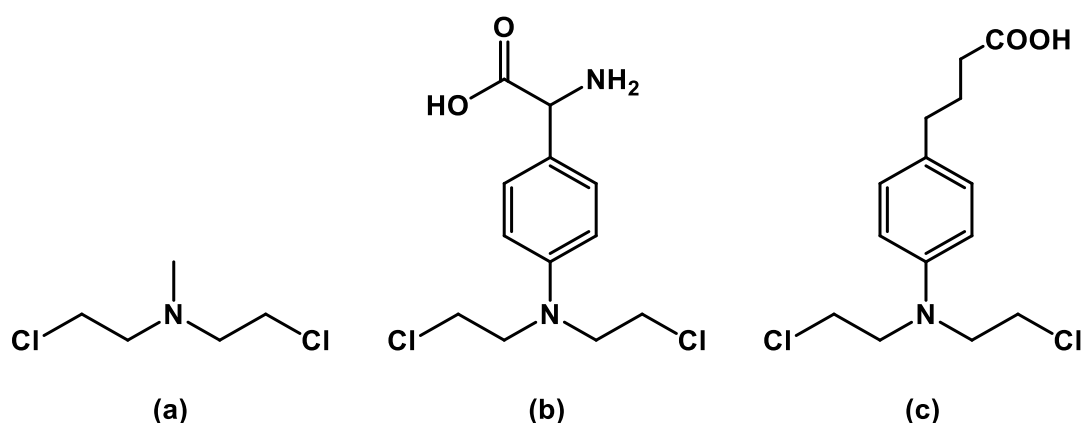


Figure 1.1: The structure of nitrogen mustard and some derivatives; a) nitrogen mustard (mechlorethamine); b) chlorambucil, and c) melphalan.

Nitrogen mustards were used as anticancer agents long before their mechanism of action was understood. It has since been found that they induce cell death by preventing the normal sequence of DNA replication, through interstrand cross-linking of DNA.²⁻⁴ DNA was not identified as the target of the mustards until after Watson and Crick proposed their model for the structure of DNA in 1953.^{15,16} Cross-linking the two DNA strands blocks DNA replication by preventing strand separation, as well as bending the DNA, leading eventually to cell death.^{3,17}

After the discovery of the effect of folate deficiency on bone marrow, a series of folic acid analogues including aminopterin and methotrexate were developed (Figure 1.2). Later, these folate antagonists were administered to children with leukaemia, and it was found that they can induce remission.^{18,19} Methotrexate was also used successfully to treat metastatic cancer in 1956.²⁰ Aminopterin and methotrexate were used as chemotherapeutic agents long before their mechanism of action was reported by Osborn *et al.* in 1958.^{5,6} Both are antimetabolites that act through inhibiting dihydrofolate reductase, a folate-requiring enzyme needed for DNA replication. This results in interference with folate synthesis, eventually leading to cell death.^{5,6}

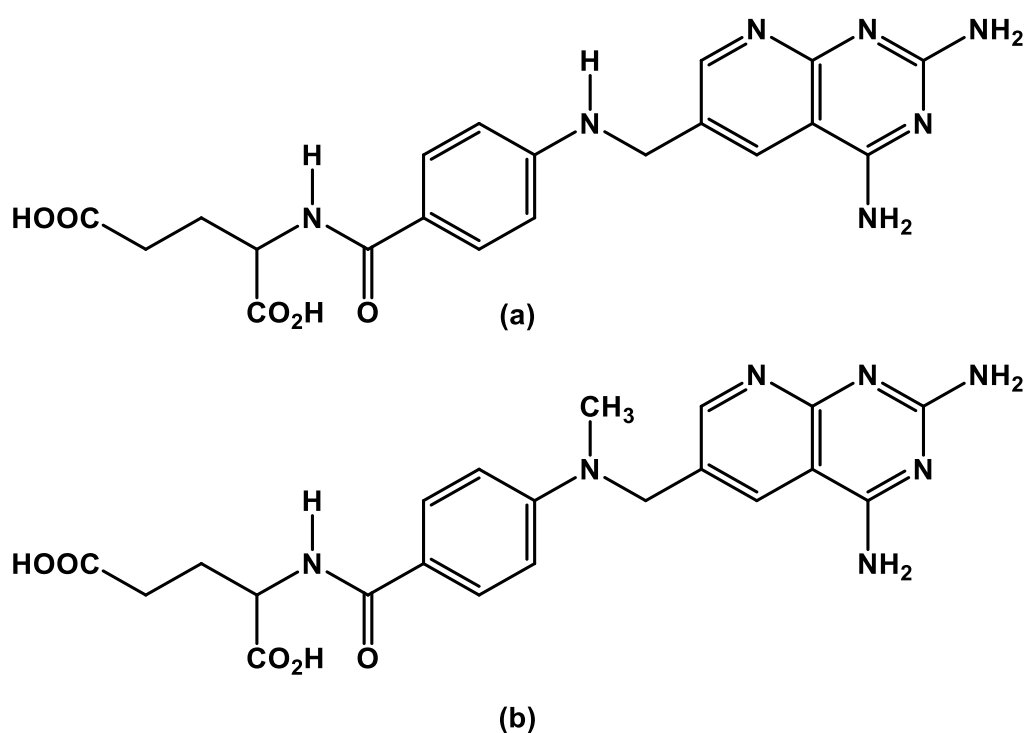


Figure 1.2: Structure of some folic acid analogues used clinically as anticancer agents: a) aminopterin, and b) methotrexate.

Over the years, many other anticancer drugs which inhibit cell growth and/or affect the integrity of DNA have been developed. The ongoing design and synthesis of metal-based anticancer drugs stems from the serendipitous discovery of the anticancer properties of cisplatin (cis-(diamminodichloro)platinum(II)) (Figure 1.3a) by Rosenberg *et al.*²¹⁻²³ Cisplatin binds covalently to DNA predominantly via intrastrand cross-links with the purine bases adenine and guanine. This process involves the two chlorine atoms of cisplatin being replaced by the N7 atoms of two adjacent purines on the same DNA strand.²⁴⁻²⁷

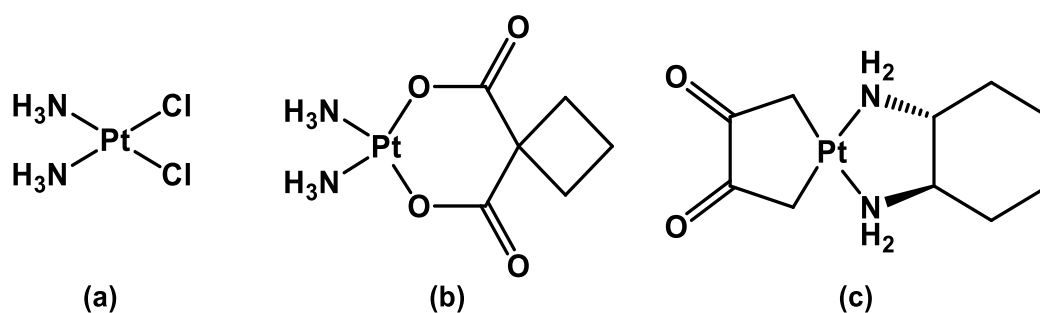


Figure 1.3: Structure of some platinum anticancer complexes: a) cisplatin; b) carboplatin, and c) oxaliplatin.

The binding of cisplatin to DNA results in bending and unwinding of the double helix, ultimately leading to the cell undergoing apoptosis.²⁸⁻³³ Cisplatin is highly cytotoxic towards a variety of tumours such as testicular, ovarian, head and neck, and bladder carcinomas, as well as lymphoma.³⁴⁻⁴¹ Unfortunately, cisplatin does not exert its cytotoxicity selectively towards cancer cells, resulting in severe side effects including nausea, ear damage, vomiting, nephrotoxicity, neurotoxicity, and emetogenesis.⁴²⁻⁴⁴ As a result of

attempts to overcome these toxic side effects, a number of less toxic platinum drugs have been developed. These include carboplatin (Figure 1.3b), which is effective for the treatment of ovarian cancer, and oxaliplatin (Figure 1.3c), which is used to treat colon cancer.

Increased understanding of cancer biology, developments in molecular biology techniques, and elucidation of the complete sequence of the human genome have all led to the development of new therapeutic approaches known as targeted therapies.⁴⁵ Targeted therapies are based on designing drugs that interfere with the activity of a specific biological target or process which is critical for cancer cell survival, such as a gene, enzyme or protein.⁴⁵ In the recent years, many drug targets have been identified for targeted therapy approaches, including DNA polymerases and topoisomerases, kinase signalling pathways, nuclear hormone receptors in breast and prostate cancer, and telomerase. Since the therapeutic activity of many anticancer drugs is a result of their binding to DNA, understanding the structure and mechanism of replication of nucleic acids has played a significant role in the development of targeted therapy.

1.2 Duplex DNA

DNA, or deoxyribonucleic acid, is a hereditary material that is present in the vast majority of living organisms. DNA is the main constituent of chromosomes, and its genetic information is used to synthesise the proteins that are required for numerous biological functions and processes.^{46,47}

DNA is a polymer made from repeating units called deoxyribonucleotides that link together through phosphodiester bonds. Each deoxyribonucleotide is composed of deoxyribose sugar, a phosphate group, and a nitrogenous base, which could be either a pyrimidine (cytosine (C) or thymine (T)), or a purine (adenine (A) or guanine (G)) (Figure 1.4).⁴⁸ The nitrogenous base is linked to deoxyribose forming a nucleoside. The nucleosides are joined together by phosphate groups that form phosphodiester bonds with the 5-hydroxyl group on one nucleoside and the 3-hydroxyl group on the neighbouring nucleoside. This linkage results in the formation of a single DNA strand.

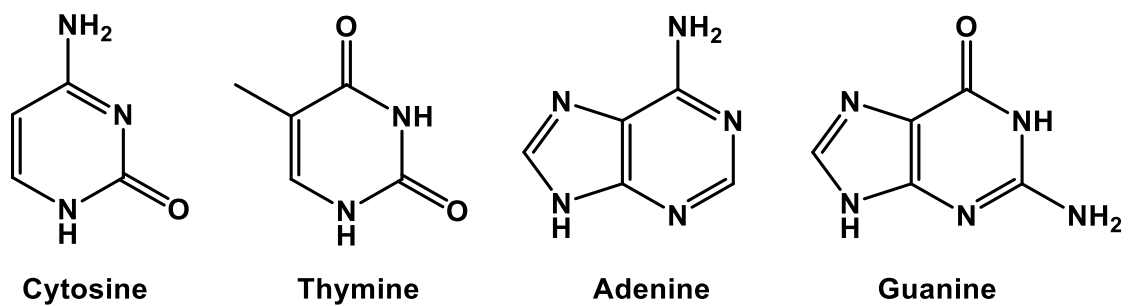


Figure 1.4: The chemical structures of the nitrogenous bases present in DNA.

B-DNA is the most common form of double-stranded DNA (dsDNA) that is found in biological systems, and its structure was first determined by Watson and Crick in 1953.¹⁵ By using results obtained from X-ray diffraction, they determined that this form of DNA is an anti-parallel, right-handed double helical molecule, with the two polynucleotide chains held together by hydrogen bonds between the pyrimidine and purine bases on opposite strands (base pairing) (Figure 1.5a).¹⁵ Base pairing occurs when adenine

residues on one strand form two hydrogen bonds with thymine residues on the opposite strand, and guanine residues form three hydrogen bonds with cytosine residues (**Figure 1.5b**). In addition to base pairing, interactions between the π electron clouds of the bases contribute to the overall stability of B-DNA.

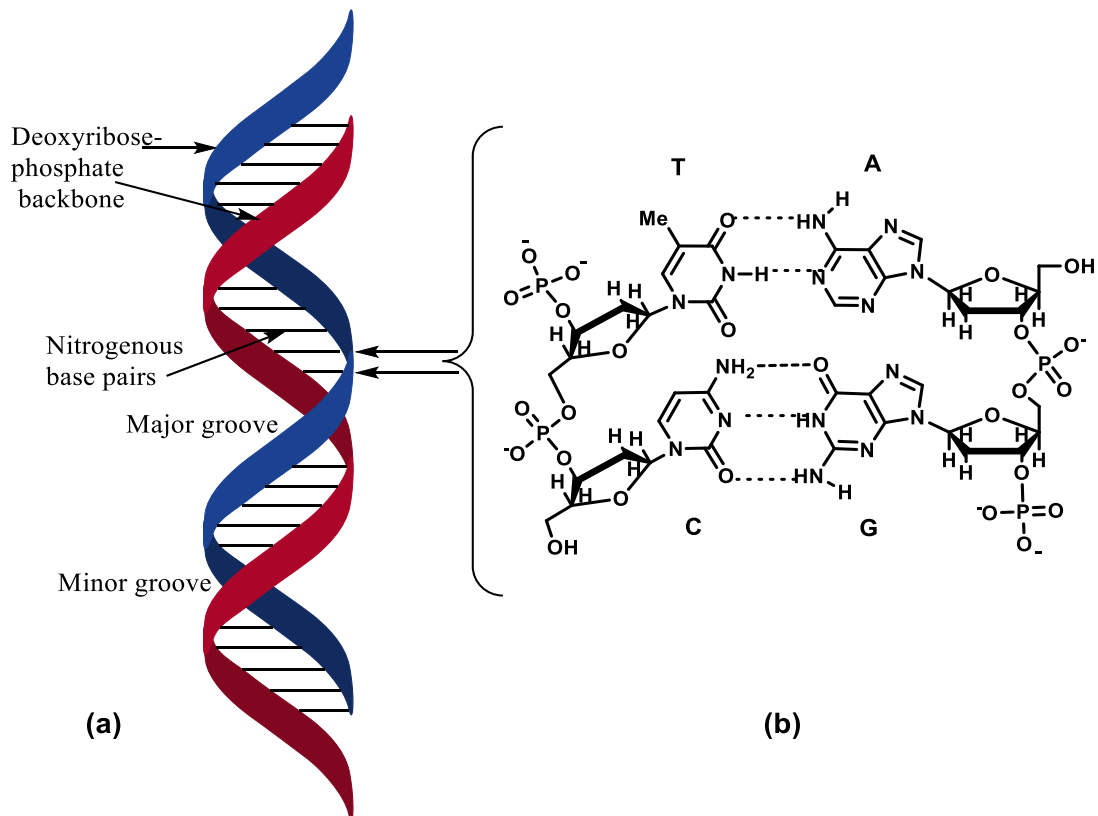


Figure 1.5: a) Schematic illustration of the structure of double-stranded DNA. b) Structures of the two types of Watson-Crick base pairs present in B-form DNA.

There are two less common forms of duplex DNA, known as A- and Z-DNA (Figure 1.6). In low humidity environments B-DNA can convert to A-DNA, which also has a right handed helical structure.⁴⁹ Duplex DNA can also adopt the Z-form structure in solutions with high salt concentrations.^{50,51} Z-DNA is a left-handed double helix, and is wider and more compact than B-DNA.⁵²

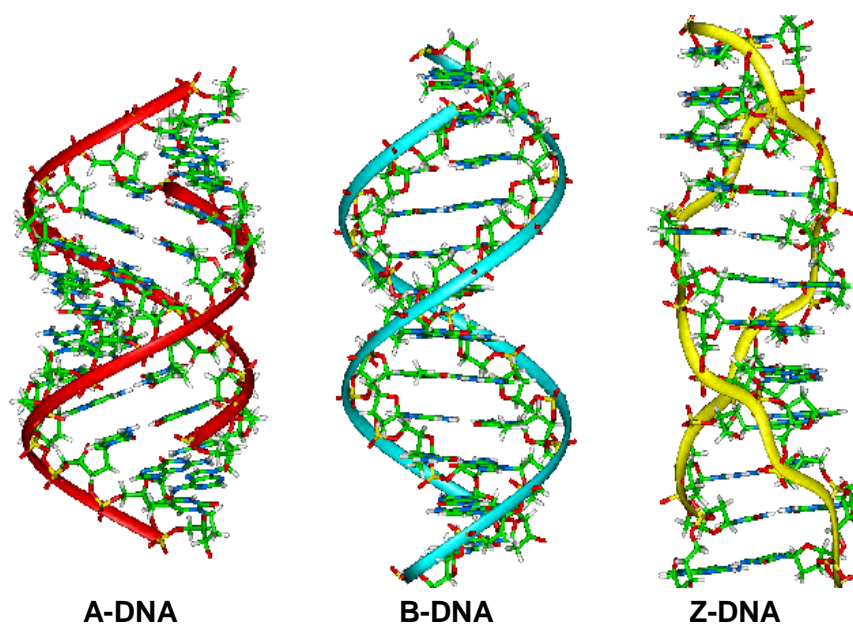


Figure 1.6: The structures of A-DNA, B-DNA and Z-DNA. Adapted from various references.^{53,54}

It has been discovered that some proteins bind to Z-DNA with high affinity and specificity, and that B-DNA can change to Z-DNA in the hippocampus of brains of patients with Alzheimer's disease.⁵⁵ These findings suggest that the Z-DNA conformation may play a biological role in a variety of cellular functions.

As a result of the geometrical configuration of the bonds between the deoxyribose sugar-phosphate backbone and the nitrogenous bases in the B-DNA structure, two different sized grooves, the major and minor grooves, form along the surface of the nucleic acid.^{46,56} A wide range of proteins, oligonucleotides and metal complexes can bind to DNA through these grooves.⁵⁷ Since the major and minor grooves vary in their hydrogen bonding characteristics, electrostatic potential, extent of hydration and size and shape, it has been found that some molecules prefer to bind in one groove

over the other. For instance, it was observed that small organic molecules with a crescent shape act as minor groove binders, while proteins and oligonucleotides act as major groove binders.⁵⁸ The interactions between DNA and groove binding molecules include van der Waals, electrostatic and hydrophobic interactions, as well as hydrogen bonding with the DNA base pairs.⁵⁹⁻⁶²

The naturally occurring antibiotics distamycin and netropsin (Figure 1.7) are examples of dsDNA minor groove binders.⁶⁰ It has been found that these molecules prefer to interact with AT-rich DNA sequences. This binding preference is attributed to the fact that AT-rich regions are less sterically demanding, and able to participate in strong electrostatic binding interactions.⁶¹ On the other hand, the interaction of minor groove binders with GC-rich dsDNA sequences is inhibited for steric reasons, owing to the formation of hydrogen bonds between the amino group of the guanines and the carbonyl oxygen atoms of cytosine residues in GC base pairs.⁵⁹

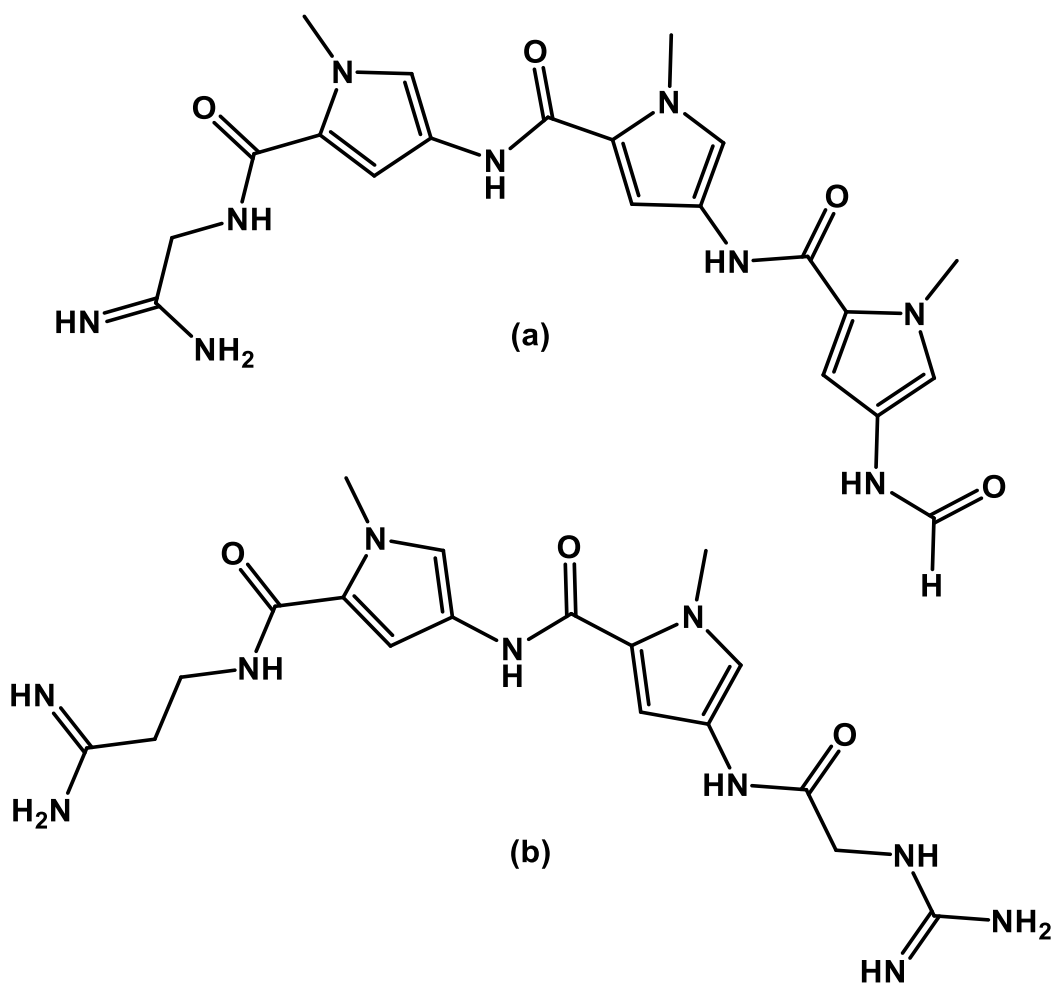


Figure 1.7: Structure of some DNA minor groove binders: a) distamycin, and b) netropsin.

The structure of double helical DNA also offers an additional binding site to the minor and major grooves. Some small aromatic molecules can insert themselves and stack between adjacent base pairs within the DNA double helix.⁵⁹ Such molecules are known as intercalators. Intercalative binding is stabilized by hydrogen bonding, charge transfer and hydrophobic interactions between the aromatic intercalator and the DNA base stack.⁶³ The interactions between the π -orbitals of the intercalating ligand and those of the

base pairs widen the gaps between the base pairs, resulting in unwinding and bending of the DNA molecule, and an increase in its length.^{47,56,64}

The DNA stain ethidium bromide (EtBr) and the anticancer drug daunomycin (Figure 1.8) are examples of organic intercalators.^{47,65} The binding of daunomycin is further stabilized by the formation of hydrogen bonds between the hydroxyl group of the daunomycin glycone ring and an adjacent guanine base. These hydrogen bonds were found to play a significant role in the biological activity of daunomycin.⁶⁵ Many intercalators have also been found to possess a positive charge, which facilitates electrostatic binding interactions with dsDNA.^{66,67}

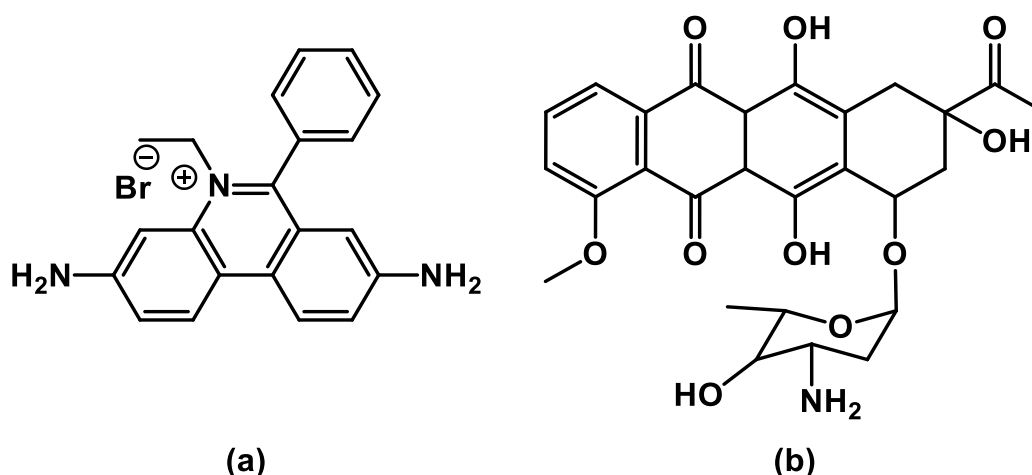


Figure 1.8: Structure of some organic intercalators: a) ethidium bromide, and b) daunomycin.

1.3 Quadruplex DNA and telomeres

In addition to the double helical structures, certain DNA sequences can form multistranded helices such as quadruplexes (G-tetraplexes), and i-motifs (i-tetraplexes) which have been identified by some crystallographic and NMR

studies.⁶⁸⁻⁷² In particular, G-quadruplex DNA has attracted considerable interest in recent years because of its ability to form in telomeric DNA sequence, and also act as an inhibitor for telomerase, the enzyme responsible for telomere maintenance.⁷³⁻⁷⁵

Telomeres are found at the ends of linear eukaryotic chromosomes, and are comprised of telomeric DNA bound to a variety of proteins. Telomeric DNA is composed of tandem repeats of noncoding double-stranded base sequences, and with a guanine-rich strand forming a protruding 3 single-strand overhang.⁶⁹ For instance, repeats of the sequence d(TTAGGG) constitute human telomeres, while repeats of the sequence d(TTTTGGGG) are found in the telomeres of the protozoa *Oxytricha novat*.^{69,76}

Telomeres play a vital role in cell growth and proliferation, as they protect chromosomes from degradation and fusion with each other.⁶⁹ Their role is to maintain the structural integrity of chromosomes by protecting their ends from being recognized as double-strand breaks during cell division.^{77,78} Normal somatic cells progressively lose telomeric repeats during cellular division, with the chromosomes shortening by 50–200 bases after each round of DNA replication.⁷⁷ Losing telomeric DNA means that important genetic information is not lost with each round of cellular division. However, when the length of telomeric DNA decreases to a critical length, dsDNA cannot replicate anymore, and the cell enters a senescent state, after which it undergoes apoptosis, and dies.⁷⁷ This process can be prevented by telomerase, a ribonucleoprotein enzyme made of protein and RNA subunits. Its biological role is to maintain telomere length by adding G-rich DNA repeat sequences

onto the 3'-end of telomeric DNA.^{77,79} Telomerase activity is typically tightly regulated during development, and exhibits minimal activity in somatic cells, which leads to a gradual shortening of telomeres as the organism ages.

In contrast, telomerase has been found to be much more active in germ cells and human tumours.⁷⁷ Stabilization of telomere lengths by telomerase contributes to more than 90% of human cancer cells effectively exhibiting cellular immortality.^{80,81}

In vivo, it has been shown that the single-stranded G-rich overhangs of telomeres are susceptible to folding into a variety of guanine-rich DNA structures known as G-quadruplexes.^{78,82} This telomeric quadruplex DNA has attracted widespread interest as a therapeutic target for cancer treatment.⁸³

G-quadruplexes are made from G-rich DNA sequences arranged to form multiple stacked guanine tetrads held together by π -stacking interactions and stabilized by monovalent cations (such as potassium or sodium) that are located between each pair of G-tetrads (Figure 1.9a).^{69,84} A G-tetrad is a square planar array of four guanine bases held together by eight Hoogsteen hydrogen bonds (Figure 1.9b).^{78,69}

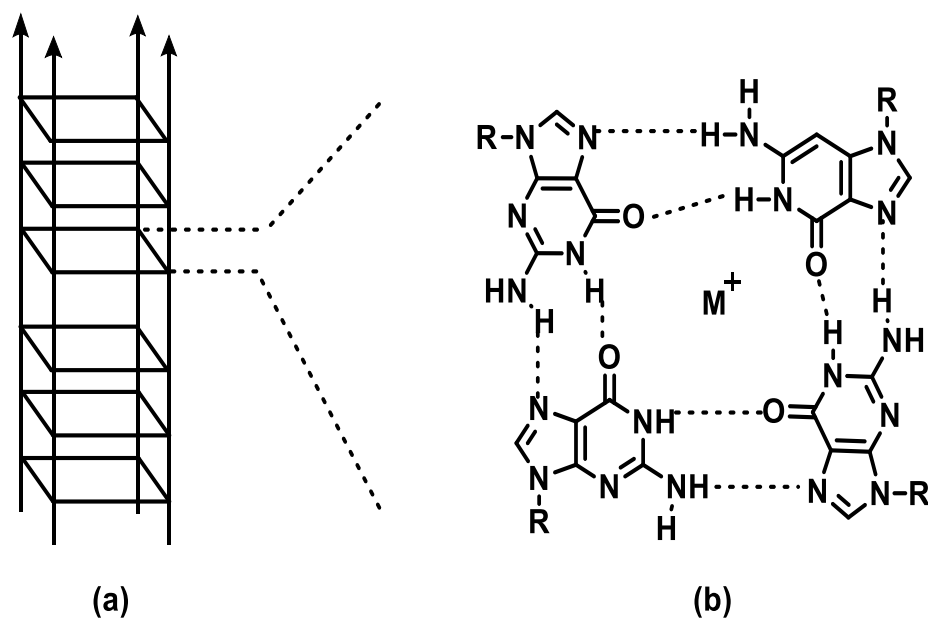


Figure 1.9: a) a schematic structure of a G-quadruplex formed by stacking of G-tetrads from four parallel DNA strands; b) structure of a G-tetrad featuring the Hoogsteen hydrogen bonding. ($M^+ = Na^+$ or K^+).

G-Quadruplex DNA exhibits a variety of three dimensional structures that are formed through either folding of a single DNA strand (intramolecular folding), or the association of two or four strands of DNA (intermolecular association). The structural diversity of G-quadruplexes is due in part to the range of strand orientations (parallel, antiparallel or hybrid) observed (Figure 1.10). These different topologies depend on a wide variety of factors, such as loop length, DNA strand sequence, number of individual G-tetrads, and the surrounding environmental conditions.⁸⁴⁻⁸⁸ The different topologies of G-quadruplex DNA provide access to a variety of chemical functional groups that can be targeted by small molecules.

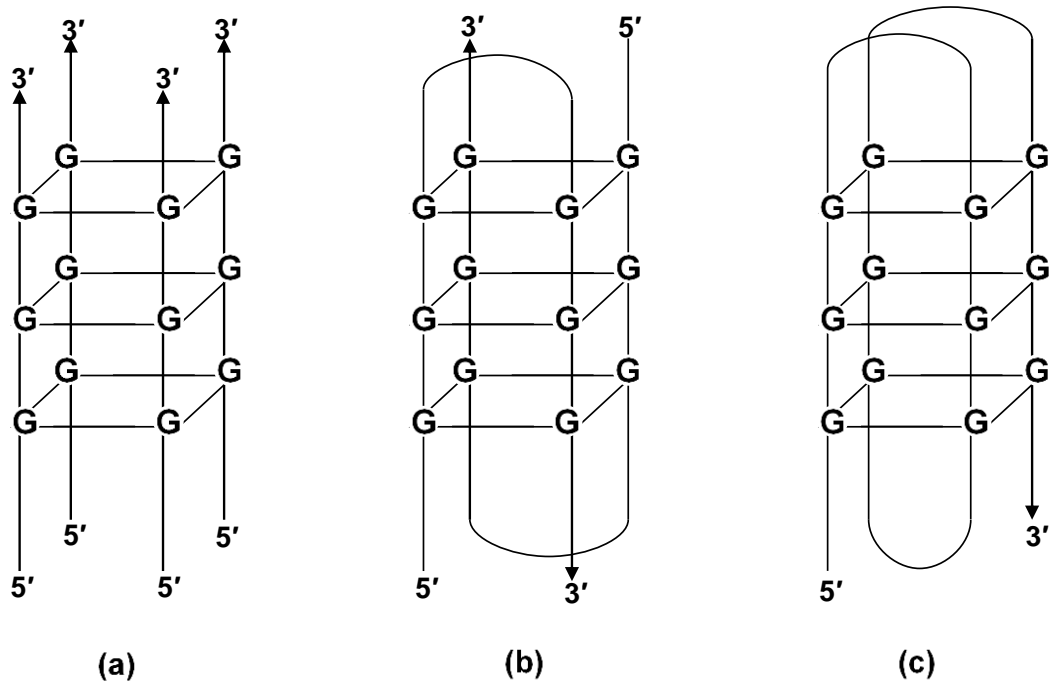


Figure 1.10: Schematic illustration of some different qDNA topologies: a) Intermolecular parallel tetramolecular G-quadruplex; b) intermolecular antiparallel bimolecular G-quadruplex; c) intramolecular antiparallel unimolecular G-quadruplex. Adapted from various references.^{89,90}

In addition to their occurrence in telomeric regions, guanine-rich DNA sequences that are susceptible to adopting G-quadruplex DNA structures are found in other locations in the human genome, including chromosomes, centromeres, fragile X syndrome repeats, the c-myc gene, retinoblastoma susceptibility genes, and human insulin genes.^{89,91-93} This indicates that G-quadruplex structures may also have a role in other diseases besides cancer. The formation of G-quadruplexes in these regions also means they may be involved in various biological functions such as regulation of transcription and translation, DNA recombination, and replication of DNA stands.^{68,94-99} However, during the last few years the majority of research has focused on the formation and stabilization of G-quadruplexes in telomeres.¹⁰⁰⁻¹⁰²

Inhibition of telomerase activity in cancer cells has attracted attention as a new approach to cancer treatment. It has been shown that the folding of telomeric DNA into G-quadruplex structures impedes telomerase from elongating telomeres.⁸² Some studies in cancer cells have shown that small molecules which bind to and stabilize G-quadruplexes have caused damage to the telomeres as a result of their dissociation from single-stranded DNA (ssDNA) templates.^{40,73-75,82,103,104} It has been shown that such molecules bind to quadruplex DNA either by intercalation between the G-tetrads or through stacking with terminal G-tetrads.¹⁰⁵ A wide range of qDNA-binding, small aromatic molecules have been investigated. These include anthraquinones (e.g. 2,6-diamidoanthraquinone), acridines (e.g. BRACO19= N-[9-[4-(dimethylamino)anilino]-6-(3-pyrrolidin-1-ylpropanoylamino)acridin-3-yl]-3-pyrrolidin-1-ylpropanamide), porphyrins (e.g. TMPyP4= tetra(*N*-methyl-4-pyridylporphine) and natural compounds (e.g. telomestatin) (Figure 1.11).^{74,106-110}

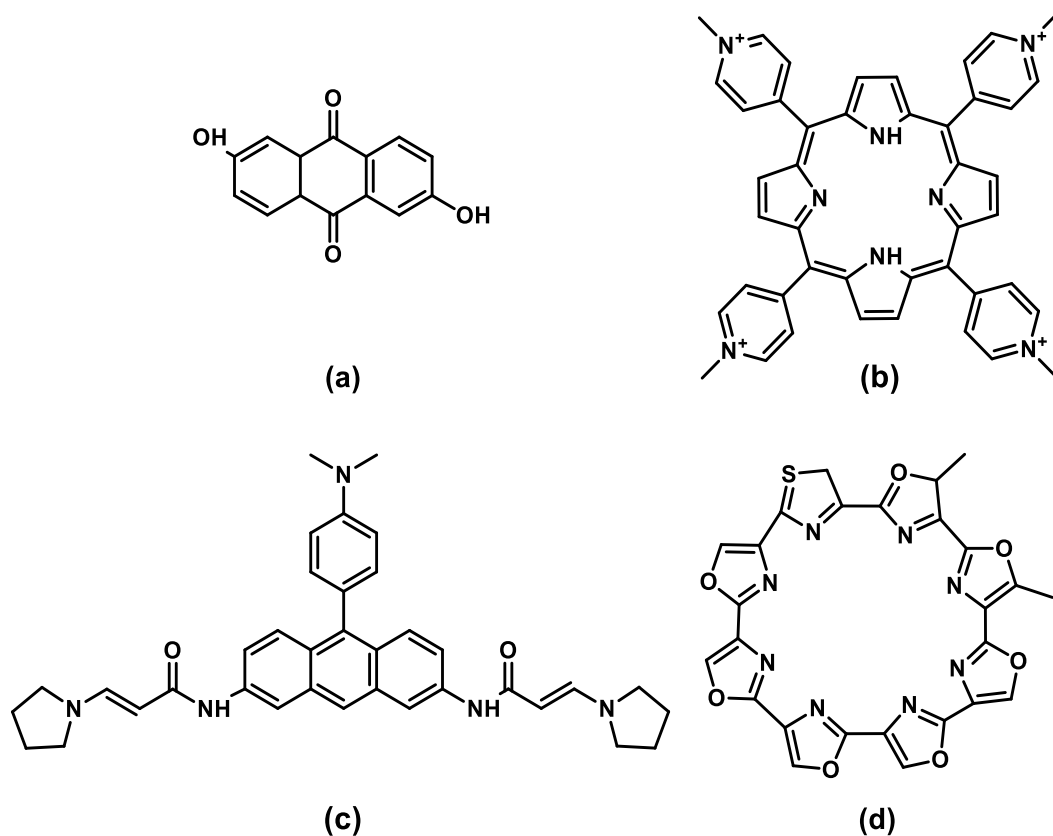


Figure 1.11: Structures of some compounds that bind to qDNA: a) 2,6-diamidoanthraquinone; b) TMPyP4; c) BRACO19, and d) telomestatin.

NMR studies conducted by Sun *et al.* revealed that 2,6-diamidoanthraquinone binds to a parallel four-stranded G-quadruplex through intercalation between the G-tetrads.⁷⁴ Further studies conducted by Wheelhouse and co-workers showed that the porphyrins like TMPyP4 could bind to both parallel and anti-parallel q-DNA intercalatively.^{73,89,111} In addition, research has shown that both the acridine BRACO19 and the natural product telomestatin can bind to quadruplex DNA and act as telomerase inhibitors.^{103,112-114} All these studies have concluded that the binding of small molecules to G-quadruplex DNA is affected by various factors including their overall charge, the length of any side chains present, and hydrogen bonding

substituents.⁷⁴ Some known double-stranded DNA binding compounds such as distamycin, daunomycin and ethidium bromide have also been found to bind to G-quadruplex DNA.^{115,116} Compounds that bind to both double-stranded DNA and G-quadruplex DNA are consequently cytotoxic at the concentrations required to inhibit telomerase.¹⁰⁴ Therefore, it is important to develop new compounds that exhibit high binding affinities and selectivity for quadruplex DNA, over duplex DNA.

1.4 Metal complexes that bind to DNA

During the last few decades there has been increased interest in transition metal complexes as potential anticancer and antibacterial therapeutics.¹¹⁷ Some metal complexes have been shown to interfere with DNA replication, DNA transcription and apoptosis, meaning they can be used to damage DNA and induce cell death.^{43,118,119} It is well known now that the biological activity of some metal complexes is due to their ability to bind to DNA.^{30,66,120} The great diversity in structures and size of transition metal complexes, as well as their electrochemical and photophysical properties, makes them attractive as selective DNA binding reagents.^{56,121,122} Therefore, the DNA binding properties of a number of metal complexes have been investigated. A large proportion of these complexes contain ruthenium(II), rhodium(III), platinum(II), platinum(IV), and titanium(IV), and their DNA-binding behaviour has been extensively investigated both *in vitro* and *in vivo*. Much attention was initially directed to square planar and octahedral complexes containing

inert metal ions such as platinum(II), rhodium(III) and ruthenium(II) with bidentate or tetradentate aromatic heterocyclic ligands.¹²¹ These metal complexes are non-covalent DNA-binding agents that act as either groove-binders or intercalators.¹²¹

1.4.1 Metal complexes that bind to dsDNA

Almost 35 years ago the Sigman group demonstrated that $[\text{Cu}(\text{phen})_2]^+$, (phen = 1,10-phenanthroline) (Figure 1.12a) binds to DNA non-covalently by interacting with the DNA minor groove, and functions as a synthetic DNA nuclease.¹²³ Since this demonstration many other studies have established that most mononuclear, inert transition metal complexes especially those bearing aromatic ligand bind in the minor groove of DNA. This includes platinum complexes such as $[\text{Pt}(\text{en})_2]^{2+}$ (en= 1,2-diaminoethane), (Figure 1.12b), and the square planar nickel(II) metalloprotein $\text{Ni(II)}^*\text{Lys-Gly-His}$ (Figure 1.12c), which was found to selectively associate with the dsDNA minor groove at A/T rich sites.^{124,125} Although most mononuclear, inert transition metal complexes act as minor groove binders, it was found that cobalt(III) ammine complexes such as $[\text{Co}(\text{NH}_3)_6]^{3+}$ and $[\text{Co}(\text{en})_3]^{3+}$ (Figure 1.12d and e, respectively) selectively interact with GG sequences in the major groove of dsDNA.^{126,127} It has been proposed that the binding preferences of metal complexes for the major or minor groove at different base sequences is due to the availability of more favourable van der Waals interactions and electrostatic potentials, coupled with opportunities for specific hydrogen bonding interactions at these regions.

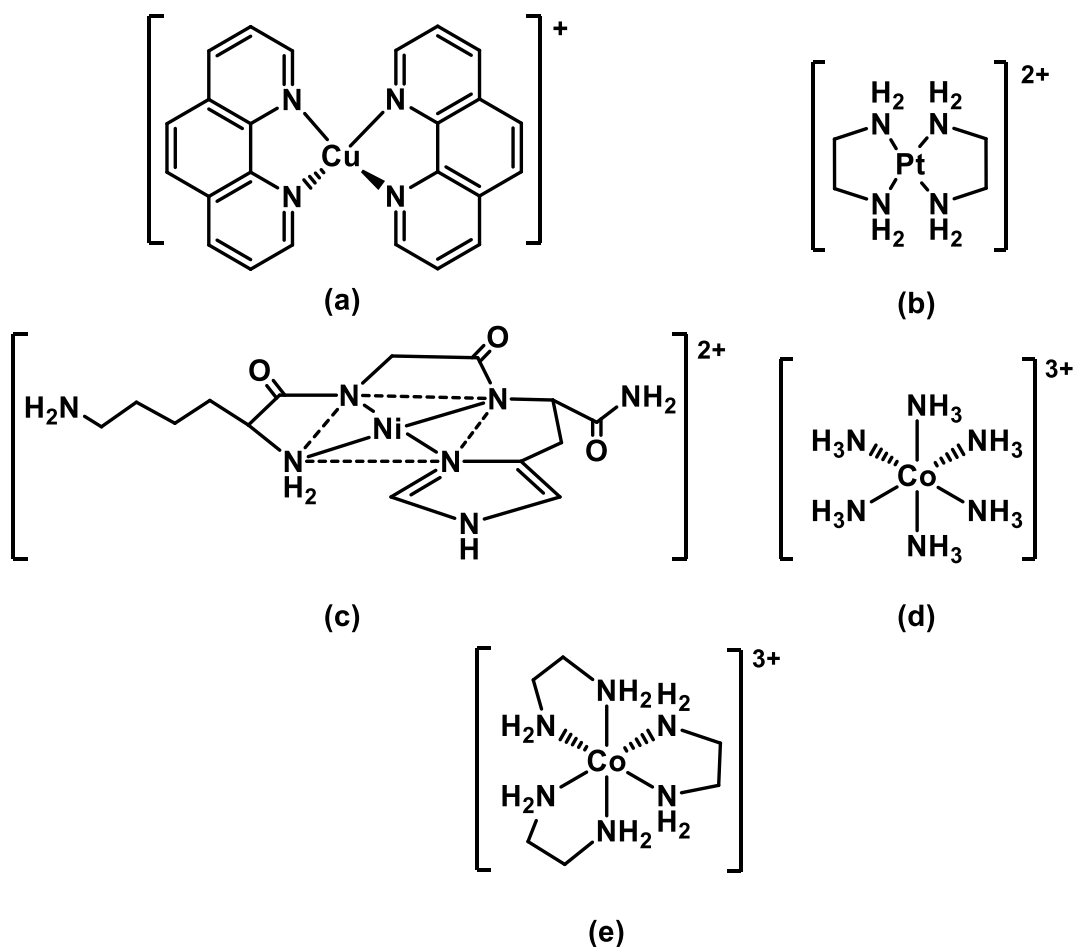


Figure 1.12: Examples of mononuclear metal complexes that bind to dsDNA: a) $[\text{Cu}(\text{phen})_2]^+$; b) $[\text{Pt}(\text{en})_2]^{2+}$; c) $\text{Ni}(\text{II})^*\text{Lys-Gly-His}$; d) $[\text{Co}(\text{NH}_3)_6]^{3+}$, and e) $[\text{Co}(\text{en})_3]^{3+}$.

While most of these complexes were found to be groove binders, a wide variety of metal complexes have also been found to intercalate with dsDNA. For example, square planar platinum(II) complexes containing an aromatic heterocyclic ligand such as terpy, phen, bipy, or phi, (terpy = 2,2':6'2''-terpyridine, phen = phenanthroline, bipy = 2,2'-bipyridine, phi = 9,10-phenanthrenequinone), have been shown to bind to double-stranded DNA noncovalently by this mechanism.¹²⁸⁻¹³⁶ The square planar geometry of Pt(II) complexes allows deeper insertion of attached intercalating ligands between

base pairs than is possible with octahedral or tetrahedral complexes.¹²⁹ $[\text{Pt}(\text{terpy})(\text{SCH}_2\text{CH}_2\text{OH})]^+$, (Figure 1.13a), synthesised by Lippard and co-workers, was the first metal compound shown to bind to dsDNA by intercalation.¹³⁰ A single crystal X-ray diffraction study revealed that $[\text{Pt}(\text{terpy})(\text{SCH}_2\text{CH}_2\text{OH})]^+$ intercalated between the base pairs of double helical DNA.¹³¹ It was shown to intercalate into calf thymus DNA (CT-DNA) with a binding constant of $2 \times 10^5 \text{ M}^{-1}$, and to increase the length of the DNA as well as stabilize it.^{132,133} Lippard and co-workers conducted further studies to investigate the intercalative properties of other platinum complexes including $[\text{Pt}(\text{bipy})(\text{en})]^{2+}$ and $[\text{Pt}(\text{phen})(\text{en})]^{2+}$ (Figure 1.13b and c). X-ray diffraction and electrophoresis studies revealed that the planar ligands phen and bipy help these complexes to intercalate and unwind DNA.¹³⁴⁻¹³⁶ It was concluded that the intercalative ability of metal complexes depends upon various factors including the structural characteristics of the complex, DNA composition and the ionic strength of the surrounding medium.¹³⁷

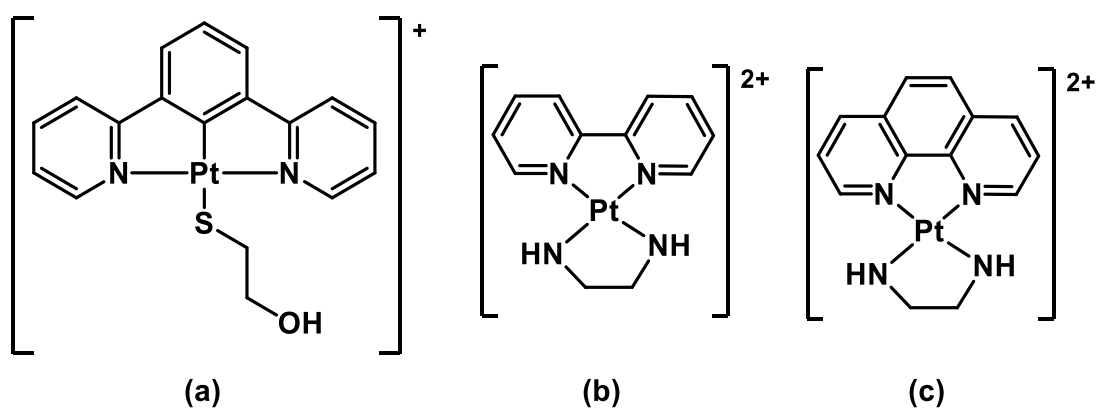


Figure 1.13: Examples of platinum metallointercalators: a) $[\text{Pt}(\text{terpy})(\text{SCH}_2\text{CH}_2\text{OH})]^+$; b) $[\text{Pt}(\text{bipy})(\text{en})]^{2+}$; c) $[\text{Pt}(\text{phen})(\text{en})]^{2+}$.

Another study involving platinum intercalators was conducted by Aldrich-Wright and co-workers. They examined the effect of a series of Pt(II) complexes with the general formula $[\text{Pt}(\text{en})(\text{Me}_x\text{phen})]^{2+}$ ($x = 1, 2$ or 4) on L1210 leukaemia cells. Their work revealed that the DNA affinity of these complexes, and their activity towards the leukaemia cells, was affected by the number and the position of the methyl groups on the phenanthroline ligand.^{138,139} This result suggests that altering the ligand structure can improve the binding affinity of metal complexes towards DNA.

Although platinum complexes were the initial focus of the majority of research into metal anticancer complexes, a large amount of interest now focuses on octahedral metalointercalators containing other transition metals. Interest in the interactions of octahedral transition metal centres with DNA stems in part from the discovery that $[\text{Ru}(\text{phen})_3]^{2+}$ and related complexes can bind non-covalently and enantioselectively to DNA.^{122,140} This is partially attributable to the greater size of the octahedral coordination sphere, which provides more surface area for interactions with DNA and, therefore, potentially enhances DNA binding selectivity. The binding properties of a wide variety of octahedral rhodium and ruthenium complexes containing aromatic ligands such as phen, phi, dppz, phzi, and eilatin (dppz = dipyrdo[3,2-*a*:2,3-*c*]phenazine, phzi = benzo[*a*]phenazin-5,6-quinone diimine, eilatin = dibenzo[*b,j*]dipyrdo[4,3,2-*de*:2,3,4-*gh*][1,10]phenanthroline) have been investigated.^{56,141,142}

It has been found that metal complexes containing phen, phi or dppz bind to duplex DNA via intercalation, by inserting these ligands to different extents in

between two base pairs. In contrast, metal complexes containing phzioreilatin bind via insertion, with this ligand displacing DNA bases out of the base stack.^{56,141,142} Studies on chiral octahedral ruthenium(II) complexes such as $[\text{Ru}(\text{DIP})_3]^{2+}$ (DIP = 4,7-diphenyl-1,10-phenanthroline) (Figure 1.14a) showed that the Δ -enantiomer binds more tightly to B-DNA, whilst $[\text{Ru}(\text{phen})_2(\text{dppz})]^{2+}$ (dppz = dipyrido[3,2-a:2,3'-c]phenazine) (Figure 1.14b) shows extremely high dsDNA binding affinity due to the expansive aromatic surface area of the dppz ligand.^{143,144}

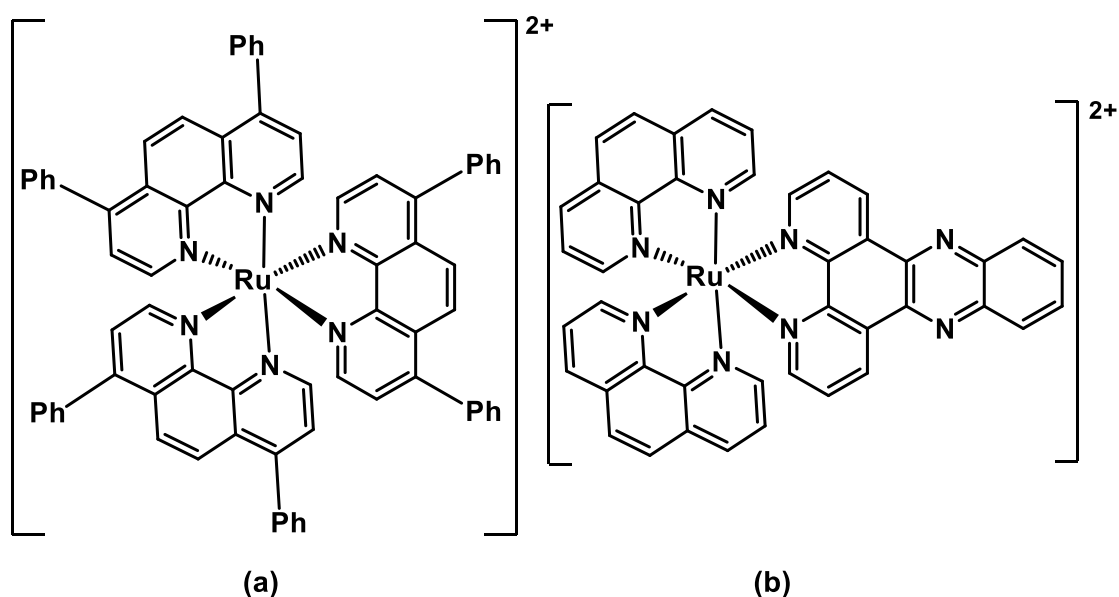


Figure 1.14: Examples of some octahedral metallointercalators: a) $[\text{Ru}(\text{DIP})_3]^{2+}$, and b) $[\text{Ru}(\text{phen})_2(\text{dppz})]^{2+}$.

The inclusion of the highly intercalative dppz ligand in the coordination sphere of a complex has been shown to generally enhance dsDNA binding affinity.^{122,143,145} These studies concluded that the structure of the

intercalating ligand present in a metal complex can affect its binding modes and selectivity toward different DNA sequences. For example, one report by Urathamakul and co-workers showed that the relative affinities of some ruthenium complexes towards a dsDNA molecule decreased in the following order: $[\text{Ru}(\text{phen})_2(\text{dppz})]^{2+} > [\text{Ru}(\text{phen})_2(\text{dpqMe}_2)]^{2+}$ (dpqMe₂ = 6,7-dimethyl-2,3-di(pyridin-2-yl)quinoxaline) $> [\text{Ru}(\text{phen})_2(\text{dpqC})]^{2+}$ (dpqC = dipyrido[3,2-*a*:2'3'-*c*](6,7,8,9-tetrahydro)phenazine) $> [\text{Ru}(\text{phen})_2(\text{dpq})]^{2+}$ (dpq = dipyrido[3,2-*d*:2'3'-*f*]quinoxaline) $> [\text{Ru}(\text{phen})_2(\text{pda})]^{2+}$ (pda = 9,10-diaminophenanthrene) $> [\text{Ru}(\text{phen})_3]^{2+}$ (Figure 1.15).¹⁴³

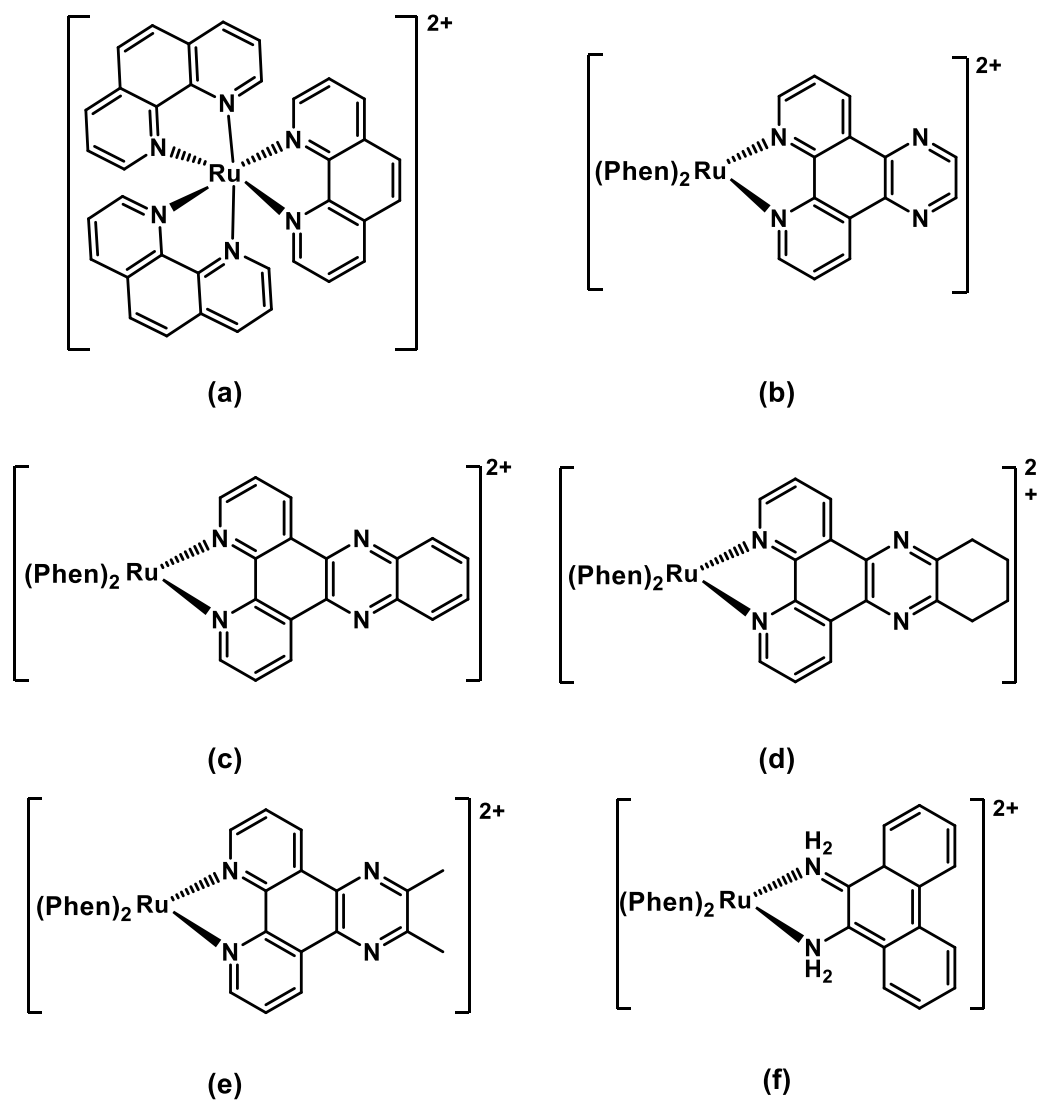


Figure 1.15: Structures of dsDNA-binding Ru(II) complexes studied by Urathamakul and co-workers: a) $[\text{Ru}(\text{phen})_3]^{2+}$; b) $[\text{Ru}(\text{phen})_2(\text{dpq})]^{2+}$; c) $[\text{Ru}(\text{phen})_2(\text{dppz})]^{2+}$; d) $[\text{Ru}(\text{phen})_2(\text{dpqC})]^{2+}$; e) $[\text{Ru}(\text{phen})_2(\text{dpqMe}_2)]^{2+}$; f) $[\text{Ru}(\text{phen})_2(\text{pda})]^{2+}$.¹⁴³

Another study conducted by Talib and co-workers found that the DNA binding affinity of some octahedral nickel(II) complexes with different ligands followed the order $[\text{Ni}(\text{phen})_3]^{2+} < [\text{Ni}(\text{phen})_2(\text{dpq})]^{2+} < [\text{Ni}(\text{phen})_2(\text{dpqC})]^{2+} < [\text{Ni}(\text{phen})_2(\text{dppz})]^{2+}$.¹⁴⁴ These studies suggest that the binding affinity of $[\text{M}(\text{phen})_3]^{2+}$ complexes can be increased by replacing one phen ligand with

other aromatic bidentate ligands which have an extended polycyclic structure.

Other studies have investigated the effect upon DNA binding of changing the identity of the metal ion present in a metallointercalator.^{146,147} For example, Arounagiri and co-workers examined the binding affinity of complexes with the general structure $[M(\text{phen})_2(\text{dppz})]^{2+}$ to CT-DNA, and found that the binding constants for interactions of these complexes followed the trend $\text{Ru(II)} > \text{Co(III)} > \text{Ni(II)}$.¹⁴⁵ Another study conducted by Talib and co-workers found that octahedral nickel(II) complexes containing aromatic ligands interacted more weakly with DNA than the corresponding ruthenium(II) complexes, and attributed this to the difference in size of the metal complexes.¹⁴⁴

1.4.2 Metal complexes that bind to quadruplex DNA

Although most of the reported quadruplex DNA stabilisers are purely organic compounds with heteroaromatic structures, recent studies have demonstrated that metal complexes can also bind to and stabilise quadruplex DNA effectively. This includes complexes in which metals are coordinated to planar aromatic ligands such as salphen (*N,N'*-bis(salicylidene)phenylenediamine), terpyridines, and phenanthrolines. A manganese(III) porphyrin was the first planar metal complex to be investigated for its potential to act as a qDNA stabilising agent.¹⁴⁸ This complex combined a central aromatic core and four flexible cationic arms

(Figure 1.16a), and showed a high affinity for the human telomeric quadruplex DNA (GGGTTA)₄. It was able to discriminate between quadruplex DNA and two different duplex DNA molecules (GC-rich and AT-rich) by a factor of 1000 in favour of the quadruplex derived from the human telomeric sequence. In contrast, a related manganese porphyrin analogue Mn-TMPyP (Figure 1.16b), and the corresponding free base TMPyP, both showed high affinity for duplex DNA^{73,149-151}. The high affinity and selectivity of the manganese(III) porphyrin shown in Figure 1.16a toward telomeric qDNA was found to be due to the combination of the central aromatic core and the four flexible cationic arms. Additional studies were conducted to investigate the ability of other metalloporphyrins with manganese(III) or nickel(II) centres to target quadruplexes formed from telomeric DNA.^{149,152} These showed that metalloporphyrins were capable of inhibiting telomerase with IC₅₀ values in the micromolar range. In addition, it was found that the nature of the metal centre and its coordination geometry plays an important role in the kinetics of binding and nature of the binding modes used in interactions with quadruplex DNA.

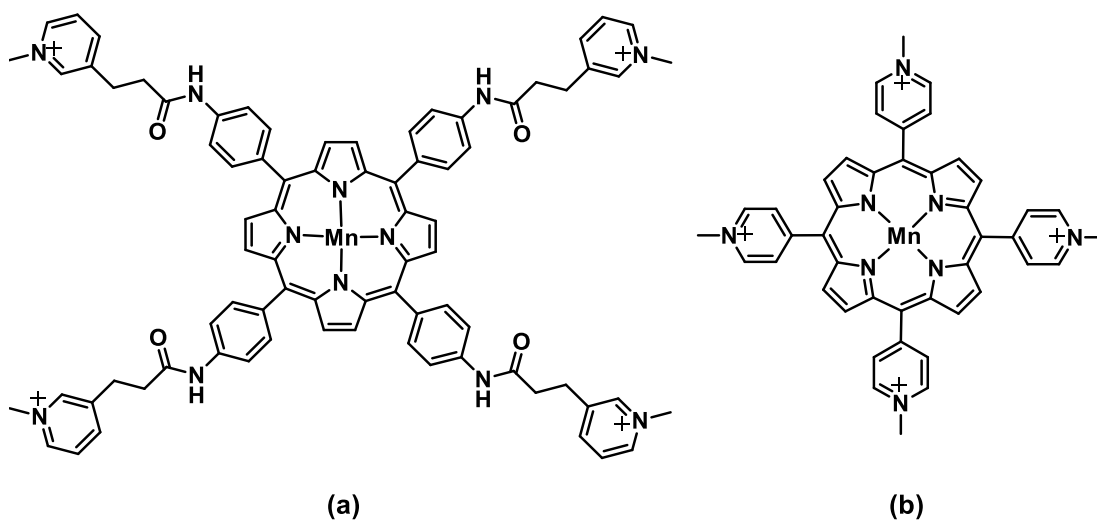


Figure 1.16: Structure of some metal porphyrin complexes that have been shown to bind to and stabilise quadruplex DNA: a) a manganese(III) porphyrin complex, and b) Mn-TMPyP4.

A different class of quadruplex-stabilizing and telomerase-inhibiting metal complexes was investigated by Reed and co-workers.¹⁵³ These were square planar platinum(II) complexes containing substituted phenanthroline ligands (Figure 1.17). FRET (Fluorescence Resonance Energy Transfer) was used to study the interactions between these platinum(II) complexes and both duplex and quadruplex DNA. It was found that the platinum(II) complexes with the piperidine-containing ligand (Figure 1.17b) induced a high degree of stabilisation of quadruplex DNA formed from the human telomeric sequence, which indicated that the piperidine substituent had a significant positive effect on the interaction between the complex and qDNA.

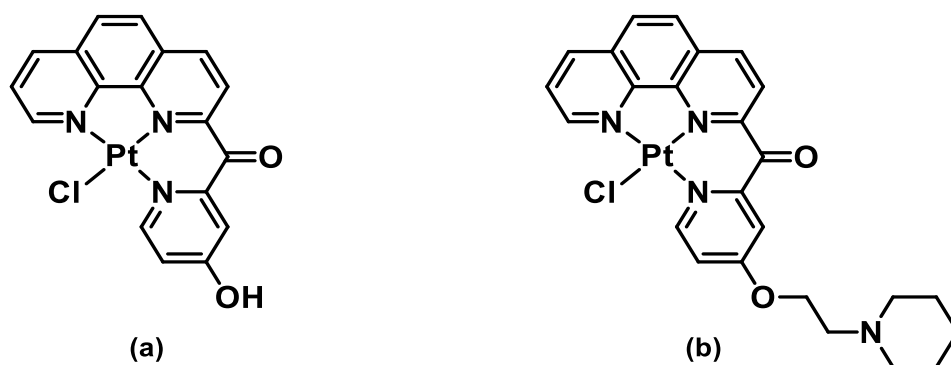


Figure 1.17: Structure of some platinum(II) complexes shown to bind to quadruplex DNA by Reed and co-workers.¹⁵³

Reed and co-workers have also reported that some nickel(II) salphen complexes can act as a new type of telomeric quadruplex DNA stabiliser and telomerase inhibitor.¹⁵⁴ Qualitative molecular modelling studies showed that these Ni(II) complexes (Figure 1.18) possess the main structural requirements to be quadruplex-stabilizing molecules. These include the π -delocalized system of the salphen ligands, which can stack on a guanine quartet, the positively charged piperidine substituents, which interact with the grooves and loops and the negatively charged phosphate backbone of the quadruplex, and finally the positively charged nickel ion that was found to lie above the centre of a G-quartet.¹⁵⁴ These planar complexes were also found to induce telomerase inhibition with $^{tel}EC_{50}$ values in the order of ~ 0.1 mM.

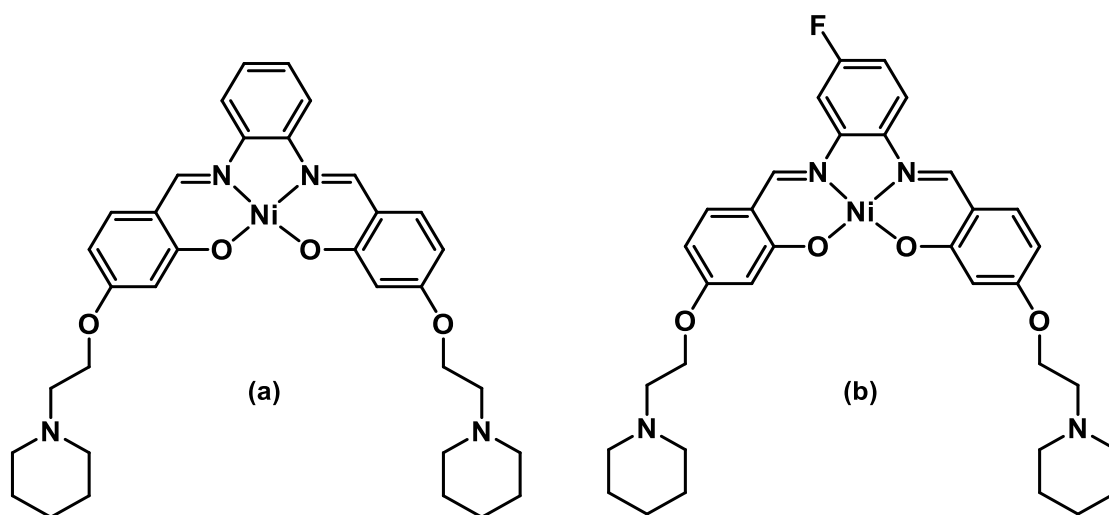


Figure 1.18: Structure of some nickel(II) salphen complexes shown to bind to quadruplex DNA by Reed and co-workers.¹⁵⁴

A later study was conducted to further explore the ability of metal Schiff base complexes as selective qDNA binders and telomerase inhibitors. This study investigated the effect of changing the number of aromatic ring systems present in the complexes shown in Figure 1.18, or the identity of side chains, on their qDNA binding properties.¹⁵⁵ In addition, the effect of changing the metal ion in the Schiff base complex, and therefore its overall geometry, on the ability to interact with the G-quadruplex DNA F21T (sequence: 5-FAM-d(GGG[TTAGGG]3)-TAMRA-3) using a FRET melting assay, was explored.¹⁵⁵ The structures of some of these complexes are presented in Figure 1.19. The results of the FRET assay clearly revealed that the square planar nickel(II) and copper(II) complexes were highly effective stabilizers of human telomeric DNA. It was found that the change in melting temperature (ΔT_m) induced by nickel salphen complexes which contained different piperidine and morpholine side chains ranged between 26.4 and 31.6 °C.

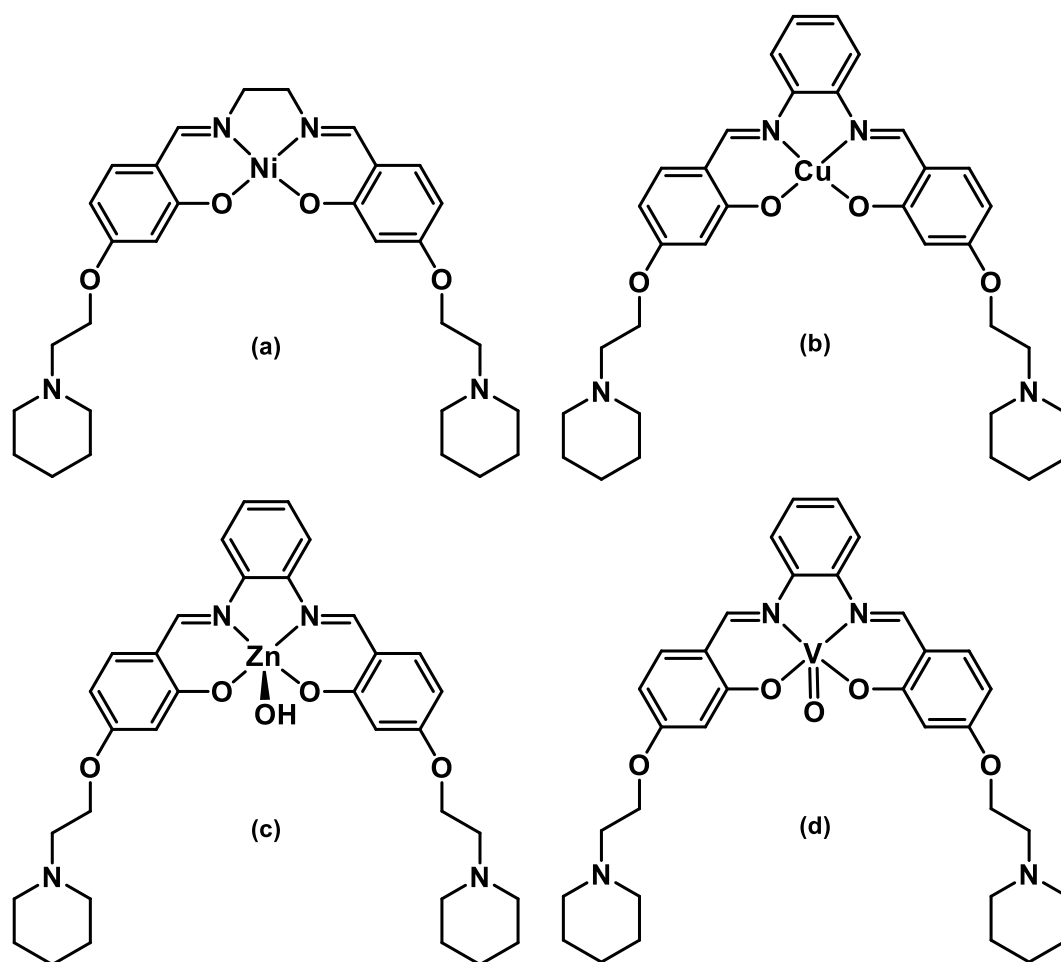


Figure 1.19: Structure of some of the metal Schiff base complexes whose qDNA-binding properties were studied by Arola-Arnal and co-workers.¹⁵⁵

These results suggested that variations in the cyclic amine substituents do not make significant differences in the binding affinity of these complexes. On the other hand, the nickel(II) salen complex in Figure 1.19a exhibited a lower ΔT_m than the corresponding salen complex in Figure 1.18a, which was attributed to the former complex having one less aromatic ring able to interact with a G-quartet of the quadruplex DNA molecule. It was also found that varying the central metal ion in the complex could dramatically affect the DNA binding properties. For example, despite the similar square planar coordination environment around the metal ion for the complexes in Figure

1.18a and Figure 1.19b, the ΔT_m value for the copper complex was found to be significantly lower.¹⁵⁵

Furthermore, the above work revealed that the geometry of the metal complex had an effect on DNA-binding properties. For example, the distorted square pyramidal zinc and vanadium complexes (Figure 1.19c and d, respectively) showed negligible or little interaction with quadruplex DNA. This was demonstrated by their ΔT_m values being considerably lower than that of the analogous square planar nickel and copper complexes. This indicates that for optimal binding between metal complexes and quadruplex DNA, the former must have a square planar geometry in which both faces are available for π - π stacking with a guanine quartet. FRET competition assays showed that these metal complexes have a high degree of selectivity for quadruplex DNA as opposed to duplex DNA.

Recently, the nickel Schiff base complexes shown in Figure 1.20 were synthesized and their interactions with a duplex DNA molecule, as well as both tetramolecular and unimolecular DNA quadruplexes, were investigated using several techniques including ESI-MS, DNA melting temperature measurements, CD spectroscopy, and FRET assays.¹⁵⁶ ESI-MS and DNA melting temperature measurements suggested that the complex in Figure 1.20b exhibits a lower affinity than that in Figure 1.20a towards a dsDNA molecule. This could be attributed to inability of the former molecules to more effectively interact with dsDNA via an intercalation binding mode as a result of the two aromatic ring systems derived from *meso*-1,2-diphenylethylenediamine. In contrast, the presence of a single aromatic

system that is coplanar with those which originated from 2,4-dihydroxybenzaldehyde in the complex shown in Figure 1.20a facilitates insertion into the stack of dsDNA base pairs.

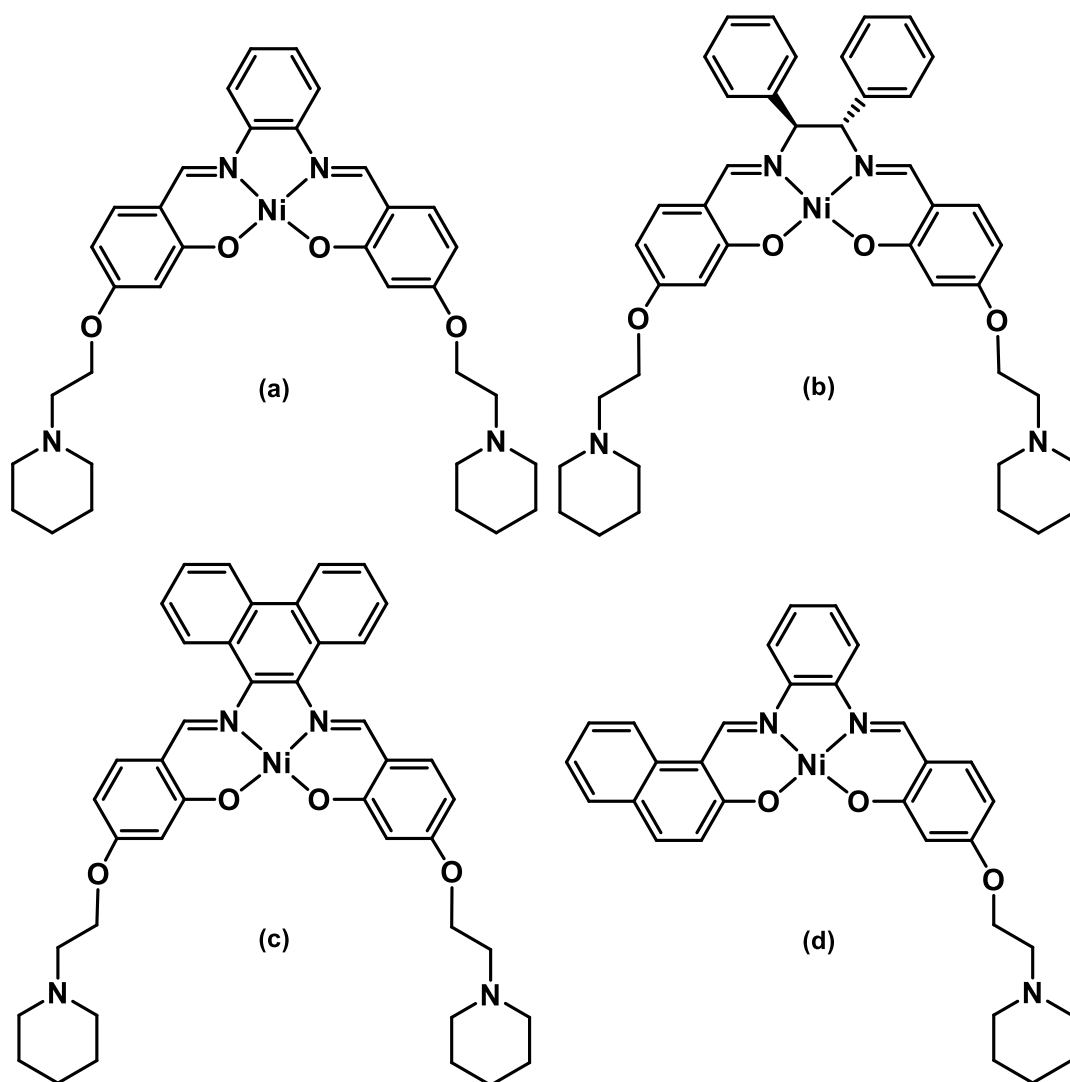


Figure 1.20: Structure of some of the metal Schiff base complexes whose qDNA-binding properties were studied by Davis and co-workers.^{156,157}

In addition, ESI-MS and CD spectroscopy suggested that the complex in Figure 1.20b shows significant binding to a tetramolecular DNA quadruplex. This could be attributed to the presence of additional binding sites in qDNA such as the terminal G-tetrads found on the ends of the nucleic acid

molecules, which allow for π - π stacking interactions between these nickel complexes and the guanine residues of the G-tetrads. Interestingly, the results of ESI-MS and FRET assays indicated that the nickel complex in Figure 1.20b did not bind as tightly to a unimolecular DNA quadruplex. These results indicate that the presence of the *meso*-1,2-diphenylethylenediamine moiety in metal complexes of this type may enhance their selectivity for some DNA quadruplexes over dsDNA.

The size and position of the aromatic surface area within the nickel Schiff base complexes was found to be important for DNA binding interactions. For example, it was found that the complex in Figure 1.20c exhibited a high affinity for dsDNA, but a limited binding to qDNA molecules.¹⁵⁷ This could be attributed to the presence of a large planar 9,10-diaminophenanthrene unit which facilitates insertion into the stack of dsDNA base pairs, but sterically hinders the approach of the nickel Schiff base molecules to the loops of the qDNA molecule. In addition, ESI-MS, CD spectroscopy and UV-Vis DNA melting studies suggested that the asymmetric complex shown in Figure 1.20d which contained a single naphthaldehyde moiety, exhibited a significant decrease in its ability to bind to dsDNA, as well as a limited binding to qDNA.¹⁵⁷ This result could be attributed to the lack of the electrostatic interactions due to the presence of only one piperidine group that can be protonated in the solution, as well as the presence of the naphthaldehyde unit which may hinder the approach of the nickel Schiff base molecules to the dsDNA and to G-quadruplexes. Furthermore, the effect of changing the length or chemical composition of side chains present in the

complexes shown in Figure 1.20, upon their DNA binding properties was also explored.¹⁵⁷ Both ESI-MS and CD spectroscopy studies revealed that the replacement of the alkyl chains by either propyl piperidine or ethyl morpholine did not result in any significant enhancements in DNA affinity or selectivity.

1.5 Aims

The results of studies described in the previous section indicate that changing the structure of nickel Schiff base complexes can enhance their binding affinity and selectivity for qDNA. These changes included increasing the number of aromatic moieties present in their structure, and the length and chemical composition of the pendant groups. However, to date, the effect of varying the position of the pendant groups on the ability of those complexes to bind to qDNA and their selectivity for qDNA over dsDNA, has not been explored.

Therefore, the aims of this project were to:

1. Synthesize the hydroxylated nickel Schiff base complexes shown in Figure 1.21.
2. Synthesize the alkylated nickel Schiff base complexes (7) – (12) shown in Figure 1.22 by reacting the complexes in Figure 1.21 with 1-(2-chloroethyl)piperidine hydrochloride. These complexes are isomers of those shown in Figure 1.18a, Figure 1.19a, and Figure 1.20a. The source of isomers stems from the identity of the dihydroxybenzaldehyde (2,3- or 2,5- isomer, as opposed to 2,4-

isomer) used during the first stage of synthetic procedure used to prepare the metal complex.

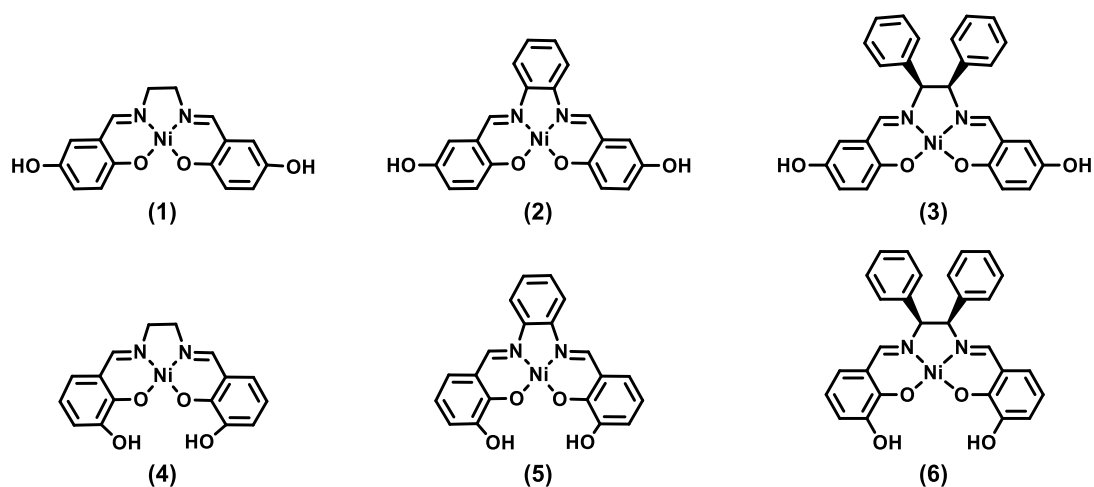


Figure 1.21: Structures of the hydroxylated nickel Schiff base complexes synthesized in this study.

3. Characterize the above complexes by mass spectrometry, as well as NMR spectroscopy, microanalysis and, where possible, X-ray crystallography.
4. Use electrospray ionization mass spectrometry and circular dichroism spectroscopy to compare the interactions between the nickel Schiff base complexes shown in Figure 1.22 with a duplex DNA molecule (D2) and a tetramolecular quadruplex DNA (Q4), with that of the isomeric complexes previously reported.

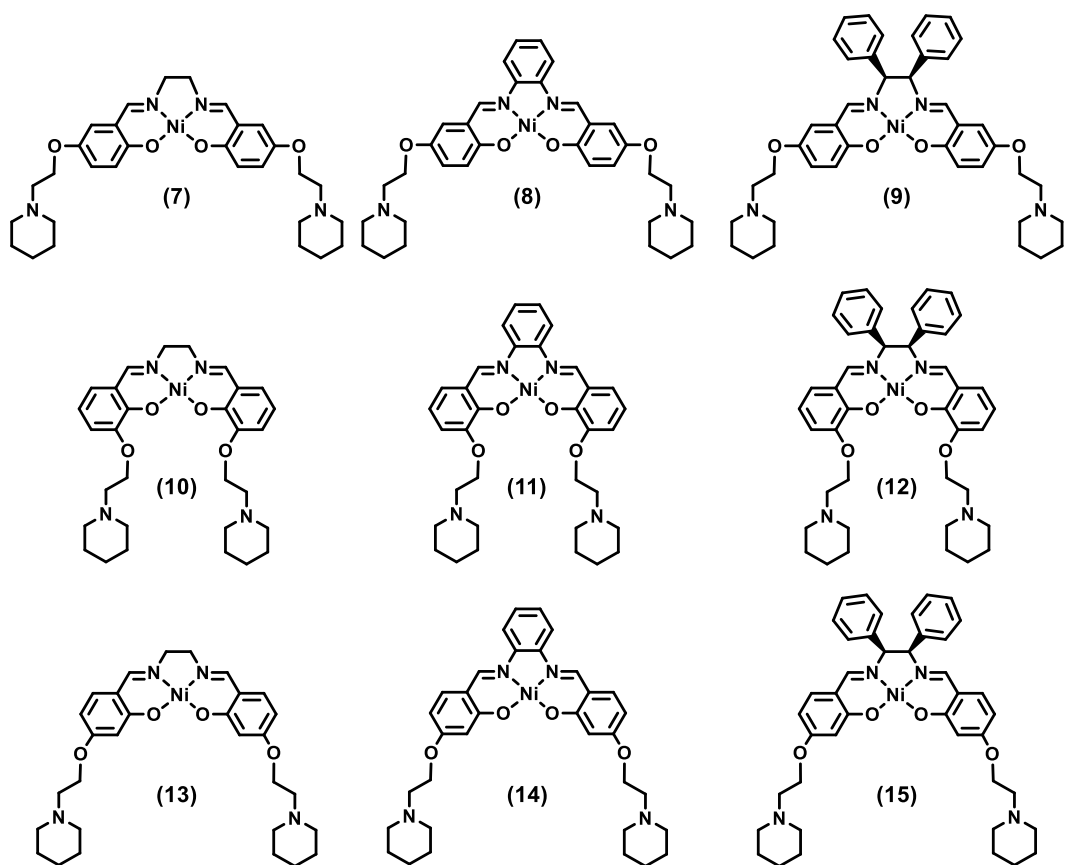


Figure 1.22: Structures of the alkylated nickel Schiff base complexes under study.

CHAPTER 2

MATERIALS AND METHODS

2.1 Chemicals

All solvents and reagents used in this study were of the highest grade commercially available. Milli-Q™ water (Millipore, Molsheim, France) was used in all experiments. Nickel compounds (**13**), (**14**) and (**15**) were obtained from PhD student Kimberley Davis (School of Chemistry, University of Wollongong, Australia). 1-(2-Chloroethyl)piperidine hydrochloride, 2,3-dihydroxybenzaldehyde, 2,5-dihydroxybenzaldehyde, magnesium sulfate (MgSO₄), 1,2-phenylenediamine, 1,2-ethylenediamine, 1,2-*meso*-diphenylethylenediamine, nickel acetate tetrahydrate (Ni(OAc)₂·4H₂O), DMSO-d₆ ((CD₃)₂SO), CDCl₃ and cesium iodide (Fluka brand) were all purchased from Sigma-Aldrich (Castle Hill, Australia). Potassium carbonate (K₂CO₃), dimethylformamide (DMF), dichloromethane (DCM), dimethyl sulfoxide (DMSO), acetic acid (CH₃COOH), methanol (MeOH), anhydrous diethyl ether (Et₂O), aluminium oxide used in column chromatography, as well as acetonitrile (ACN), ammonia and ammonium acetate (NH₄OAc) that were used in HPLC purification of oligonucleotides and ESI-MS experiments, were all purchased from Ajax Finechem (Seven Hills, Australia). All oligonucleotides were obtained either from Geneworks (Adelaide, South Australia) or Sigma-Aldrich (Castle Hill, Australia).

2.2 Characterisation of nickel Schiff base complexes

2.2.1 Physical measurements

Elemental microanalysis determination for the elements carbon, hydrogen, nitrogen and nickel were performed at the Campbell Microanalytical Laboratory at the Chemistry Department of the University of Otago, New Zealand. NMR spectra of the nickel complexes dissolved either in DMSO- d_6 or $CDCl_3$ were obtained using a Varian Inova-500 MHz NMR spectrometer at 25 °C. The chemical shifts of the resonances observed in 1H and ^{13}C NMR spectra were reported in ppm (δ) relative to either tetramethylsilane (TMS) or the solvent peak as an internal standard. In 1H NMR spectra, the signal from the small amount of $CHCl_3$ present in $CDCl_3$ solvent was reported at 7.26 ppm, while the signal from the small amount of CD_3SOCD_2H present in DMSO- d_6 solvent was reported at 2.50 ppm. For ^{13}C NMR spectra, the resonance from the $CDCl_3$ solvent was set to 77.7 ppm, while that from DMSO- d_6 solvent was assigned to 39.6 ppm. Hydrogen and carbon resonances were fully assigned through the use of 2D experiments including Correlation Spectroscopy (COSY), Nuclear Overhauser Effect Spectroscopy (NOESY), Heteronuclear Single-Quantum Correlation (HSQC) and Heteronuclear Multiple-Bond Correlation (HMBC) spectroscopy. Electrospray ionisation (ESI) mass spectra of alkylated nickel Schiff base complexes were obtained using a Waters Quattro ESI mass spectrometer (Milford, Massachusetts, USA), using solutions prepared in $H_2O:MeOH$ (50:50).

2.2.2 Crystallography

X-ray structural studies were performed by Dr Anthony C. Willis at the Research School of Chemistry, the Australian National University, Canberra, Australia. The X-ray diffraction measurements performed on complexes **(5)**, **(8)** and **(10)** were carried out at 150 K on an Xcalibur diffractometer with Atlas detector using Mo K α radiation, $\lambda = 0.71073 \text{ \AA}$. Data reduction and cell refinement were accomplished using *CrysAlis PRO* software.¹⁵⁸ The structures were solved with SIR92, and refined using the program CRYSTALS.^{159,160} Molecular graphics were produced using PLATON.¹⁶¹

During refinement of **(5)** hydrogen atoms bonded to C were positioned geometrically and the water H atoms were based on peaks from a difference electron density map and potential H-bonded contacts. The H atoms were initially refined with soft restraints on the bond lengths and angles to regularize their geometry (C-H in the range 0.93-0.98 \AA , O-H = 0.82 \AA) and with $U_{\text{iso}}(\text{H})$ in the range 1.2-1.5 times U_{eq} of the parent atom, after which the positions were refined with riding constraints.

During refinement of **(8)**, the H atoms were all located in a difference map, but those bonded to C were repositioned geometrically. The H atoms were initially refined with soft restraints on the bond lengths and angles to regularize their geometry (C-H in the range 0.93-0.98 \AA , O-H = 0.83 \AA) and with $U_{\text{iso}}(\text{H})$ in the range 1.2-1.5 times U_{eq} of the parent atom, after which the positions were refined with riding constraints except for those bonded to O

which were allowed to refine freely. The largest features in the final difference electron density map are located midway between bonded atoms.

During refinement of **(10)** the program PLATON was used to identify a twinning relationship in the data. Application of a twinning correlation within CRYSTALS to allow for overlapping reflections, based on the above relationship, gave a small improvement in the agreement factors. The final refined values for the twin elements were 0.704(5) and 0.296(5). Hydrogen atoms bonded to C were positioned geometrically and the water H atoms were based on peaks from a difference electron density map and potential H-bonded contacts. The H atoms were initially refined with soft restraints on the bond lengths and angles to regularize their geometry (C-H in the range 0.93-0.98 Å, O-H = 0.82 Å) and with $U_{\text{iso}}(\text{H})$ in the range 1.2-1.5 times U_{eq} of the parent atom, after which the positions were refined with riding constraints.

2.3 *Oligonucleotides*

2.3.1 Purification of single-stranded oligonucleotides

Single-stranded oligonucleotides (D2A, D2B and q4) were purchased from either Sigma-Aldrich (Castle Hill, Australia), or Geneworks (South Australia), as freeze-dried 'trityl-off' derivatives. The base sequences of DNA molecules which were used in this study are presented in Table 2.1. These oligonucleotides were purified using high performance liquid chromatography (HPLC) by following previously reported procedures.^{157,162,163} Purified DNA

solutions were then freeze-dried using a Savant speedVac (Selby-Biolab, Australia) prior to storage at -20 °C.

When required, freeze-dried samples were dissolved in 1000 μL of Milli-Q™ water. Diluted solutions (300 \times dilution factor) were prepared by adding 2 μL of one of the above DNA solutions to 598 μL of Milli-Q™ water. In order to determine the concentration of the final DNA solutions, the absorbance at 260 nm was measured, and the molar absorption coefficients (ϵ) of the individual nitrogenous bases present in the DNA sequence were used to obtain an overall value of ϵ for the oligonucleotide itself. Values of ϵ for the purine and pyrimidine bases were obtained from the website, Oligonucleotides Properties Calculator.¹⁶⁴

Table 2.1: Properties of the DNA molecules used in this study.

<i>Oligonucleotide sequence</i>	<i>DNA label</i>	<i>Mass (Da)</i>
GCTGCCAAATACCTCC	D2A	4786.2
GGAGGTATTTGGCAGC	D2B	4977.3
(GCTGCCAAATACCTCC/GGAGGTATTTGGCAGC)	D2	9763.5
TTGGGGGT	q4	2496.7
(TTGGGGGT) ₄	Q4	9986.6

2.3.2 Preparation of dsDNA (D2)

Appropriate quantities of single-stranded DNA (ssDNA) solutions (D2A and D2B) were mixed together in an Eppendorf tube and dried using the Savant SpeedVac before being dissolved in an appropriate volume of NH_4OAc solution (100 mM, pH 7.4) to give a final dsDNA concentration of 1 mM. The

DNA was then annealed by heating the resulting DNA solution in a water bath at 61 °C (the melting temperature of the DNA plus 15 °C)¹⁶⁴ for 15 min, after which it was allowed to cool slowly to room temperature overnight.

2.3.3 Preparation of qDNA (Q4)

An appropriate quantity of solution containing the ssDNA q4 was placed in an Eppendorf tube, dried and then redissolved in sufficient NH₄OAc solution (150 mM, pH 7.4) to give a final concentration of 1 mM. The DNA was then annealed by heating the resulting solution in a water bath at 90 °C for 15 min, after which it was allowed to cool slowly to room temperature overnight.

2.4 Reactions of oligonucleotides with nickel Schiff base complexes

2.4.1 ESI-MS experiments

Stock solutions of nickel complexes (1 mM) were prepared in a mixture of acetic acid:MeOH (1:99) for all DNA-binding studies. Reaction mixtures containing different ratios of DNA (10 μM) and nickel complex were prepared in NH₄OAc solution (100 and 150 mM for D2 and Q4, respectively). This gave mixtures with final DNA:metal complex ratios of 1:1, 1:3, 1:6 and 1:9. The volumes of different reagent solutions used to prepare these reaction mixtures are presented in Table 2.2.

Table 2.2: Volume of stock solutions used to prepare nickel/DNA samples for analysis by ESI-MS.

<i>DNA:metal complex ratio</i>	<i>Volume of DNA (1 mM stock) (μL)</i>	<i>Volume of metal complex (1 mM stock) (μL)</i>	<i>Volume of buffer (μL)</i>
1:1	1	1	98
1:3	1	3	96
1:6	1	6	93
1:9	1	9	90

ESI-MS was used to investigate the binding of nickel complexes to dsDNA and qDNA. A Waters Q-ToF UltimaTM ESI mass spectrometer (Manchester, UK) was used to acquire mass spectra in negative ion mode. The instrument was calibrated using a cesium iodide (CsI) solution (1 mg/mL), prior to acquiring the spectra of samples containing DNA and nickel complexes. The samples were injected into the mass spectrometer using a Harvard model 22 syringe pump (Natick, USA) at a constant flow rate (10 μ L/min). The parameters used to obtain the spectra for all experiments are listed in Table 2.3.

Table 2.3: ESI-MS conditions used for the analysis of DNA/metal complex solutions.

<i>MS parameter</i>	<i>Setting</i>
Capillary (kV)	2.50
Cone (V)	60
Source temperature ($^{\circ}$ C)	25
Desolvation temperature ($^{\circ}$ C)	80
Desolvation gas flow (L/Hr)	100

2.4.2 CD Experiments

A Jasco J-810 spectropolarimeter and 0.1 cm path length quartz cell was used to obtain CD spectra between 200 and 400 nm. The instrument parameters used to acquire these spectra are listed in Table 2.4.

Table 2.4: Instrument parameters used to acquire all CD spectra of nickel/DNA samples.

<i>CD parameter</i>	<i>Setting</i>
Sensitivity	standard
Scanning speed	100 nm/min
Response	4 s
Band width	1 nm
Number of accumulations	6
Temperature	25 °C

The CD spectra were obtained first for a 300 μ L solution containing either D2 or Q4 (20 μ M) dissolved in NH_4OAc solution of the appropriate concentration. Aliquots of a stock solution (Table 2.5) containing both the same type of DNA (20 μ M) and nickel complex (0.6 mM), were then added to the initial DNA solution in order to produce samples with DNA:metal complex ratios of 1:1, 1:3, 1:6 and 1:9. CD spectra were obtained after each new solution was made.

Table 2.5: Volumes of the DNA/metal complex stock required for CD samples.

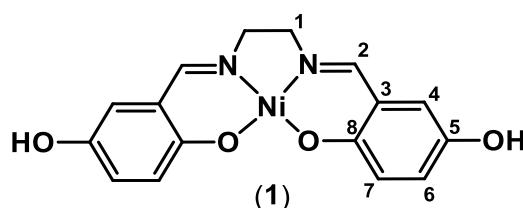
<i>DNA: metal complex ratio</i>	<i>Volume of DNA/nickel complex stock solution added (μL)</i>
1:1	10.4
1:3	23.0
1:6	41.7
1:9	53.6

CHAPTER 3

SYNTHESIS AND CHARACTERISATION OF NICKEL SCHIFF BASE COMPLEXES.

3.1 *Synthesis of hydroxylated nickel Schiff base complexes*

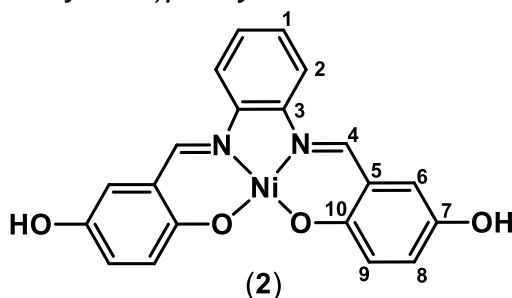
N, N'-Bis-5-(hydroxysalicylidine)ethylenediaminenickel(II) (1)



This compound was prepared by following a previously reported method.¹⁵⁵ 2,5-Dihydroxybenzaldehyde (676 mg, 4.89 mmol) and 1,2-ethylenediamine (197 mg, 3.30 mmol) were dissolved in MeOH (50 mL), forming a transparent light orange solution. The mixture was heated with constant stirring under reflux for 30 min, after which Ni(OAc)₂·4H₂O (1.24 g, 4.96 mmol) was added, forming a chocolate brown coloured precipitate. Refluxing was continued for another 3 h. After this time, the solution was allowed to cool to room temperature. The red-brown solid present was collected by vacuum filtration, and then washed with MeOH (100 mL), diethyl ether (50 mL) and water (50 mL). The compound was then dried under vacuum for a further 1 h. Yield: 0.81 g, 92.0 %. Microanalysis calc. for C₁₆H₁₄N₂NiO₄·4H₂O: C = 44.80; H =

5.17; N = 6.53; Ni = 13.68 %. Found: C = 44.83; H = 4.25; N = 6.53; Ni = 14.00 %. ^1H NMR (500 MHz, DMSO- d_6): δ 3.36 (s, 4H, H1); 6.55 (d, 2H, J = 8.74 Hz, H7); 6.58 (d, 2H, J = 2.38 Hz, H4); 6.73 (dd, 2H, J = 2.39 and 8.74 Hz, H6); 7.77 (s, 2H, H2); 8.55 (s, 2H, OH); ^{13}C NMR (125 MHz, DMSO- d_6): δ 58.36 (C1); 115.09 (C4); 119.57 (C3); 120.47 (C7); 124.43 (C6); 146.18 (C5); 158.72 (C8); 162.42 (C2);

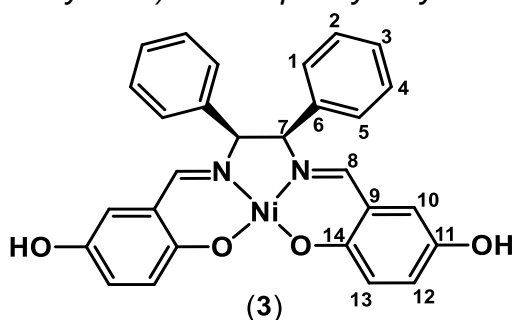
N, N'-Bis-5-(hydroxysalicylidine)phenylenediaminenickel(II) (2)



This compound was prepared by following a previously reported method.¹⁵⁴ 2,3-Dihydroxybenzaldehyde (695 mg, 5.03 mmol) and 1,2-phenylenediamine (239 mg, 2.21 mmol) were dissolved in MeOH (50 mL), forming a transparent light yellow solution. This was heated under reflux with constant stirring for 30 min, during which time the solution changed to a dark orange colour. Ni(OAc) $_2$ ·4H $_2$ O (1.27 g, 5.09 mmol) was subsequently added, and a dark red-brown precipitate formed immediately. The reaction mixture was heated under reflux for a further 3 h, after which the solution was allowed to cool to room temperature. The precipitate that remained was collected by vacuum filtration and then washed sequentially with MeOH (100 mL), diethyl ether (50 mL) and water (50 mL). The compound was then dried under vacuum for 2 h. Yield: 1.00 g, 98.0 %. Microanalysis calc. for C $_{20}$ H $_{14}$ N $_2$ NiO $_4$ ·1.25H $_2$ O: C =56.19; H =3.89; N = 6.55 %. Found: C =56.14; H

= 3.68; N = 6.49 %. ^1H NMR (500 MHz, DMSO- d_6): δ 6.76 (d, 2H, J = 8.7 Hz, H9); 6.90 (s, 2H, H6); 6.92 (broad s, 2H, H8); 7.29 (m, 2H, H1); 8.13 (m, 2H, H2); 8.80 (s, 2H, H4); 8.82 (s, 2H, OH). ^{13}C NMR (125 MHz, DMSO- d_6): 115.15 (C6); 116.44 (C2); 119.51 (C5); 121.07 (C9); 127.25 (C8); 127.57 (C1); 142.81 (C3); 146.78 (C7); 155.71 (C4); 160.80 (C10).

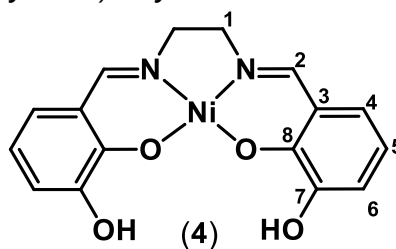
N, N'-Bis-5-(hydroxysalicylidine)meso-diphenylethylenediaminenickel(II) (**3**)



2,5-Dihydroxybenzaldehyde (675 mg, 4.89 mmol) and 1,2-*meso*-diphenylethylenediamine (537 mg, 2.53 mmol) were dissolved in MeOH (50 mL), forming a transparent light yellow solution. This was heated under reflux with constant stirring for 30 min. During this time the solution changed to an orange colour. Ni(OAc) $_2$ ·4H $_2$ O (1.24 g, 4.96 mmol) was subsequently added, and a dark green precipitate formed immediately. This solution was heated under reflux for a further 3 h. After the solution was allowed to cool to room temperature, the precipitate was isolated by vacuum filtration and dried. The green solid was then washed with MeOH (100 mL), diethyl ether (50 mL) and water (50 mL), before being dried under vacuum for a further 1 h. Yield: 0.98 g, 79.0 %. Microanalysis calc. for C $_{28}$ H $_{22}$ N $_2$ NiO $_4$ ·2H $_2$ O: C = 61.69; H = 4.81; N = 5.14; Ni = 10.77 %. Found: C = 61.72; H = 4.57; N = 5.14; Ni = 11.00 %. ^1H NMR (500 MHz, DMSO- d_6): δ 5.02 (s, 2H, H7); 6.40 (d, 2H, J = 2.6 Hz, H10); 6.62 (d, 2H, J = 9.1 Hz, H13); 6.78 (dd, 2H, J = 2.7, 9.00 Hz, H12);

7.27 (m, 6H, H2, 3 and 4); 7.40 (broad s, 4H, H1 and 5); 7.45 (s, 2H, H8); 8.52 (s, 2H, OH); ^{13}C NMR (125 MHz, DMSO- d_6): δ 76.40 (C7); 115.06 (C10); 119.44 (C9); 120.63 (C13); 125.23 (C12); 128.70 (C3); 128.83 (4C, C2 and C4); 129.60 (4C, C1 and C5); 136.38 (C6); 146.40 (C11); 159.07 (C14); 162.34 (C8).

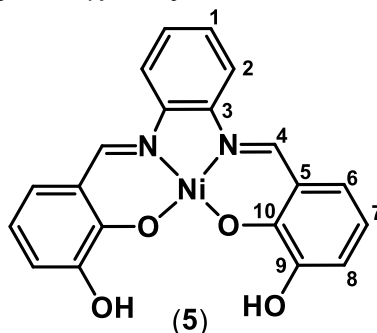
N, N'-Bis-3-(hydroxysalicylidine)ethylenediaminenickel(II) (**4**)



This compound was prepared by following a previously reported method.¹⁵⁵ 2,3-Dihydroxybenzaldehyde (676 mg, 4.89 mmol) and 1,2-ethylenediamine (197 mg, 3.27 mmol) were dissolved in MeOH (50 mL), forming a light yellow suspension. This stirred reaction mixture was heated under reflux for 30 min, during which time the solution colour changed to dark orange. Ni(OAc) $_2$ ·4H $_2$ O (1.24 g, 4.96 mmol) was then added, and a dark green precipitate formed immediately. This mixture was heated under reflux for a further 3 h. After the reaction was completed, the mixture was allowed to cool to room temperature, and the green solid isolated by vacuum filtration and dried. It was then washed with MeOH (100 mL), diethyl ether (50 mL) and water (50 mL), before being dried under vacuum for a further 2 h. Yield: 0.70 g, 80.0 %. Microanalysis calc. for C $_{16}$ H $_{14}$ N $_2$ NiO $_4$ ·H $_2$ O: C = 51.25; H = 4.30; N = 7.47; Ni = 15.65 %. Found: C = 51.09; H = 3.94; N = 7.43; Ni = 15.60 %. ^1H NMR (500 MHz, DMSO- d_6): δ 3.43 (s, 4H, H1); 6.38 (t, 2H, J = 7.68 Hz, H5); 6.69 (dd, 2H, J = 1.54 and 7.49 Hz, H6); 6.74 (dd, 2H, J = 1.53 and 8.06 Hz,

H4); 7.88 (s, 2H, C2); 8.16 (broad s, OH). ¹³C NMR (125 MHz, DMSO-d₆): δ 58.45 (C1); 114.81 (C5); 114.95 (C6); 119.61 (C3); 122.40 (C4); 148.15 (C7); 153.13 (C8); 163.21 (C2).

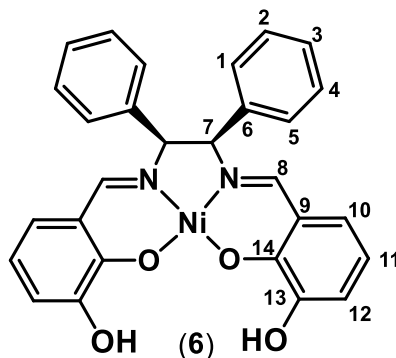
N, N'-Bis-3-(hydroxysalicylidine)phenylenediaminenickel(II) (**5**)



2,3-Dihydroxybenzaldehyde (695 mg, 5.03 mmol) and 1,2-phenylenediamine (284 mg, 2.63 mmol) were dissolved in MeOH (50 mL), forming a transparent dark yellow solution. This was heated for 30 min at reflux with constant stirring, during which time the solution colour changed to dark orange. Ni(OAc)₂·4H₂O (1.27 g, 5.10 mmol) was then added to the mixture, and immediately resulted in a deep red-brown precipitate. This solution continued to be heated under reflux for 3 h, after which it was allowed to cool to room temperature. The precipitate that had formed was separated by vacuum filtration and dried. It was subsequently washed with MeOH (100 mL), diethyl ether (50 mL) and water (50 mL), before being dried under vacuum for a further 2 h. Yield: 0.69 g, 68.0 %. The product was purified by crystallization from a MeOH-DMSO (70:30) mixture. Microanalysis calc. for C₂₀H₁₄N₂NiO₄·2H₂O: C = 54.47; H = 4.11; N = 6.35; Ni = 13.31%. Found: C = 54.57; H = 3.48; N = 6.22; Ni = 13.20 %. ¹H NMR (500 MHz, DMSO-d₆): δ 6.54 (t, 2H, *J* = 7.63 Hz, H7); 6.81 (d, 2H, *J* = 6.67 Hz, H8); 7.09 (d, 2H, *J* = 8.10 Hz, H6); 7.35 (m, 2H, H1); 8.17 (m, 2H, H2); 8.51 (s, 2H,

H4); 9.12 (s, 2H, OH). ^{13}C NMR (125 MHz, DMSO- d_6): δ 115.84 (C7); 116.13 (C8); 116.83 (C2); 119.70 (C5); 123.88 (C6); 128.12 (C1); 142.66 (C3); 148.66 (C9); 154.99 (C10); 157.21 (C4).

N, N'-Bis-3-(hydroxysalicylidine) meso-diphenylethylenediaminenickel(II) (**6**)

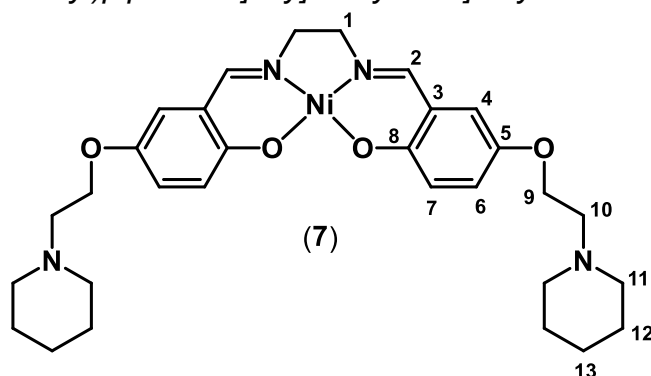


2,3-Dihydroxybenzaldehyde (676 mg, 4.89 mmol) and 1,2-*meso*-diphenylethylenediamine (537 mg, 2.53 mmol) were dissolved in MeOH (50 mL), forming a transparent light yellow solution. The mixture was heated with constant stirring under reflux for 30 min. During this time the solution changed colour to dark orange. Ni(OAc) $_2$ ·4H $_2$ O (1.23 g, 4.96 mmol) was added to the reaction mixture, and a dark green precipitate formed immediately. Heating under reflux was continued for another 3 h, after which the solution was allowed to cool to room temperature, and the resulting precipitate was isolated by vacuum filtration. The solid was then washed with MeOH (100 mL), diethyl ether (50 mL) and water (50 mL), before being dried under vacuum for a further 2 h. Yield: 1.20 g, 97.0 %. Microanalysis calc. for C $_{28}$ H $_{22}$ N $_2$ NiO $_4$ ·1.5H $_2$ O: C = 62.72; H = 4.70; N = 5.22 %. Found: C = 62.68; H = 4.41; N = 5.19 %. ^1H NMR (500 MHz, DMSO- d_6): δ 5.08 (broad, s, 2H, H7); 6.34 (t, 2H, J = 8.03 Hz, H11); 6.61 (d, 2H, J = 6.76 Hz, H10); 6.70 (d, 2H, J = 5.91 Hz, H12); 7.26-7.28 (m, 6H, H2, H3 and H4); 7.42 (br, s, (4H,

H1 and H5); 7.57 (s, 2H, C8); 8.34 (s, 2H, OH). ^{13}C NMR (125 MHz, DMSO- d_6): δ 76.72 (C7); 115.33 (C11); 115.71 (C12); 119.74 (C9); 122.97 (C10); 128.98 (C3); 129.13 (C2 and C4); 129.83 (C1 and C5); 136.35 (C6); 148.37 (C13); 153.73 (C14); 163.45 (C8).

3.2 Synthesis of alkylated nickel Schiff base complexes

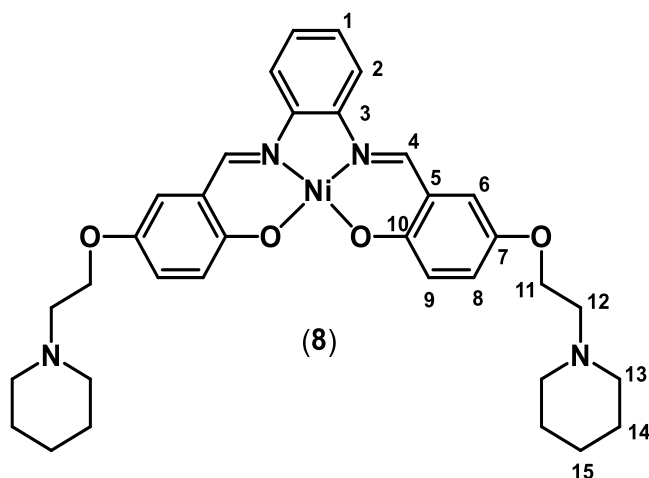
N,N'-Bis[5-[[1-(2-ethyl)piperidine]oxy]salicylidine]ethylenediaminenickel(II) (7)



A suspension of compound (1) (107 mg, 0.30 mmol), 1-(2-chloroethyl) piperidine hydrochloride (216 mg, 1.17 mmol) and K_2CO_3 (284 mg, 2.05 mmol) was made in anhydrous DMF (10 mL) and stirred for 72 h under N_2 . During this time a green precipitate appeared in the bright brown solution. After the end of the reaction, the DMF was removed from the mixture under low pressure to yield a dark green solid. This was then dissolved in DCM (30 mL), and insoluble material removed by gravity filtration. The filtrate was then washed with water seven times, and then dried using MgSO_4 , before the DCM was allowed to evaporate. The desired compound was subsequently obtained as a dark green solid. Yield 0.11 g, 63.0 %. ESI-MS calc.

$[C_{30}H_{40}N_4O_4Ni+H]^+ = 579.4$, $[C_{30}H_{40}N_4O_4Ni+2H]^{2+} = 289.7$. Found: $[C_{30}H_{40}N_4O_4Ni+H]^+ = 579.1$, $[(C_{30}H_{40}N_4O_4Ni + 2H)]^{2+} = 290.2$. Microanalysis calc. for $C_{30}H_{40}N_4NiO_4$: C = 62.20; H = 6.96; N = 9.67 %. Found: C = 62.18; H = 6.98; N = 9.53 %. 1H NMR (500 MHz, $CDCl_3$): δ 1.45 (m, 4H, H13); 1.60 (m, 8H, H12); 2.48 (broad s, 8H, H11); 2.71 (t, 4H, $J = 6.04$ Hz, H10); 3.41 (s, 4H, H1); 3.97 (t, 2H, $J = 6.04$ Hz, H9); 6.46 (d, 2H, $J = 2.66$ Hz, H4); 6.90 (dd, 2H, $J = 2.66$ and 9.29 Hz, H6); 6.94 (d, 2H, $J = 9.18$ Hz, H7); 7.35 (s, 2H, H2). ^{13}C NMR (125 MHz $CDCl_3$): δ 24.18 (C13); 25.90 (C12); 55.05 (C11); 58.07 (C10); 58.44 (C1); 66.70 (C9); 112.99 (C4); 118.47 (C3); 122.57 (C7); 124.92 (C6); 148.39 (C5); 160.52 (C8); 161.20 (C2).

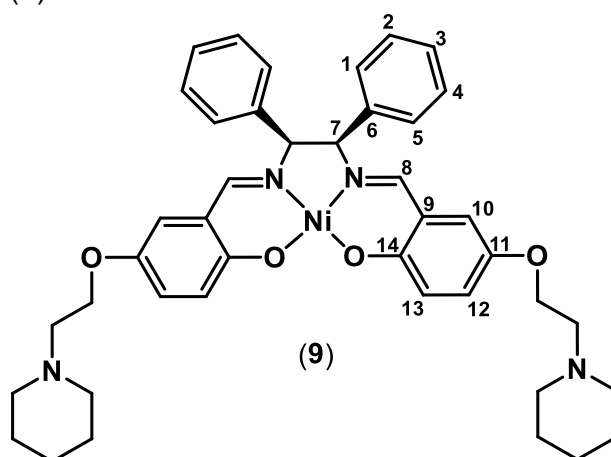
N,N'-Bis[5-[[1-(2-ethyl)piperidine]oxy]salicylidine]phenyldiaminenickel(II)
(8)



This compound was prepared by following a previously reported method.¹⁵⁴ Compound **(2)** (122 mg, 0.30 mmol) was suspended in anhydrous DMF (10 mL), along with 1-(2-chloroethyl)piperidine hydrochloride (215.7 mg, 1.17 mmol) and K_2CO_3 (284 mg, 2.05 mmol) and stirred for 72 h under N_2 . During this time a brown precipitate appeared, and the K_2CO_3 disappeared. After the end of the reaction time, the DMF was removed from the mixture under low

pressure to yield a red-brown solid. This was then dissolved in DCM (30 mL) and washed with water five times, and then dried using MgSO₄, before the DCM was allowed to evaporate under low pressure to yield a dark red-brown crystalline product. Yield: 0.10 g, 53.0 %. ESI-MS calc: [C₃₄H₄₀N₄O₄Ni+H]⁺ = 628.4, [C₃₄H₄₀N₄O₄Ni+2H]²⁺ = 314.7. Found: [C₃₄H₄₀N₄O₄Ni+H]⁺ = 627.2, [C₃₄H₄₀N₄O₄Ni +2H]²⁺ = 314.2. Microanalysis calc. for C₃₄H₄₀N₄NiO₄·2H₂O: C = 61.56; H = 6.68; N = 8.44; Ni = 8.85 %. Found: C = 61.37; H = 6.52; N = 8.13; Ni = 8.70 %. ¹H NMR (500 MHz, CDCl₃): δ 1.47 (m, 4H, H15); 1.63 (t, 8H, J = 5.57 Hz, H14); 2.51 (broad s, 8H, H13); 2.75 (t, 4H, J = 6.16 Hz, H12); 4.04 (t, 4H, J = 6.16 Hz, H11); 6.68 (d, 2H, J = 2.64 Hz, H6); 7.02 (dd, 2H, J = 2.93 and 9.38 Hz, H8); 7.09 (d, 2H, J = 9.38 Hz, H9); 7.18-7.20 (m, 2H, J = 2.93, H1); 7.69-7.71 (m, 2H, J = 3.51 Hz, H2); 8.16 (s, 2H, H4). ¹³C NMR (125 MHz, CDCl₃): δ 24.35 (C15); 26.09 (C14); 55.23 (C13); 58.19 (C12); 66.85 (C11); 112.43 (C6); 114.85 (C2); 118.56 (C5); 123.33 (C9); 127.29 (C1); 127.59 (C8); 142.89 (C3); 149.18 (C7); 153.28 (C4); 162.80 (C10).

N,N'-Bis[5-[[1-(2-ethyl)piperidine]oxy]salicylidine]meso-diphenylethylene-diaminenickel(II) (**9**)

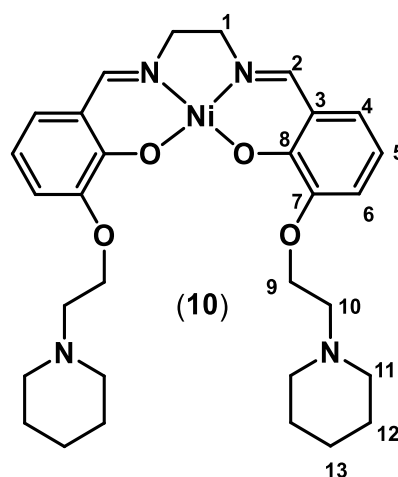


The synthesis of this complex was monitored using thin layer chromatography (TLC). A suspension of compound (**3**) (166 mg, 0.3 mmol), 1-(2-chloroethyl) piperidine hydrochloride (222 mg, 1.2 mmol) and K_2CO_3 (294 mg, 2.1 mmol) in anhydrous DMF (10 mL) was stirred for 6 d under N_2 . TLC analysis showed that after this time the starting material was still present in the reaction mixture. Therefore, the reaction was heated to 50 °C for a further 48 h under N_2 at 50 °C. The reaction was stopped after 48 h when TLC showed that no starting material remained in the mixture. After this time, the precipitate present was removed by gravity filtration. The DMF was then evaporated under low pressure to yield a red solid, which was then dissolved in DCM (30 mL), and washed with water seven times. All precipitates which appeared during the washing process were removed by gravity filtration. After the washing step, the DCM solution was dried with $MgSO_4$, and evaporated yielding 0.05 g of a red solid. An ESI mass spectrum of the resulting solid dissolved in MeOH:H₂O (50:50) did not show any ions which could be assigned to complex (**9**). In addition, the ¹H NMR spectrum of the product contained many broad and overlapping signals, indicating that it was

likely to be a mixture of compounds. In other attempts to synthesise complex (9), the same procedure as above was followed but different concentrations of either the hydroxylated precursor complex or 1-(2-chloroethyl) piperidine hydrochloride were used. Again ESI mass spectra and ^1H NMR spectra did not show any sign of complex (9) in the products obtained. After these failed attempts to synthesise complex (9), it was decided to remove this compound from the list of target molecules to be used in DNA-binding studies.

N,N'-Bis[3-[[1-(2-ethyl)piperidine]oxy]salicylidine]ethylenediaminenickel(II)

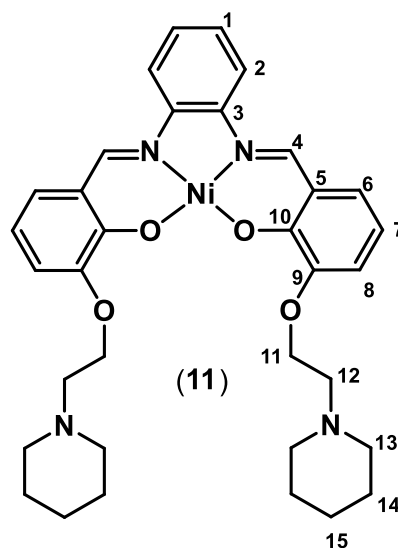
(10)



A suspension of compound (4) (107 mg, 0.30 mmol), 1-(2-chloroethyl) piperidine hydrochloride (216 mg, 1.17 mmol) and K_2CO_3 (283 mg, 2.05 mmol) was made in anhydrous DMF (10 mL) and stirred for 72 h under N_2 . During this time, a dark yellow precipitate appeared, and the K_2CO_3 disappeared. Upon completion of the reaction, the DMF was removed under low pressure to yield a red solid, which was dissolved in DCM (30 mL). After removal of some insoluble materials by gravity filtration, the filtrate was washed with water five times, dried with MgSO_4 and the DCM evaporated, to

yield a brown solid. Yield: 90.0 mg, 53.0 %. ESI-MS calc: $[C_{30}H_{40}N_4O_4Ni+H]^+$ = 579.4, $[C_{30}H_{40}N_4O_4Ni+2H]^{2+}$ = 289.7. Found: $[C_{30}H_{40}N_4O_4Ni+H]^+$ = 579.1, $[C_{30}H_{40}N_4O_4Ni + 2H]^{2+}$ = 290.2. Microanalysis calc. for $C_{30}H_{40}N_4NiO_4 \cdot 2H_2O$: C = 58.56; H = 7.21; N = 9.10; Ni = 9.54 %. Found: C = 58.31; H = 7.04; N = 8.96; Ni = 9.40 %. 1H NMR (500 MHz, $CDCl_3$): δ 1.45 (broad s, 4H, H13); 1.64 (m, 8H, H12); 2.56 (broad s, 8H, H11); 2.93 (t, 4H, H10); 3.40 (s, 4H, H1); 4.13 (t, 4H, H9); 6.45 (t, 2H, $J = 7.40$ Hz, H5); 6.72 (d, 2H, $J = 7.40$ Hz, H4); 6.76 (d, 2H, $J = 6.87$ Hz, H6); 7.49 (s, 2H, H2). ^{13}C NMR (125 MHz, $CDCl_3$): δ 24.31 (C13); 25.96 (C12); 55.27 (C11); 57.61 (C10); 58.54 (C1); 66.11 (C9); 113.96 (C5); 114.56 (C6); 120.18 (C3); 124.14 (C4); 149.95 (C7); 155.83 (C8); 161.66 (C2).

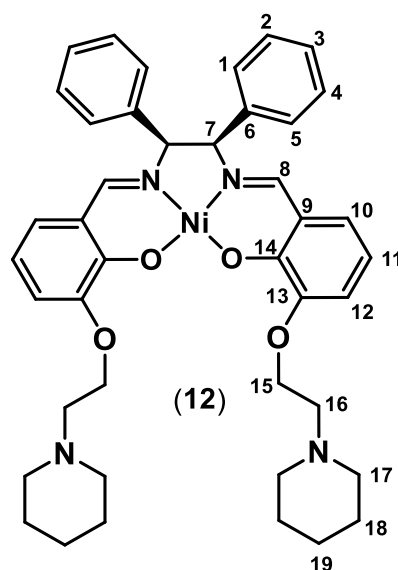
N,N'-Bis[3-[[1-(2-ethyl)piperidine]oxy]salicylidine]phenylenediaminenickel(II) (11)



A suspension of compound (5) (122 mg, 0.3 mmol), 1-(2-chloroethyl)piperidine hydrochloride (216 mg, 1.17 mmol) and K_2CO_3 (284 mg, 2.05 mmol) in anhydrous DMF (10 mL) was stirred for 96 h under N_2 . After this time, the DMF was removed from the reaction mixture under low

pressure to yield a red solid. This was subsequently added to DCM (30 mL), and the insoluble portion was removed by gravity filtration. The filtrate was then washed with water five times, and dried with MgSO₄, before the DCM was removed under low pressure to afford the product as a dark red solid. Yield: 0.05 g, 26.0 %. ESI-MS cal: [C₃₄H₄₀N₄O₄Ni+H]⁺ = 628.4, [C₃₄H₄₀N₄O₄Ni+2H]²⁺ = 314.7. Found: (C₃₄H₄₀N₄O₄Ni+H)⁺ = 627.2, [C₃₄H₄₀N₄O₄Ni+2H]²⁺ = 314.3. Microanalysis calc. for C₃₄H₄₀N₄NiO₄·H₂O: C = 61.56; H = 6.68; N = 8.44 %. Found: C = 61.62; H = 6.38; N = 8.37 %. ¹H NMR (500 MHz, CDCl₃): δ 1.46 (m, 4H, H15); 1.61 (m, 8H, H14); 2.56 (s, 8H, H13); 2.96 (t, 2H, J = 6.72, H12); 4.14 (t, 2H, J = 6.72 Hz, H11); 6.56 (t, 2H, J = 7.68 Hz, H7); 6.79 (d, 2H, J = 7.36 Hz, H8); 6.95 (d, 2H, J = 7.68 Hz, H6); 7.21-7.22 (m, 2H, H1); 7.69-7.70 (m, 2H, H2); 8.24 (s, 2H, H4); ¹³C NMR (125 MHz, CDCl₃): δ 24.30 (C15); 25.96 (C14); 55.29 (C13); 57.60 (C12); 66.08 (C11); 114.82 (C2); 115.19 (C7); 115.3 (C8); 119.85 (C5); 124.64 (C6); 127.29 (C1); 142.85 (C3); 150.42 (C9); 154.13 (C4); 157.53 (C10).

N,N'-Bis[3-[[1-(2-ethyl)piperidine]oxy]salicylidine]meso-diphenylethylene-diaminenickel(II) (**12**)



A suspension of compound (**6**) (165 mg, 0.3 mmol), 1-(2-chloroethyl)piperidine hydrochloride (221 mg, 1.2 mmol), and K_2CO_3 (292 mg, 2.1 mmol) in anhydrous DMF (25 mL) was stirred for 72 h under N_2 . The reaction was monitored by TLC. After the end of this period, the DMF was removed from the reaction mixture under low pressure to yield a dark brown slurry. This was then dissolved in DCM (30 mL), and the resulting solution filtered under gravity to eliminate excess insoluble starting materials. The filtrate was then washed with water seven times, and dried with $MgSO_4$, before the DCM was evaporated to afford the desired product as a yellowish brown solid. This product was purified by using column chromatography on alumina, using DCM/methanol (95/5, v/v) as the eluent, to yield the desired compound (0.11 g, 46.0 %). ESI-MS cal: $[C_{42}H_{48}N_4O_4Ni+H]^+$ = 731.6, $[C_{42}H_{48}N_4O_4Ni+2H]^{2+}$ = 365.8. Found: $[C_{42}H_{48}N_4O_4Ni+H]^+$ = 731.4, $[(C_{42}H_{48}N_4O_4Ni + 2H)]^{2+}$ = 366.3. Microanalysis calc. for $C_{42}H_{48}N_4NiO_4 \cdot H_2O$: C = 67.30; H = 6.72; N = 7.47 %. Found: C = 67.40; H = 6.67; N = 7.54 %. 1H NMR (500 MHz, $CDCl_3$): δ 1.45-1.46 (m, 4H, H19); 1.63 (m, 8H, H18); 2.56

(m, 8H, H17); 2.96 (t, 4H, $J = 6.61$ Hz, H16); 4.14 (t, 4H, $J = 6.60$ Hz, H15); 4.77 (s, 2H, H7); 6.38 (t, 2H, $J = 7.73$ Hz, H11); 6.52 (d, 2H, $J = 7.89$ Hz, H10); 6.74 (d, 2H, $J = 7.61$ Hz, H12); 7.22 (t, 4H, H1 and H5); 7.26-7.28 (m, 6H, H2, H4 and H8); 7.38 (broad s, 2H, H3). ^{13}C NMR (125 MHz, CDCl_3): δ 24.25 (C19); 25.92 (C18); 55.25 (C17); 57.58 (C16); 65.95 (C15); 77.23 (C7); 114.20 (C11); 114.86 (C12); 129.00 (C9); 124.08 (C10); 128.43 (C2 and C4); 128.81 (C1 and C5); 129.53 (C3); 135.04 (C6); 150.14 (C13); 156.31 (C14); 162.34 (C8).

3.3 Discussion of Synthetic methods

3.3.1 Hydroxylated nickel Schiff base complexes

Nickel Schiff base complexes were synthesized according to a general literature method.^{154,155} The hydroxylated Schiff base complexes were first synthesized by the reaction of different diamines with either 2,5- or 2,3-dihydroxybenzaldehyde in order to form the free Schiff base ligand. Subsequent addition of nickel acetate resulted in formation of the corresponding nickel complex. The reaction procedure is outlined in Figure 3.1, with complex (**2**) as an example. The hydroxylated nickel Schiff base complexes were intensely coloured, and insoluble in common organic solvents such as methanol, ethanol, and chloroform. They were, however, soluble in DMSO and DMF.

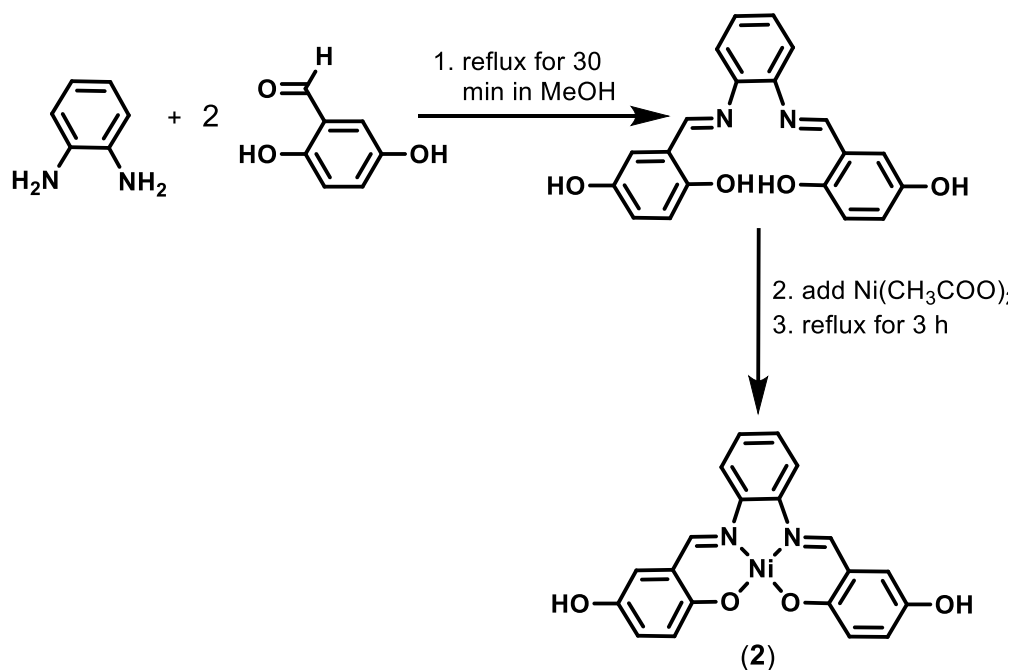
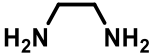
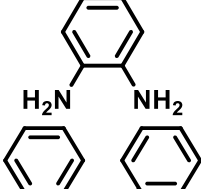
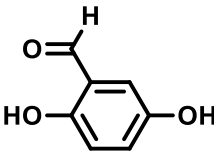
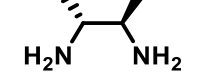
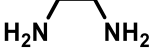
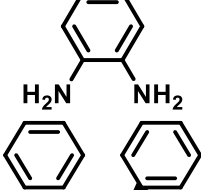
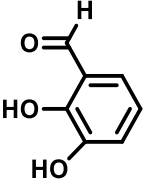
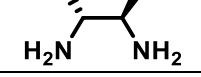
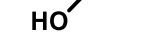


Figure 3.1: Reaction scheme for the synthesis of nickel Schiff base complex (2).

The desired nickel Schiff base complexes were obtained as microcrystalline powders in good purity and yields (Table 3.1), except for complex (5), which was contaminated with an excess of free Schiff base ligand. Therefore, it was purified via crystallisation from MeOH/DMSO before being used as the starting material for preparing the corresponding alkylated complex.

The structures of all the synthesized nickel Schiff base complexes were confirmed by using MS, ¹H NMR and ¹³C NMR spectral data. Further support for the structures of some of the complexes was provided by X-ray crystallography, while the purity of the complexes was further assured by elemental analysis data.

Table 3.1: Yields of hydroxylated nickel Schiff base complexes.

Nickel complex	Structure of diamine	Structure of dihydroxybenzaldehyde	Yield (%)
(1)			92
(2)			98
(3)			79
(4)			80
(5)			68
(6)			97

Routine 1-dimensional ^1H and ^{13}C NMR spectra were not sufficient to fully assign the structures of complexes (1)-(6). Therefore, 2D techniques including COSY (Correlation Spectroscopy), NOESY (Nuclear Overhauser Effect Spectroscopy), HSQC (Heteronuclear Single-Quantum Correlation) and HMBC (Heteronuclear Multiple-Bond Correlation) experiments were employed. The approach taken to assigning the NMR spectra of the hydroxylated nickel Schiff base complexes is discussed below, using complexes (2) and (4) as examples. The same process was applied in order to assign the NMR spectra of all the other hydroxylated complexes.

The proton resonances in the ^1H NMR spectra were assigned on the basis of their chemical shifts, integration, multiplicity and coupling constants. For example, the ^1H NMR spectrum of the Schiff base complex (2) (Figure 3.2)

exhibited three singlets at 8.82, 8.70 and 6.91 ppm which integrate to two hydrogen atoms each. As it was expected that the -OH group would give rise to a very deshielded singlet, the resonance at 8.82 ppm was tentatively assigned to these protons.

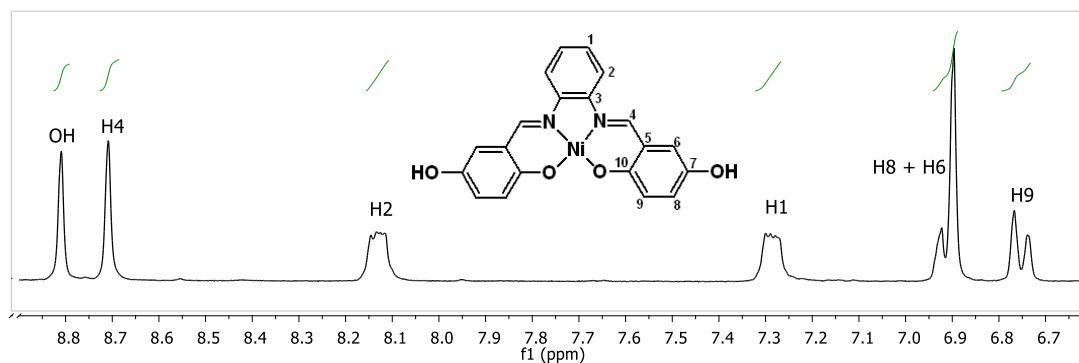


Figure 3.2: ¹H NMR spectrum of complex (2).

In addition, since imine groups are electron withdrawing, their protons are also found at relatively high chemical shifts. Therefore, the singlet at 8.70 ppm was tentatively assigned to the -N=CH protons (H4). The asymmetric doublet centred at 6.72 ppm appears to be half of an AB pattern arising from coupled protons with similar chemical shifts. The other half of the AB pattern is present at 6.91 ppm, but has one of its two resonances obscured by overlap with another, larger singlet. The AB pattern is tentatively assigned to H8 and H9, while the most likely assignment for the overlapping singlet is H6. Evidence for these assignments is provided by the similarity of the chemical shifts for H6, H8 and H9 in the spectrum of (2), with that of the corresponding hydrogen atoms in the starting material, 2,5-dihydroxybenzaldehyde. Similar reasoning led to the conclusion that the two characteristic multiples at 7.29 and 8.13 ppm should be assigned to H1 and H2, respectively. COSY and

NOESY spectra were then obtained to provide support for the above assignments as well as complete the identification of resonances to individual protons in situations where ambiguity remained, e.g. (H1/H2) and (H6/H8/H9).

COSY NMR spectra contain cross peaks owing to through-bond coupling interactions between pairs of protons which are two or three bonds apart. For example, the COSY spectrum of complex (**2**) (Figure 3.3a) shows two strong sets of cross-peaks associated with resonances at 7.29 and 8.13 ppm, consistent with their assignment to H1 and H2. Additional cross-peaks are present for the AB pattern of signals at 6.72 and 6.91 ppm arising from H8 and H9, as expected. However, COSY is not capable of allowing definitive assignment of the individual protons within each of the above pairs of resonances. Therefore a NOESY spectrum was acquired to obtain further information and complete the assignment.

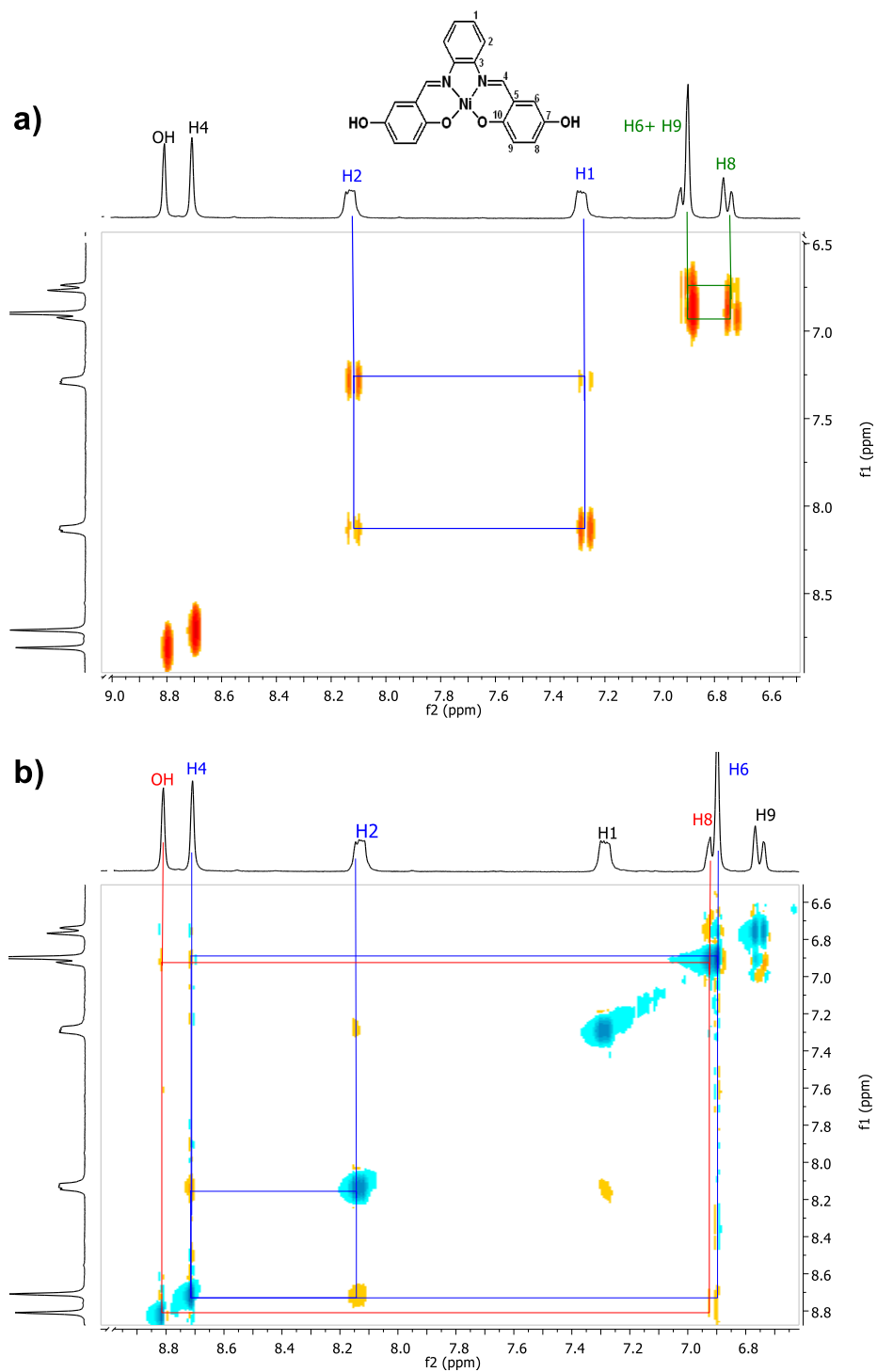


Figure 3.3: a) COSY spectrum of complex (2); b) NOESY spectrum of complex (2). Selected key correlations are highlighted.

NOESY is similar to COSY in that it examines the interactions between protons in close proximity to each other within the structure of a molecule.

However, NOESY identifies pairs of protons that are located close to each other through space, even though they may be several bonds apart. The NOESY spectrum of complex **(2)** (Figure 3.3b) shows two strong sets of couplings involving the imine proton (H4). The first of these also involves the resonance at 8.13 ppm, allowing it to be identified definitively as H2, and the signal at 7.29 ppm to H1. The second set of cross peaks involved the overlapping set of resonances at 6.90 ppm. This provided support for assigning the intense singlet at this chemical shift to H6. Another, weaker correlation can be observed between the -OH resonance at 8.82 ppm and that at 6.92 ppm. The latter was therefore assigned to H8. Additional cross peaks arising from interactions between H1 and H2, as well as H8 and H9, are also present in the NOESY spectrum.

The ^{13}C NMR spectrum of complex **(2)** (Figure 3.4a) shows ten resonances which corresponds to the number of distinct carbon environments expected for this complex. Since the ^1H NMR spectrum of **(2)** had now been fully assigned, a HSQC spectrum was obtained in an effort to assign each of the resonances in the ^{13}C NMR spectrum. The HSQC spectrum in Figure 3.4b shows correlations between signals in the ^{13}C NMR spectrum at 115.15, 116.44, 121.07, 127.25, 127.57 and 155.71 ppm, and individual resonances in the proton spectrum. This enabled the corresponding ^{13}C NMR resonances to be readily assigned, leaving a further four ^{13}C signals to still be attributed to specific carbon atoms. The latter four resonances did not show any cross peaks in the HSQC spectrum as they are all due to quaternary carbon atoms. These were then assigned based on their chemical shifts. Initially the most upfield of these signals at 119.51 ppm was assigned

to C5, as it is the only quaternary carbon not directly bound to an O or N atom. The signal at 142.81 ppm was then assigned to C3 owing to its proximity to the imine group, while the two other signals at 146.78 and 160.80 ppm were assigned to C7 and C10, respectively. The latter signal is the most deshielded of all ten resonances owing to being directly attached to an electronegative oxygen atom, as well as in close proximity to the nickel cation.

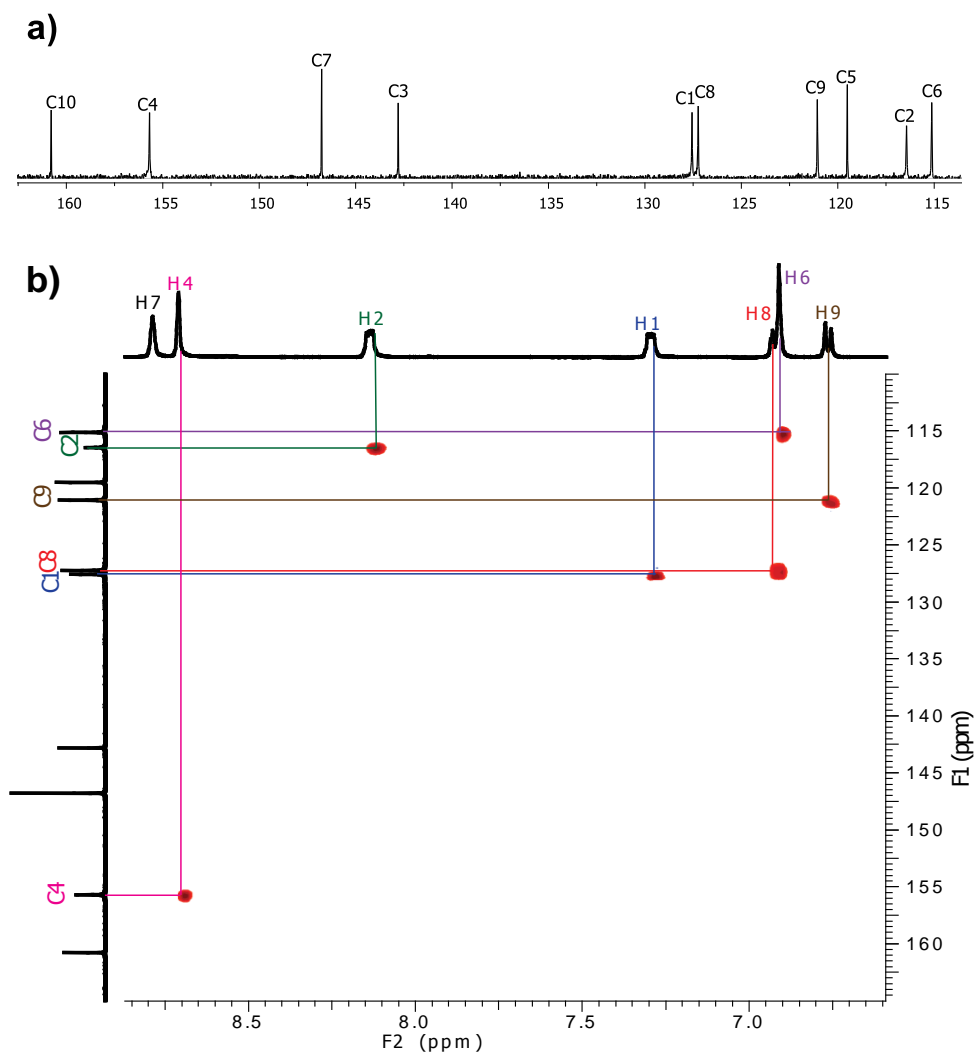


Figure 3.4: a) ^{13}C NMR spectrum of complex (2); b) HSQC spectrum of complex (2), with C-H correlations highlighted.

The NMR spectra of complex (4) were fully assigned using a similar approach to that used for (2). The ^1H NMR spectrum of this complex is shown in Figure 3.5a, together with an expansion of the aromatic region, for clarity.

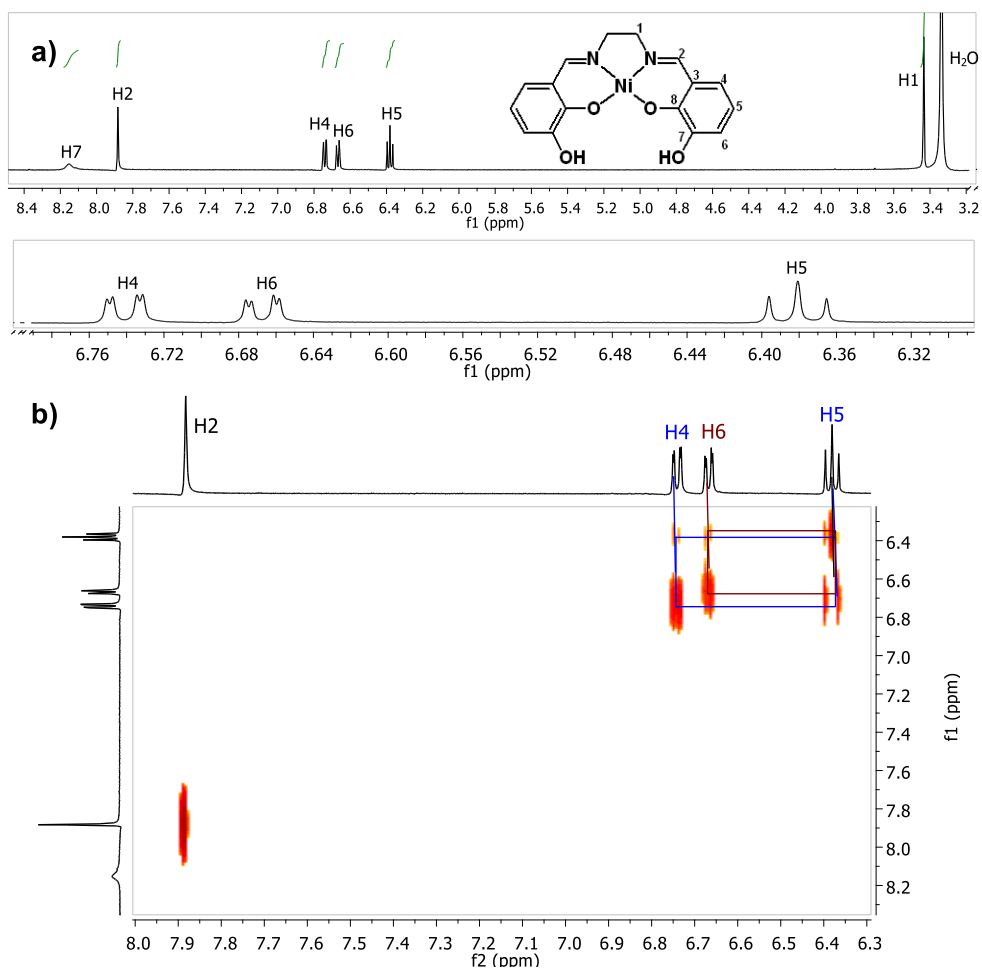


Figure 3.5: a) ^1H NMR spectrum of complex (4); b) COSY spectrum of complex (4). Key correlations are highlighted.

Based on their characteristic chemical shifts, the upfield singlet at 3.43 ppm was assigned to the aliphatic protons H1, whilst the broad singlet at 8.16 ppm was assigned to the OH protons. There is also a characteristic downfield singlet present at 7.88 ppm, which was assigned to the imine proton (H2). The triplet at 6.38 ppm was assigned to H5, as it was expected to show two

very similar couplings to H4 and H6. The latter protons gave rise to the two doublets of doublets at 6.67 and 6.74 ppm, although at this stage it was not possible to definitively assign these multiplets to individual protons. This required the use of COSY and NOESY experiments. The COSY spectrum of complex (4) (Figure 3.5b) showed, as expected, two strong sets of couplings involving H5, one to H4 and the other to H6. This provided further support for the assignment of H5 made earlier; however, it still did not allow definitive assignment of specific ^1H resonances to H4 and H6. A strong coupling was observed between the signal at 6.74 ppm, and that assigned to H2 in the NOESY spectrum of complex (4) (Figure 3.6). As this coupling was expected between H4 and H2 owing to their close proximity through space, the signal at 6.74 ppm was then assigned to H4. This in turn now allowed the other doublet of doublets at 6.67 ppm to be assigned to H6.

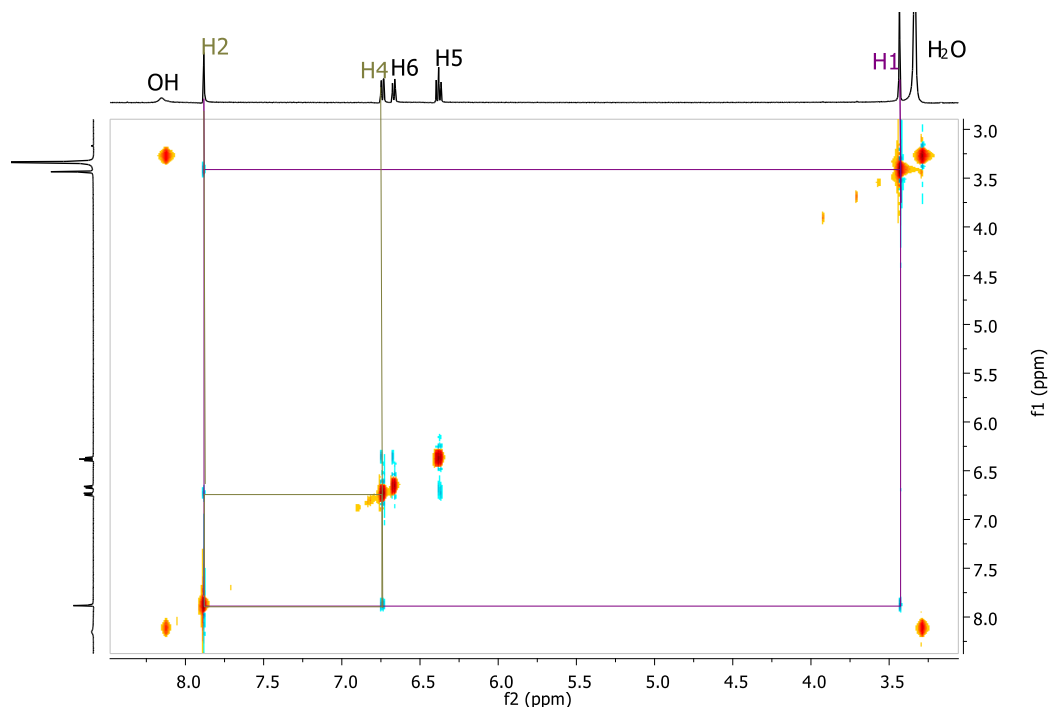


Figure 3.6: NOESY spectrum of complex (4). Key correlations are highlighted.

The ^{13}C NMR spectrum of complex (4) (Figure 3.7a) showed the expected number of signals for this complex.

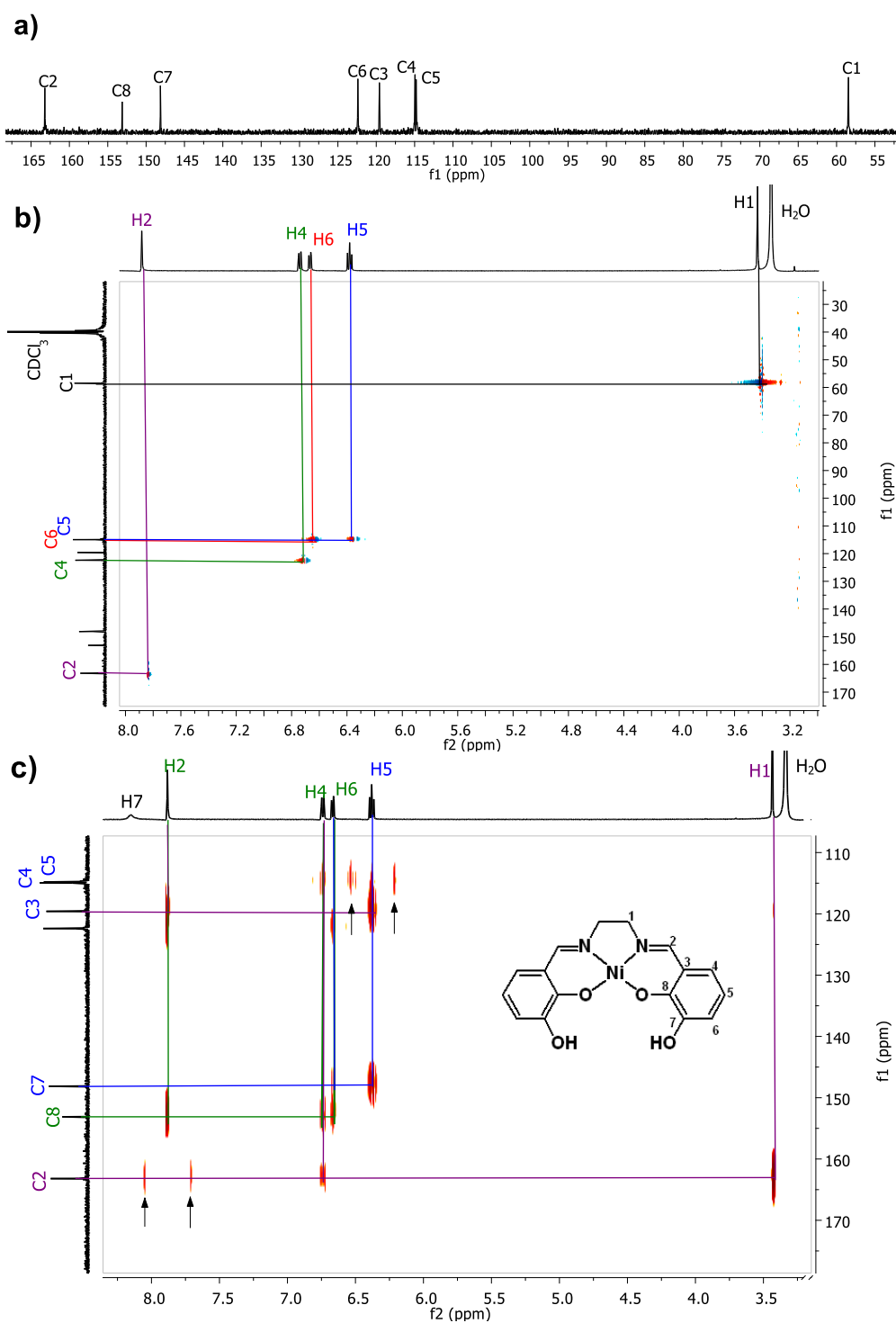


Figure 3.7: a) ^{13}C spectrum of complex (4); b) HSQC spectrum of complex (4); and c) HMBC spectrum of complex (4), with C-H correlations highlighted. Two artefacts in the HMBC spectrum are highlighted with arrows.

Again, a HSQC spectrum (Figure 3.7b) was used to assign those resonances arising from carbon signals with at least one directly bound hydrogen atom. By using this approach, resonances at 58.45, 114.81, 114.95, 122.40 and 163.2 ppm could be assigned to specific carbon atoms. The remaining carbon resonances at 119.60, 148.15 and 153.13 ppm were all therefore deduced to arise from quaternary carbon atoms, which do not show any cross-peaks in HSQC spectra. On this occasion, an HMBC spectrum (Figure 3.7c) was obtained in an effort to assign these signals. HMBC spectra reveal correlations between carbon and hydrogen nuclei which are typically separated by two or three bonds within a molecule, and may in some instances be separated by four or more bonds in conjugated systems.

The HMBC spectrum in Figure 3.7c shows cross peaks between the ^{13}C resonance at 163.21 ppm assigned to C2, and ^1H resonances previously assigned to H1 and H4. In addition, two sets of artefacts are present in the spectrum, one at lower field which is due to the one-bond correlation between C2 and H2, and another at higher field, which is due to the one-bond correlation between C5 and H5. Figure 3.7c also shows two or three cross peaks for each of the quaternary carbon signals identified above. Of these, the resonance at 119.60 ppm was tentatively assigned to C3 in view of its more shielded chemical shift, which is consistent with this carbon atom not being directly attached to a highly electronegative atom. Evidence supporting this assignment was provided by the two cross peaks in the HMBC spectrum involving the resonance at 119.60 ppm, and those from H2 and H5. These cross peaks were expected, as C3 is two bonds away from H2, and three bonds away from H5. While C8 is also expected to show a strong cross peak

with H2, it would not be expected to do so with H5 which is four bonds distant. In addition, C8 would be expected to give a less shielded resonance owing to its proximity to both Ni and O atoms. Therefore the ^{13}C resonance at 119.60 ppm was assigned to C3, despite the surprising absence of a cross peak with H4 in the HMBC spectrum. The ^{13}C resonance at 153.15 ppm was then assigned to C8, primarily on the basis of the observed cross peak with H2. In addition, this ^{13}C signal showed cross peaks with resonances from both H4 and H6. The remaining quaternary carbon resonance at 148.15 ppm was therefore assigned to C7, and as expected showed cross peaks with the resonances arising from protons H5 and H6.

3.3.2 Alkylated nickel Schiff base complexes

The nickel Schiff base complexes used for DNA binding studies were prepared by reacting the hydroxylated nickel Schiff base compounds with 1-(2-chloroethyl)piperidine hydrochloride in the presence of K_2CO_3 . This reaction was performed using DMF as the solvent, under an inert atmosphere of nitrogen gas. Figure 3.8 summarises the conditions used for these reactions by using the synthesis of complex **(8)** from **(2)** as an example.

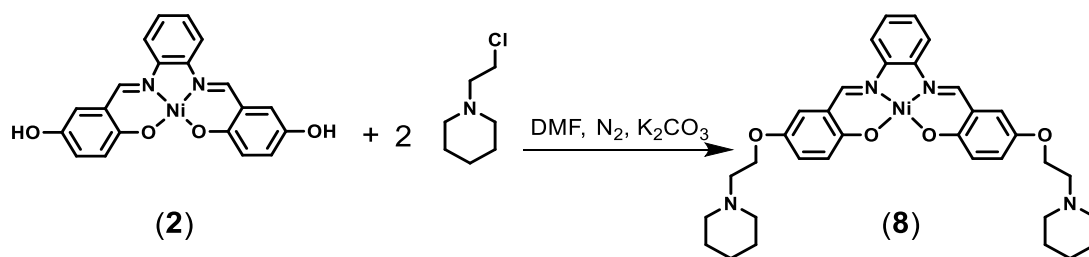

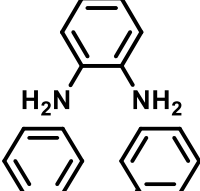
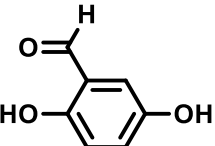
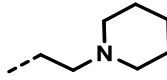
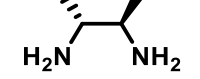

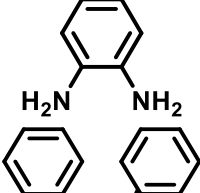
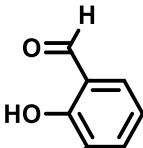
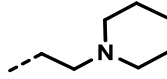
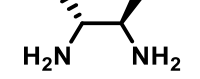


Figure 3.8: Reaction scheme for the synthesis of nickel Schiff base complex (8).

The alkylated nickel Schiff base complexes were synthesised according to a modified literature method.¹⁵⁴ In all cases with the exception of the procedure for preparing complex (12), the concentration of the hydroxylated precursor complex was 0.03 mM, instead of the 0.01 mM stated in the literature method. In addition, although the desired alkylated nickel Schiff base complexes precipitated as a coloured solid over the course of reaction, they were not isolated immediately by filtration. Instead all of the DMF present in the reaction mixture was removed by applying heat under vacuum, and any unreacted starting material was subsequently removed by washing with water several times. It was found that this isolation procedure improved the overall yield of each of the complexes. The yields obtained for each of the alkylated complexes synthesised are summarised in Table 3.2.

Table 3.2: Yields of alkylated nickel Schiff base complexes.

Nickel complex	Structure of diamine	Structure of diamine	Structure of alkyl group	Yield (%)
(7)				63
(8)				53
(9)				-
(10)				53
(11)				26
(12)				46

The structure of all alkylated nickel complexes was confirmed using ESI-MS as well as a suite of 1D and 2D ^1H and ^{13}C NMR spectroscopic techniques. The procedure employed to fully assign the ^1H and ^{13}C NMR spectra of a typical complex is described below, using **(8)** as an example.

Figure 3.9 illustrates the full ^1H NMR spectrum of complex **(8)**, with expansions of the upfield and downfield regions of the spectrum showing the assignments of individual protons.

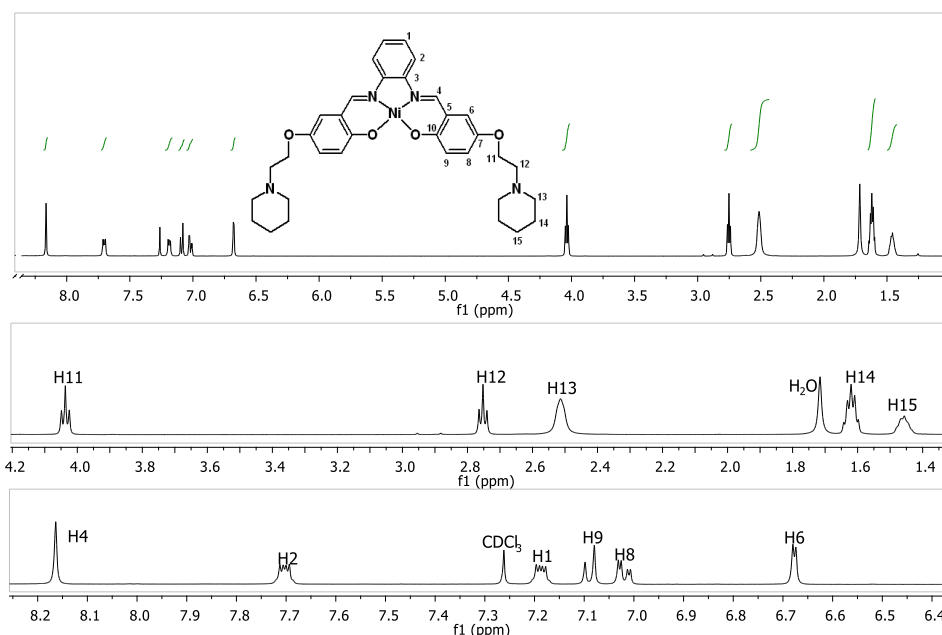


Figure 3.9: ^1H NMR spectrum of complex (**8**).

In the aromatic region of the spectrum, two distinctive multiplets are present at 7.19 and 7.70 ppm, which strongly resemble signals assigned to H1 and H2 in the spectra of related complexes also containing the phenylenediamine unit. The COSY spectrum of (**8**) (Figure 3.10) shows that the above two multiplets are coupled to each other, but to no other ^1H resonances, providing support for the same assignment in the case of the current complex. Identification of which of the two resonances should be assigned to H1, and which to H2, was then achieved using NOESY spectroscopy. The key to this assignment was knowing that the most deshielded ^1H resonance in the entire spectrum was assigned to the imine hydrogen atom, H4. Inspection of the NOESY spectrum (Figure 3.11) shows a clear cross peak involving H4 and the resonance at 7.70 ppm, identifying the latter as H2, and therefore also enabling the assignment of the ^1H resonance at 7.19 ppm to H1.

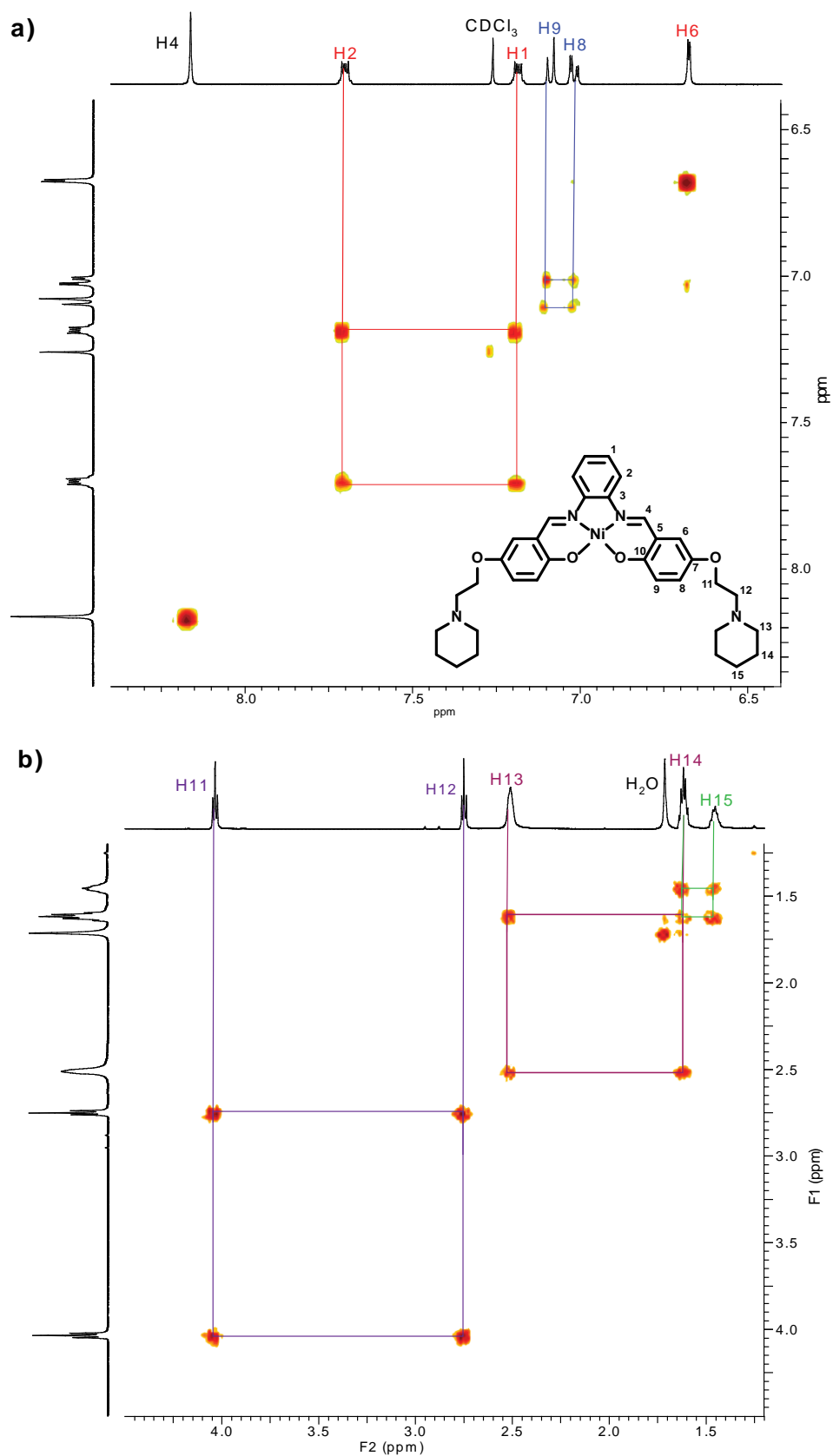


Figure 3.10: a) Expanded view of the aromatic region of the COSY spectrum of complex (**8**); b) Expanded view of the aliphatic portion of the COSY spectrum of complex (**8**) selected key correlations are highlighted.

Also apparent in the aromatic region of the ^1H NMR spectrum is a set of three multiplets shown by the COSY spectrum to be due to a set of three coupled protons. The first of these is a doublet at 6.67 ppm with a coupling constant of 2.6 Hz, which is indicative of *meta* proton coupling, as expected for H6 owing to the effect of H8 located four bonds away. The remaining signals strongly resemble an AB pattern, in which the two upfield resonances centred at 7.02 ppm have been further split into doublets with the same coupling constant as that found for H6. These upfield signals were therefore assigned to H8. The larger coupling for H8 was equal to 9.4 Hz, which is as expected identical to that observed for the other two resonances in this AB pattern, centred at 7.09 ppm, which were therefore assigned to H9. These assignments were supported by the pattern of cross peaks observed for this group of three multiplets in the COSY spectrum.

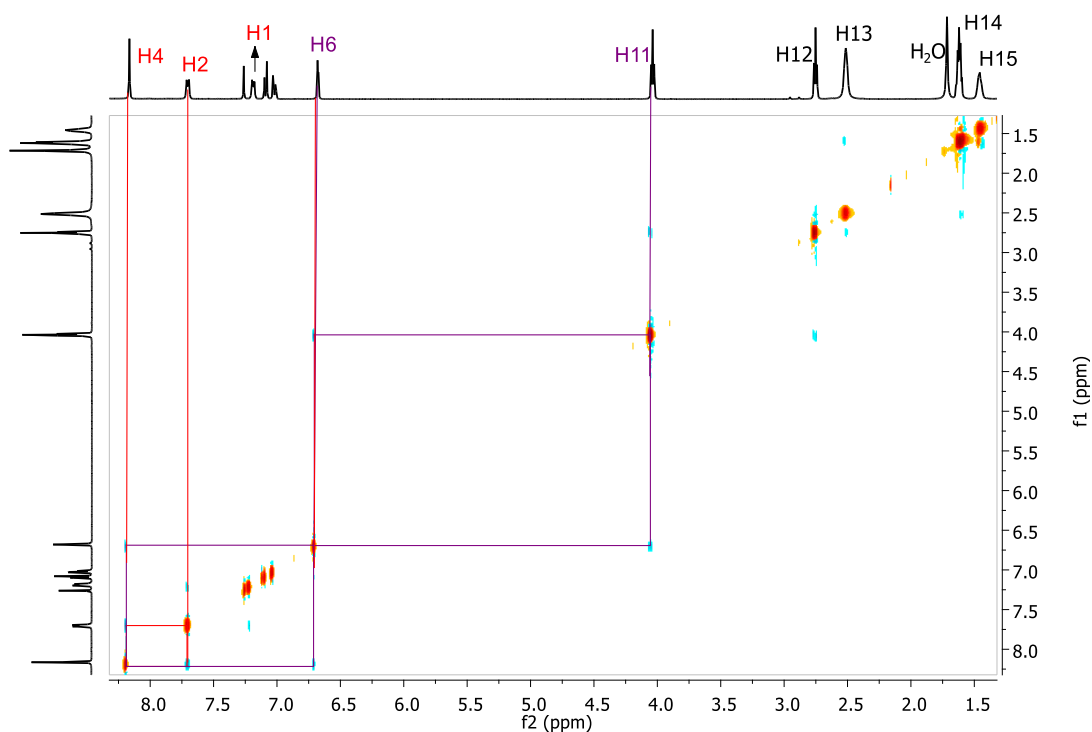


Figure 3.11: NOESY spectrum of complex (8), with key correlations highlighted.

Because of their aliphatic character, the proton signals for the piperidine groups all appear in the upfield region of the ^1H NMR spectrum. The two characteristic triplets at 2.75 and 4.04 ppm integrate to four protons each. Therefore, based on their chemical shifts, integration and splitting pattern, they were assigned to H12 and H11, respectively. Evidence in support of these specific assignments was provided by the NOESY spectrum (Figure 3.11), which showed a clear cross peak between H6 and the triplet at 4.04 ppm. This indicates that the latter multiplet must arise from H11, as it is the nearer of the two methylene groups to H6. This left three resonances in the ^1H spectrum at 1.50, 1.60 and 2.51 ppm, which required assignment. The first of these could be readily assigned to H15, owing to its smaller integration compared to that of the two other resonances, as well its chemical shift. The multiplet at 1.60 ppm was coupled to each of the other two multiplets arising from the piperidine group in the COSY spectrum, allowing it to be assigned to H14, and leaving the last broad signal at 2.51 ppm to be assigned to H13. This signal was the most deshielded of the ^1H resonance arising from the piperidine group, owing to the proximity of H13 to an electronegative nitrogen atom.

The ^{13}C NMR spectrum of complex (**8**) is presented in Figure 3.12a, and showed the expected number of signals. An HSQC spectrum was also obtained to facilitate assignment of resonances due to carbon atoms with at least one hydrogen attached. For example, the ^{13}C signals at 24.35, 26.09 and 55.23 ppm could be assigned to C15, C14 and C13, respectively.

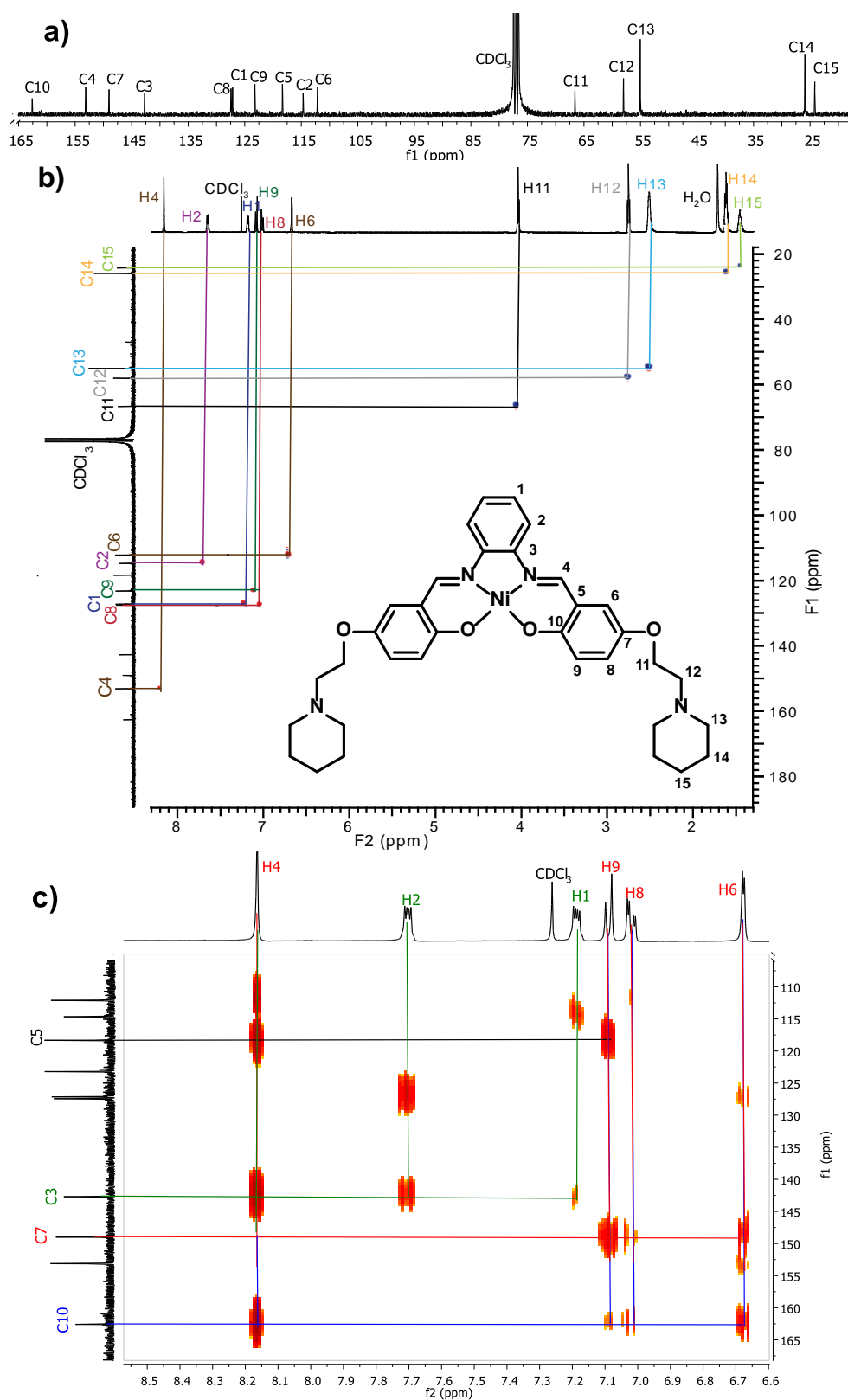


Figure 3.12: a) ^{13}C NMR spectrum of complex (8); b) HSQC spectrum of complex (8); c) HMBC spectrum of complex (8), with C-H correlations highlighted.

In addition, the two carbon resonances at 127.92 and 127.59 ppm show cross peaks with proton resonances which were assigned to H1 and H8, respectively, thereby allowing the assignment of the former ^{13}C signals to C1 and C8. Some carbon resonances did not exhibit any HSQC cross peaks owing to the fact they arise from quaternary carbon atoms, and therefore required a HMBC spectrum in order to facilitate their assignment. The HMBC spectrum in Figure 3.12c shows two or three cross peaks for each of the four carbon resonances identified as arising from quaternary carbon atoms. Of these, the most shielded is at 118.56 ppm. This suggests that this resonance should be assigned to C5, as it is the only one of the four quaternary carbon atoms not directly bonded to an O or N atom. Evidence in support of this assignment is provided by the presence of cross peaks in the HMBC spectrum involving H4, which is located only two bonds from C5, and H9. Perhaps surprisingly, there was no cross peak involving C5 and H6, which are also only two bonds distant. The next most shielded quaternary carbon resonance is present at 142.89 ppm, and shows cross peaks in the HMBC spectrum with the ^1H signals arising from H2 and H4. Such cross peaks were expected for C3, as it is two bonds away from H2, and three bonds away from H4. Therefore the signal at 142.89 ppm was assigned to C3. The two remaining quaternary carbon resonances are at 149.18 and 162.80 ppm. The first of these showed cross peaks in the HMBC spectrum with H6, H8 and H9, while for the second cross peaks involving H4, H6, H8 and H9 were observed. These two carbon resonances were assigned to C7 and C10, respectively. The observation of a cross peak with H4 was strong evidence in favour of assigning the ^{13}C resonance at 162.80 ppm to C10, as this

hydrogen atom is located three bonds away from C10, but is four bonds away from C7. Therefore a strong cross peak would not be expected for C7 and H4.

The fully assigned ^1H NMR spectrum of complex (**10**) is presented in Figure 3.13, with expansions of both the aromatic and aliphatic regions also shown for clarity. The procedure followed to assign the proton resonances present in the aromatic portion of the spectrum was identical to that used for assigning signals in the corresponding region of the spectrum of (**4**) (Section 3.3.1), and will therefore not be discussed here. In addition, the assignment of resonances in the aliphatic region of the spectrum was accomplished using a similar approach to that followed for complex (**8**), which also contains two piperidine groups.

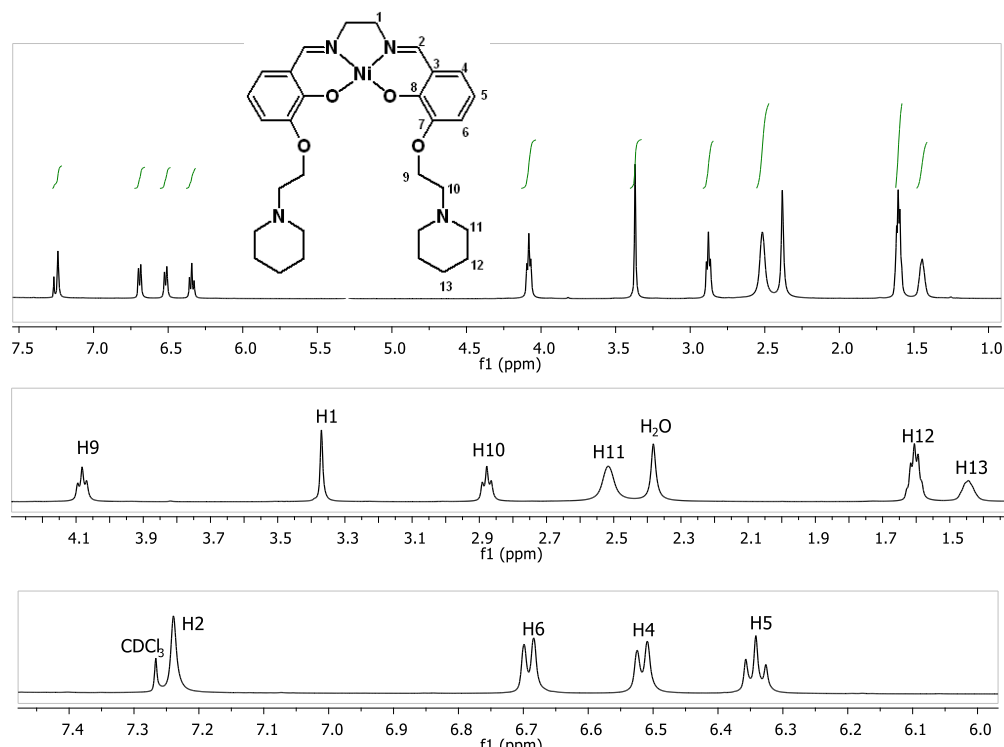


Figure 3.13: ^1H NMR spectrum of complex (**10**).

The remaining assignments shown in Figure 3.13 were made with the support of information provided by the COSY and NOESY spectra illustrated in Figure 3.14 and Figure 3.15, respectively. Both of the latter spectra contained cross peaks reflecting the existence of similar coupling patterns to those observed in the corresponding spectra of complexes containing similar structural moieties to (10). For example, the aromatic region of the ^1H and COSY NMR spectra of (4) and (10) both contain two doublets and a triplet attributable to H4, H5 and H6.

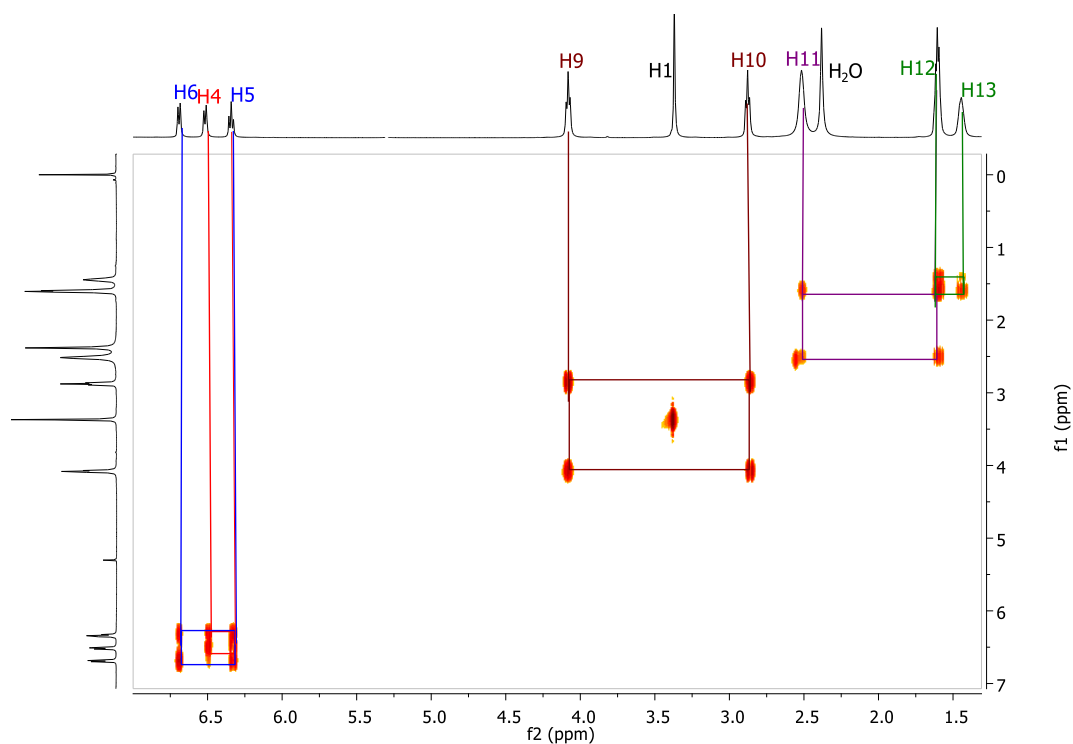


Figure 3.14: COSY spectrum of complex (10). Key correlations are highlighted.

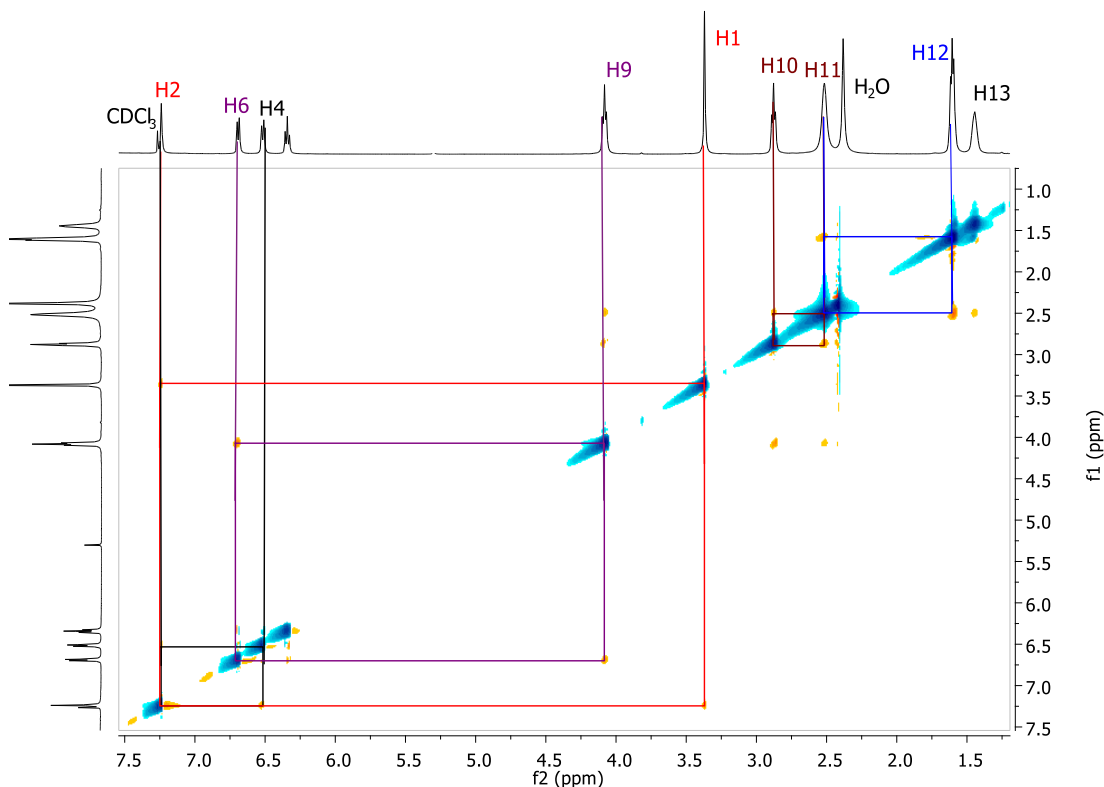


Figure 3.15: NOESY spectrum of complex **(10)**. Key correlations are highlighted.

Figure 3.16a presents the ^{13}C NMR spectrum of complex **(10)**, which contained the expected number of carbon signals. Assignment of the carbon signals in the aromatic region of the spectrum was based on a comparison of their chemical shifts to those of ^{13}C resonances in the spectrum of complex **(4)**, while the carbon signals in the aliphatic portion were assigned after comparing their chemical shifts to those of ^{13}C resonances in the spectrum of complex **(8)**. These assignments were supported by analysis of the HSQC spectrum of **(10)** shown in Figure 3.16b. For example, the presence of cross peaks for ^1H resonances assigned to H10 and H1, with the two close carbon signals at 57.61 and 58.54 ppm, allowed the latter resonances to be assigned to C10 and C1, respectively. The ^{13}C NMR resonance at 124.14

ppm was similarly assigned to C4 owing to the presence of a cross peak involving H4. By using the remaining HSQC cross-peaks, all the protonated carbon resonances were subsequently assigned.

Long range C-H correlations were used to assign the remaining signals in the ^{13}C spectrum. The HMBC spectrum in Figure 3.16c shows cross peaks which involved the carbon resonance at 120.18 ppm, and those from H2 and H5. This enabled the ^{13}C resonance to be assigned to C3, as it is positioned two bonds away from H2, and three bonds away from H5. In addition, the ^{13}C resonance at 149.95 ppm exhibited cross peaks with resonances from H5, H6 and H9. Consequently this ^{13}C resonance was assigned to C7, allowing the only remaining unassigned carbon resonance, at 155.83 ppm, to be assigned to C8. Consistent with this assignment, the spectrum showed cross peaks involving this ^{13}C resonance and those from H2, H4 and H6.

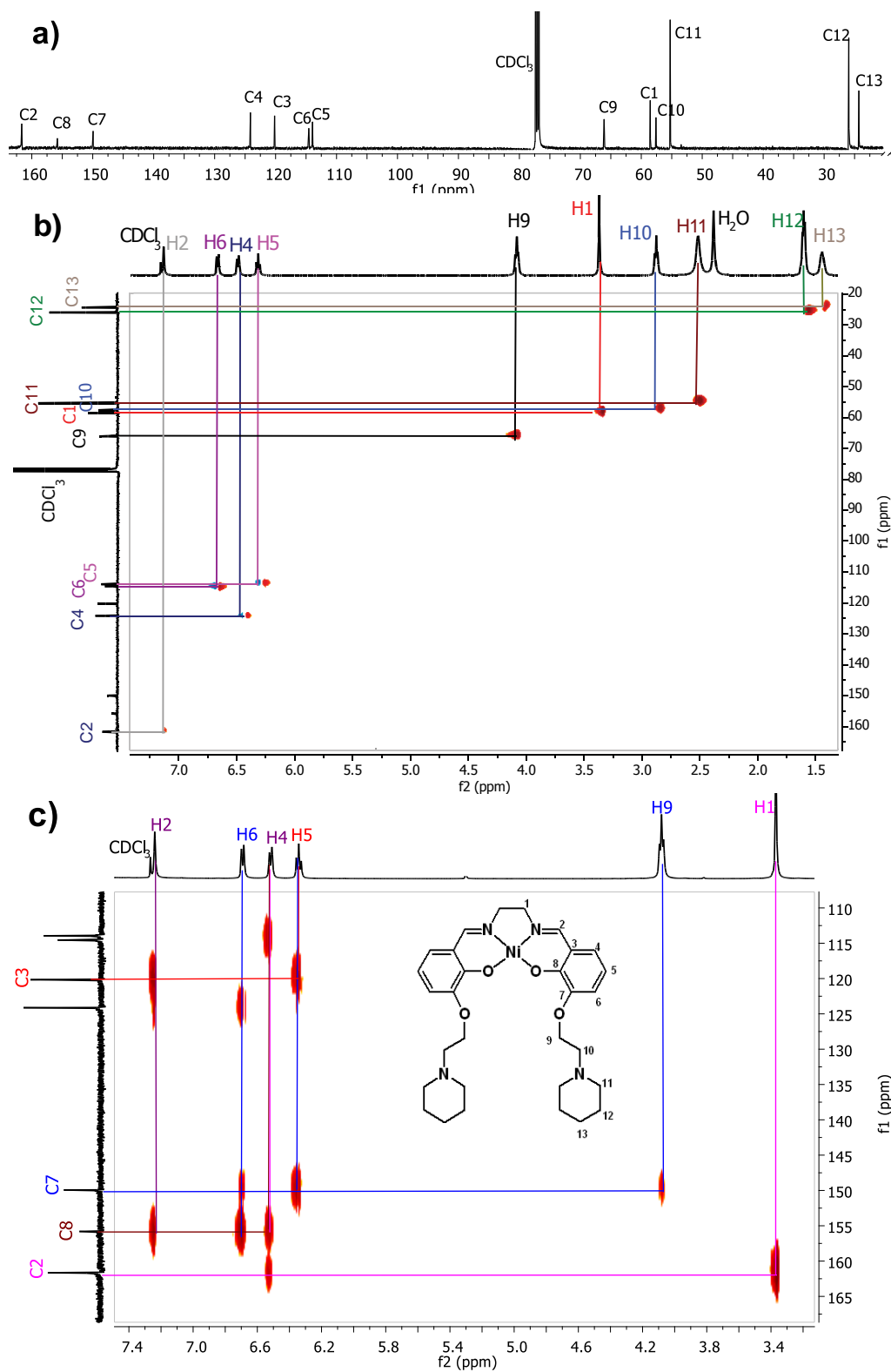


Figure 3.16: a) The ^{13}C NMR spectrum of complex (10); b) HSQC spectrum of complex (10); c) HMBC spectrum of complex (10). Key correlations are highlighted.

3.4 Crystallographic Data

Single-crystal X-ray diffraction analyses and structure determinations were performed by Dr. Anthony Willis, of the Research School of Chemistry, Australian National University. Crystals of complex (5) suitable for single-crystal X-ray analysis were obtained by slow evaporation from a methanol/DMSO solvent mixture. Crystals of (8) were obtained by slow diffusion of diethyl ether into a solution of (8) in DCM. Crystals of (10) were obtained by slow evaporation from a DCM/ petroleum spirit (1:3) solvent mixture. ORTEPs showing the solid state structures of these complexes and the numbering systems for the non-hydrogen atoms, are presented in Figure 3.17. Details of collected crystallographic data and structural refinements for the three complexes are summarised in Table 3.3.

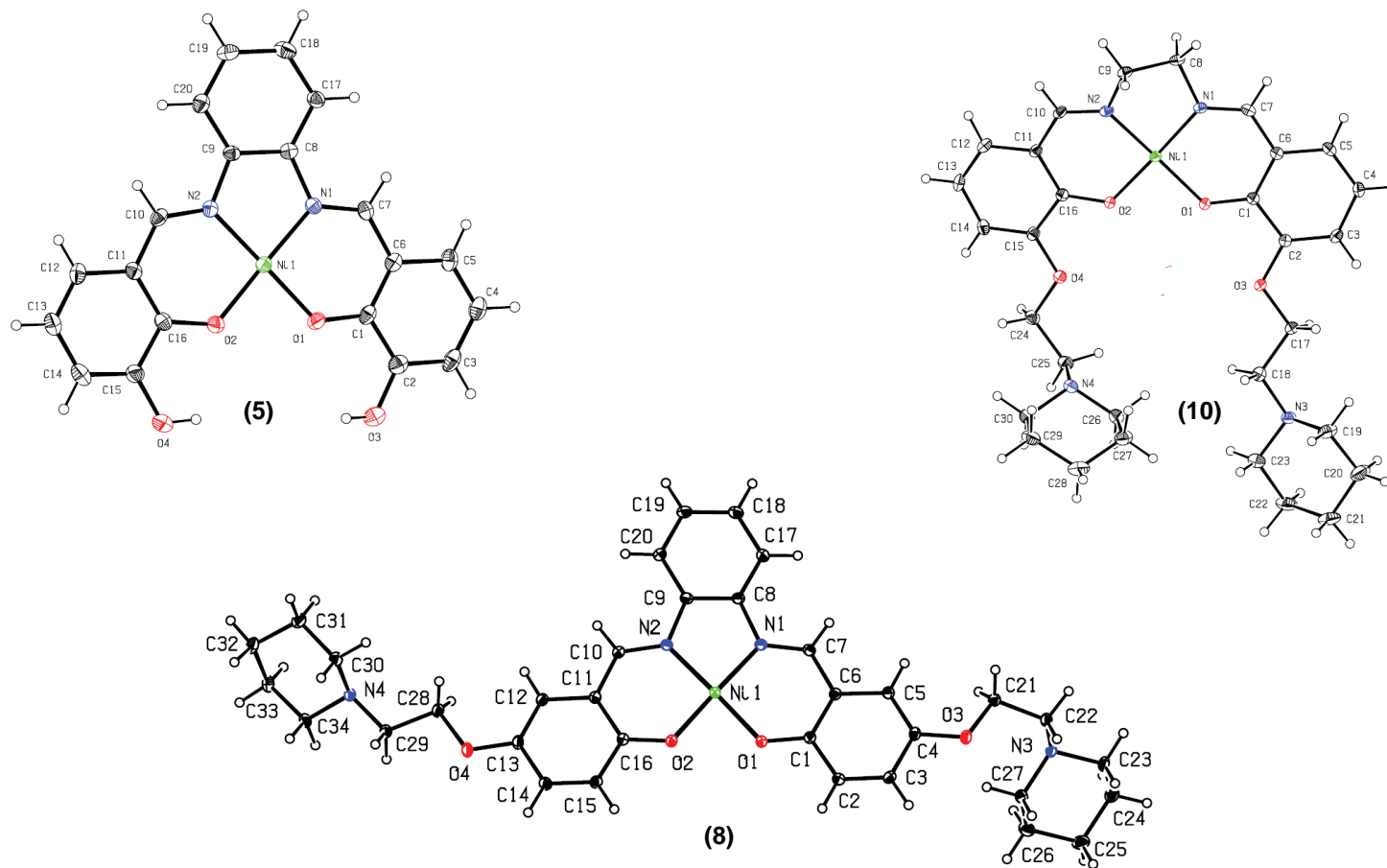


Figure 3.17: ORTEPs for the molecular structures of complexes (5), (8) and (10).

Table 3.3: Summary of crystallographic data for complexes **(5)**, **(8)** and **(10)**.

	(5)	(8)	(10)
Formula	(C ₂₀ H ₁₄ N ₂ NiO ₄) ₃ ·H ₂ O	C ₃₄ H ₄₀ N ₄ NiO ₄ ·H ₂ O	C ₃₀ H ₄₀ N ₄ NiO ₄ ·H ₂ O
<i>M</i>	1233.18	645.44	597.40
Crystal system	Triclinic	Triclinic	Monoclinic
Space group	<i>P</i> -1	<i>P</i> -1	<i>P</i> 2 ₁ / <i>n</i>
<i>a</i> (Å)	12.2000(4)	8.1440 (1)	10.1567(3)
<i>b</i> (Å)	15.0224(5)	11.8552 (2)	8.5596(4)
<i>c</i> (Å)	15.4129(6)	15.6018 (3)	33.2575 (13)
α (°)	74.102(3)	93.0064 (17)	-
β (°)	71.068 (3)	90.4792 (16)	98.602 (3)
γ (°)	69.971(3)	90.5565(15)	-
<i>V</i> (Å ³)	2467.88(16)	1504.13 (4)	2858.79(19)
<i>D</i> _x (Mg m ⁻³)	1.659	1.425	1.388
<i>Z</i>	2	2	4
Number of unique reflections	12283	8259	8148
Refinement	R[F ² > 2σ (F ²)] = 0.058 wR(F ²) = 0.106	0.030 0.074	0.060 0.106

It was observed that the nickel ion in all three crystal structures has adopted a square planar coordination geometry. All bond lengths and angles involving the central nickel ions (Table 3.4) are consistent with standard values.^{155,156} The arrangement of the phenylenediamine moieties in **(5)** and **(8)** results in N2-C9-C8-N1 torsion angles of 4.21(5)° and -2.42(15)°, respectively. In contrast, the arrangement of the ethylenediamine moiety in complex **(10)** results in the same torsion angle increasing to -38.02 (3)°.

Table 3.4: Selected bond lengths (Å) and angles (°) for nickel Schiff base complexes.

Bonds	(5)	(8)	(10)
Ni-O1	1.847(2)	1.8320 (9)	1.8674(17)
Ni-O2	1.843(3)	1.8354 (9)	1.8717(19)
Ni-N1	1.855(3)	1.8557 (11)	1.855(2)
Ni-N2	1.862(3)	1.8512 (10)	1.855(2)
O1-Ni-O2	83.82(11)	83.07 (4)	86.49(8)
O2-Ni-N2	95.12(12)	95.44 (4)	94.17(9)
O1-Ni-N2	178.25(12)	177.84 (4)	175.35(9)
O2-Ni-N1	178.58(12)	177.81 (4)	175.42(9)
O1-Ni-N1	94.76(12)	95.17 (4)	94.55(9)
N1-Ni-N2	86.29(13)	86.35 (5)	85.16(10)

Complex **(5)** crystallised in a triclinic crystal system with space group *P*-1. Three molecules of the Schiff base complex called **(5A)**, **(5B)** and **(5C)** were present, with the central nickel ions labelled Ni1, Ni2 and Ni3, respectively. One water molecule was also present in the asymmetric unit. Both oxygen atoms coordinated to the nickel atom of **(5A)** were participating in hydrogen

bonding interactions with the oxygen atom on the lattice water molecule, with the distances for O1-O13 and O2-O13 being 2.83 (6) and 2.91 (6) Å, respectively. In addition, both the phenolic and the coordinated oxygen atoms of the neighbouring (**5B**) and (**5C**) molecules were sufficiently close to one another to enable intermolecular O–H...O hydrogen bonds to form, with the distances for H11-O6, H12-O6, H7-O9, and H8-O9 being 2.14, 2.09, 2.11 and 2.10 Å, respectively.

In the crystal lattice of (**5**) (Figure 3.18), molecules (**5A**) and (**5B**) are arranged in a twisted co-facial manner which results in close contacts between carbon atoms on the benzylic and phenylenediamine moieties of separate nickel molecules. As a result the bond distances for the C6-C31, C10-C38, C11-C39, and C18-C26 contacts involving carbon atoms on molecules (**5A**) and (**5B**) were 3.39, 3.31, 3.34, and 3.35 Å, respectively (Figure 3.18a). Molecules (**5B**) and (**5C**) assemble in such a way to produce short contacts between the benzylic carbons on one molecule, and the phenolic oxygens on the adjacent molecule. This results in distances for C36-O11, C36-O12, C41-O7 and C41-O8 equal to 3.35(5), 3.13(4), 3.27(4) and 3.38(5) Å, respectively. The most notable contact between (**5B**) and (**5C**) involved Ni3 and the phenolic oxygen O7, which were located 3.30 Å apart (Figure 3.18b). The only contact observed between complexes (**5A**) and (**5C**) was between the phenolic oxygen atom O11 on complex (**5A**) and the hydrogen atom H71, which is bonded to C7 on complex (**5C**), at a distance of 2.59 Å.

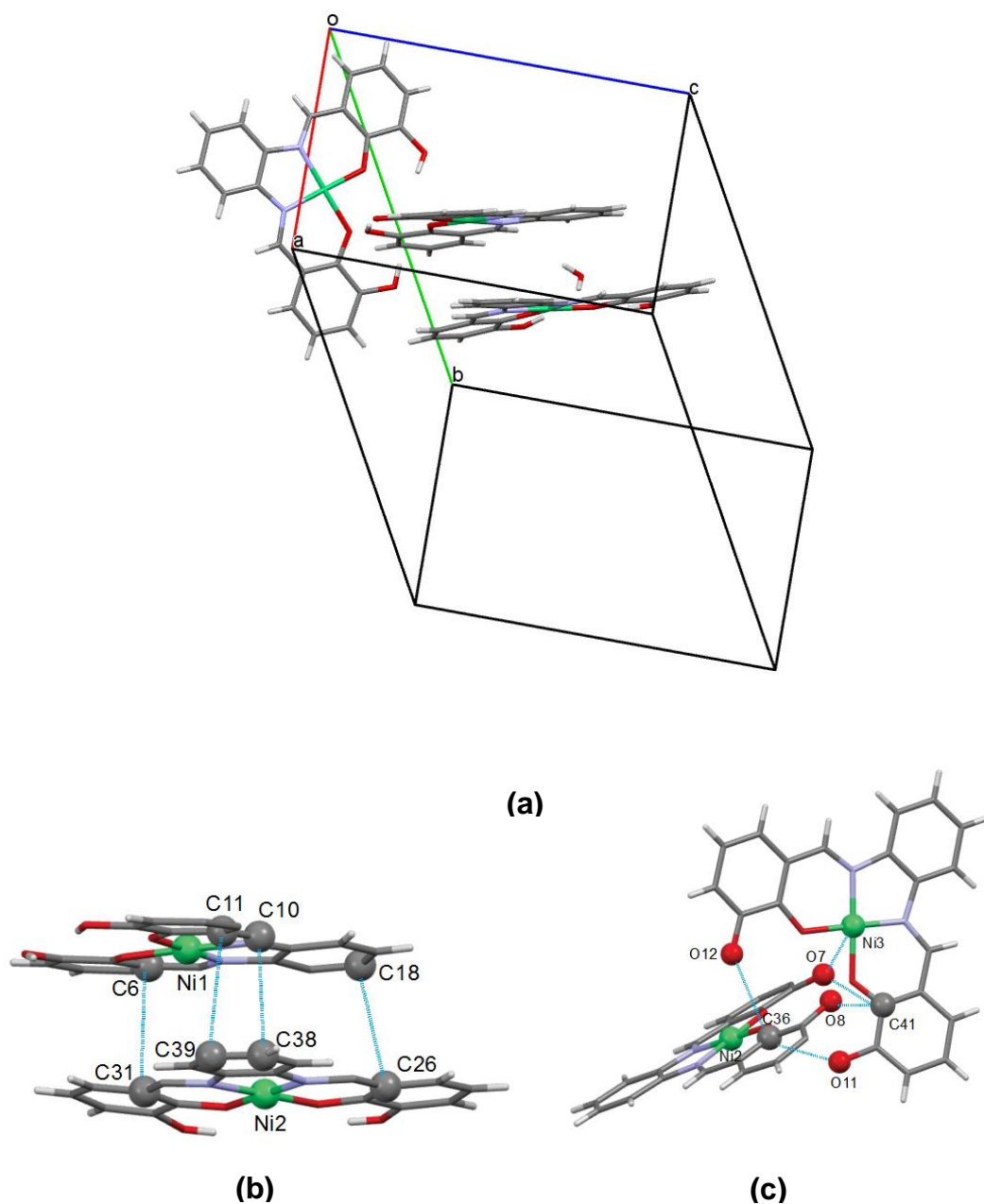


Figure 3.18: Different perspectives of the stacking of the three nickel complexes in the lattice of complex (**5**): a) all three nickel complexes in the crystal lattice; b) the short contacts between complexes (**5A**) and (**5B**); c) the short contacts between (**5B**) and (**5C**). Some hydrogen atoms were omitted for clarity.

Complex **(8)** also crystallised in the triclinic space group $P-1$, but with one metal complex and one water molecule in the asymmetric unit. There were hydrogen bonds between the oxygen atoms coordinated to the nickel ion, and the oxygen atom on the water molecule, with the distances for H1-O1 and H1-O2 being 2.21 (3) Å and 2.36 (3) Å, respectively. In contrast, complex **(10)** belongs to the monoclinic crystal system with the space group $P2_1/n$. One full metal complex and one H₂O molecule comprise the asymmetric unit of the structure of **(10)**. The oxygen atoms coordinated to the nickel ion and the phenolic oxygen atoms are involved in hydrogen bonding interactions with the hydrogen atoms of the lattice water molecules, with the distances for H1-O1, H1-O3, H2-O2 and H2-O4, being 2.36, 2.36, 2.49, and 2.31 Å, respectively.

In the crystal lattice of **(8)**, the two nickel Schiff base molecules possess a crystallographic inversion centre, and they are arranged in a slipped co-facial manner (Figure 3.19). The same arrangement has been previously reported in the crystal lattice of the complex N,N'-bis-4-(hydroxysalicylidine)meso-diphenylethylenediaminenickel(II).¹⁵⁶ The shortest intermolecular distance between the two molecules in the solid state structure of **(8)** is that between the nitrogen atom N1 (coordinated to the nickel ion) and carbon atom C16 on the benzylic moiety. These two atoms were located 3.27(16) Å apart.

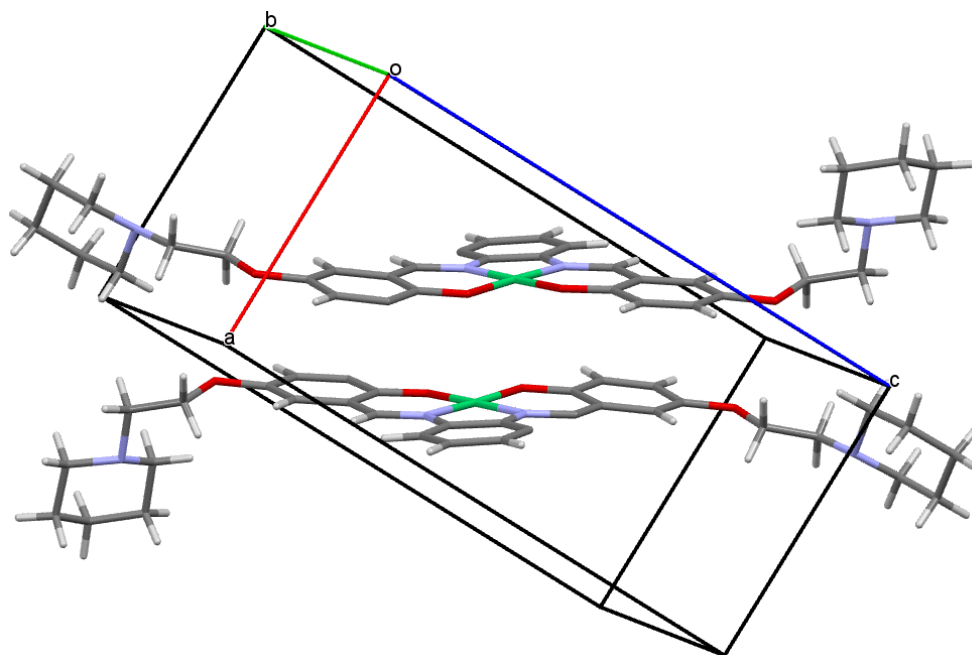


Figure 3.19: Perspective view of the stacking of pairs of complexes in the lattice of complex **(8)**.

The structure of complex **(10)** was distinctly bowed around the central coordination environment (Figure 3.20). As a consequence the six membered chelate rings coordinated to the nickel ion are not completely coplanar with each other. This is shown by the angle of 11.01° between the Ni1-O1-C1-C6-C7-N1 and Ni1-O2-C16-C11-C10-N2 planes. For comparison, the angles between the same planes in complexes **(5)** and **(8)** were only 0.57° and 2.21° , respectively.

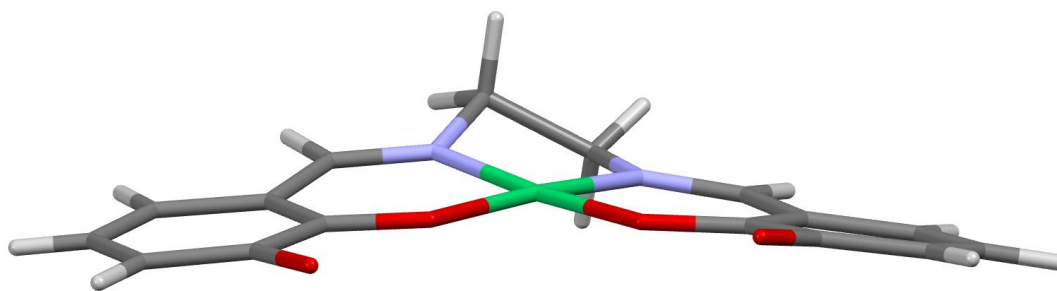


Figure 3.20: View of complex **(10)** highlighting the non co-planar arrangement of the six membered chelate rings around the nickel ion. The ethyl piperidine moieties were omitted for clarity.

Two molecules in the unit cell of complex **(10)** are related by a crystallographic inversion centre and assemble in a co-facial manner (Figure 3.21). The same arrangement was previously reported to be present in the solid state structure of the complex **(15)**, and results in the two nickel complexes sit neatly on top of one another ¹⁵⁶

This arrangement results in short contacts between the aliphatic carbon atom C9 of the ethylenediamine moiety and the two nickel-coordinated oxygen atoms O1 and O2 in the adjacent molecule. These pairs of atoms were found to be 3.28(3) and 3.27(3) Å, respectively apart. The shortest intermolecular distance between the two molecules is 3.19 Å between the two nickel ions.

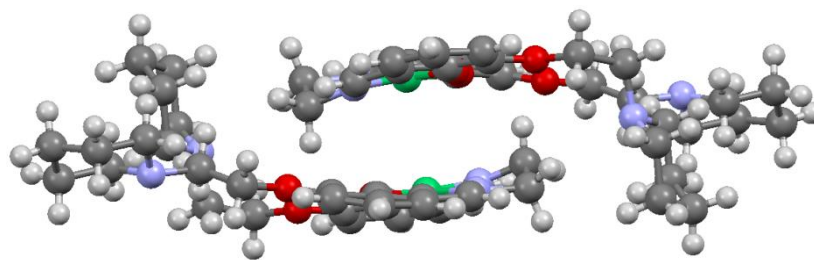


Figure 3.21: Perspective view of the stacking of pairs of complexes in the lattice of complex (10).

CHAPTER 4

DNA BINDING EXPERIMENTS

4.1 Introduction

The ability of the nickel “salphen” complexes, which were prepared via a procedure that employed 2,4- dihydroxybenzaldehyde, to bind to the dsDNA molecule D2, and the tetramolecular quadruplex Q4, has been investigated previously using ESI-MS, CD spectroscopy and UV melting temperature measurements.^{156,157} It was found that the presence of the aromatic system in the “top” of the nickel Schiff base complexes may have enabled partial insertion of the nickel molecules between the base pairs of the dsDNA. In contrast, the extent of binding of nickel Schiff base complexes containing either the *meso*-1,2-diphenylethylenediamine moiety in the “top” of the Schiff base to dsDNA was far less extensive. Both classes of nickel molecules exhibited significant levels of binding to both tetramolecular and unimolecular quadruplex DNA molecules. Examining the effect of changing the length and chemical composition of the pendant groups in nickel Schiff base complexes on their DNA-binding properties has also been previously explored.¹⁵⁵⁻¹⁵⁷ It was found that changing the length of the alkyl group connecting the piperidine rings to the Schiff base sometimes had a small effect on affinity towards either dsDNA or qDNA. Changing the piperidine groups to morpholines did not result in any enhancements in DNA affinity or selectivity. To date the effect of varying the position of the pendant groups on the Schiff base on the ability of the nickel complexes to bind to qDNA, as well as their

selectivity for qDNA over dsDNA, has not been explored. This chapter presents the results of ESI-MS and CD spectroscopic studies designed to determine whether such structural changes have a significant effect on DNA-binding properties.

4.2 Results and discussion

4.2.1 DNA binding experiments performed using nickel complexes containing the 1,2-phenylenediamine moiety

Initially, the DNA-binding properties of the three isomeric nickel complexes containing a single aromatic ring in the “top” of the Schiff base ligand was explored. The structures of these complexes are shown in Figure 4.1. Complex (**14**) has been shown in a number of studies to have significant affinity for different types of DNA.^{155,156}

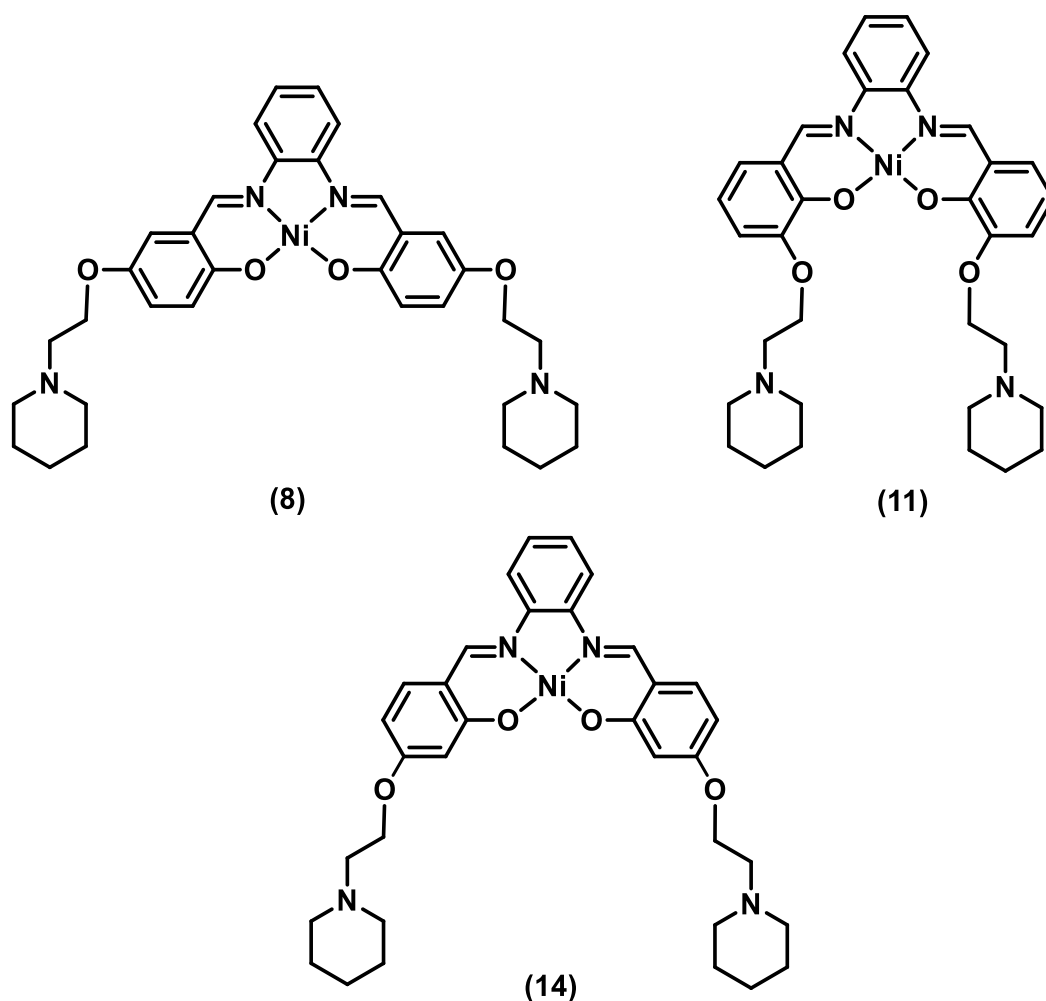


Figure 4.1: Structures of nickel Schiff base complexes containing the 1,2-phenylenediamine moiety, with ethyl piperidine pendant groups attached at different locations on the Schiff base.

In the first instance ESI mass spectra were obtained using solutions containing different ratios of the three nickel Schiff base complexes shown in Figure 4.1 and the dsDNA molecule D2 (Table 2.1). Figure 4.2 shows the ESI mass spectra of a solution containing D2 alone, as well as those containing different ratios of D2 and complex (8), which was prepared by a synthetic procedure that used 2,5-dihydroxybenzaldehyde in the first step.

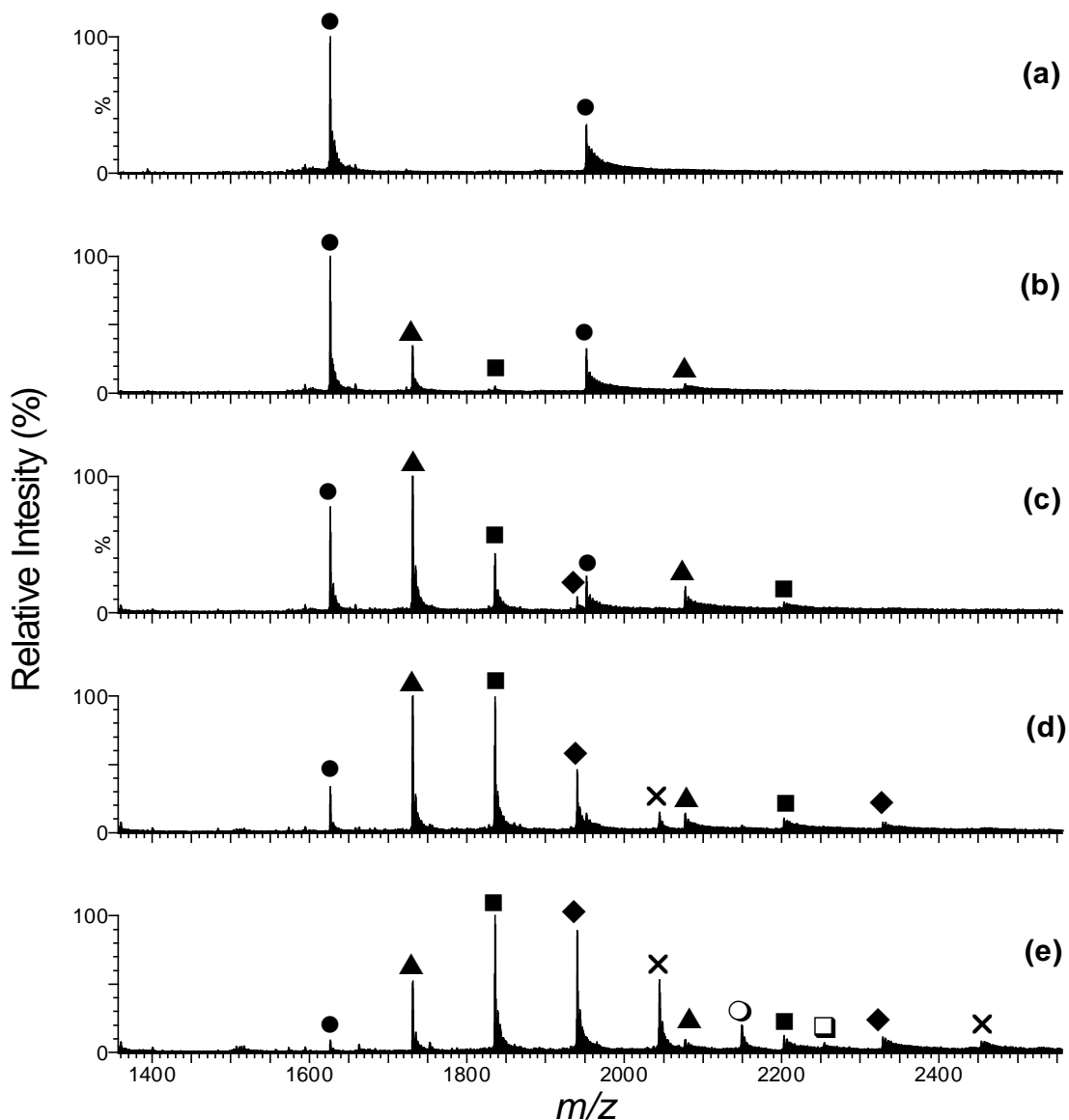


Figure 4.2: Negative ion ESI mass spectra of solutions containing D2 and different ratios of **(8)**. (a) Free D2; (b) D2:**(8)** = 1:1; (c) D2:**(8)** = 1:3; (d) D2:**(8)** = 1:6; (e) D2:**(8)** = 1:9. ● = free D2; ▲ = [D2 + **(8)**]; ■ = [D2 + 2**(8)**]; ◆ = [D2 + 3**(8)**]; × = [D2 + 4**(8)**]; ○ = [D2 + 5**(8)**]; □ = [D2 + 6**(8)**].

The ESI mass spectra of free D2 (Figure 4.2a) contains ions at m/z 1626.5 and 1952.0, which are attributed to $[D2 - 6H]^{6-}$ and $[D2 - 5H]^{5-}$, respectively. The addition of **(8)** to D2 led to the appearance of new ions with an overall charge of either 6- or 5-, which correspond to non-covalent complexes containing one or more intact nickel molecules bound to D2. For example, in

Figure 4.2b, ions of low abundance with a 6- overall charge appear at m/z 1731.2, and are attributable to non-covalent complexes containing one nickel molecule bound to D2. These may be described as $[D2 + (\mathbf{8})]$. The same non-covalent complex also gave rise to ions with an overall charge of 5- and very low abundance at m/z 2077.7. Examination of the spectra in Figure 4.2a-d shows that the relative abundance of ions from $[D2 + (\mathbf{8})]$ increased as the D2:($\mathbf{8}$) ratio was increased, whilst at the same time the relative abundance of ions from free D2 decreased. This trend is consistent with more extensive formation of non-covalent complexes as the amount of ($\mathbf{8}$) in solution was increased. Further evidence of this is provided by the appearance of ions with a 6- charge and very low abundance in Figure 4.2b at m/z 1835.8, which are assigned to $[D2 + 2(\mathbf{8})]$. The relative abundance of these ions increased steadily as the ratio of ($\mathbf{8}$) with respect to D2 became greater, and they were the ions of greatest abundance in the spectrum of a solution containing a D2:($\mathbf{8}$) with a ratio of 1:9. Concurrently, ions corresponding to non-covalent complexes consisting of higher numbers of nickel molecules bound to D2 were also seen in medium to high abundance. This includes ions with a 6- charge at m/z 1940.4 and 2045.2, which can be assigned to $[D2 + 3(\mathbf{8})]$ and $[D2 + 4(\mathbf{8})]$, respectively. Furthermore, the spectrum of a solution containing a 1:9 ratio of D2:($\mathbf{8}$) (Figure 4.2e), showed 6- ions of very low abundance at m/z 2149.5 and 2253.6, which can be assigned to non-covalent complexes consisting of five and six nickel molecules bound to D2, respectively.

In summary, the spectra in Figure 4.2 show that the abundance of ions corresponding to non-covalent complexes consisting of increasingly larger numbers of nickel molecules bound to D2 grew as the amount of **(8)** in solution was increased. At the same time ions from free D2 diminished in abundance as expected. Similar trends were observed for ESI mass spectra of solutions containing D2 and the analogous complexes **(14)** and **(11)**, confirming the ability of the latter nickel complexes to also bind to D2. This was not a surprising result in the case of complex **(14)**, as its ability to form non-covalent complexes with this dsDNA has been previously reported.¹⁵⁶ In order to compare the binding affinity of complexes **(8)**, **(11)** and **(14)** towards D2, a series of spectra were obtained of solutions containing the same ratio (1:6) of D2 and the nickel complexes. These spectra are shown in Figure 4.3.

In each spectrum, ions at m/z 1626.5 and 1952.0 are present which are attributable to free dsDNA. However, the abundances of these ions vary from one spectrum to another, suggesting that the nickel complexes are binding to different extents to the DNA. For example, ions at m/z 1626.5 from D2 are of lowest abundance in Figure 4.3d, which is a spectrum of a solution containing a 1:6 ratio of D2 and **(14)**. This supports the hypothesis that **(14)** has a higher affinity towards D2 than either **(8)** or **(11)**. Evidence in support of this is provided by the observation that the abundance of ions from non-covalent complexes containing three, four or five nickel complexes bound to D2 appears to be slightly greater in the case of the spectrum shown in Figure 4.3d. Therefore it appears that complex **(14)**, which was prepared via a synthetic pathway which employed 2,4-dihydroxybenzaldehyde, has the

highest affinity of the three isomeric complexes for D2. In this thesis, “affinity” is used to describe the overall binding of a nickel complex for a DNA molecule based on observation of the amounts of free DNA observed and the number of nickel molecules bound. There may, however, be different binding modes as more nickel molecules bind, and/or binding of each successive nickel molecule may or may not be independent.

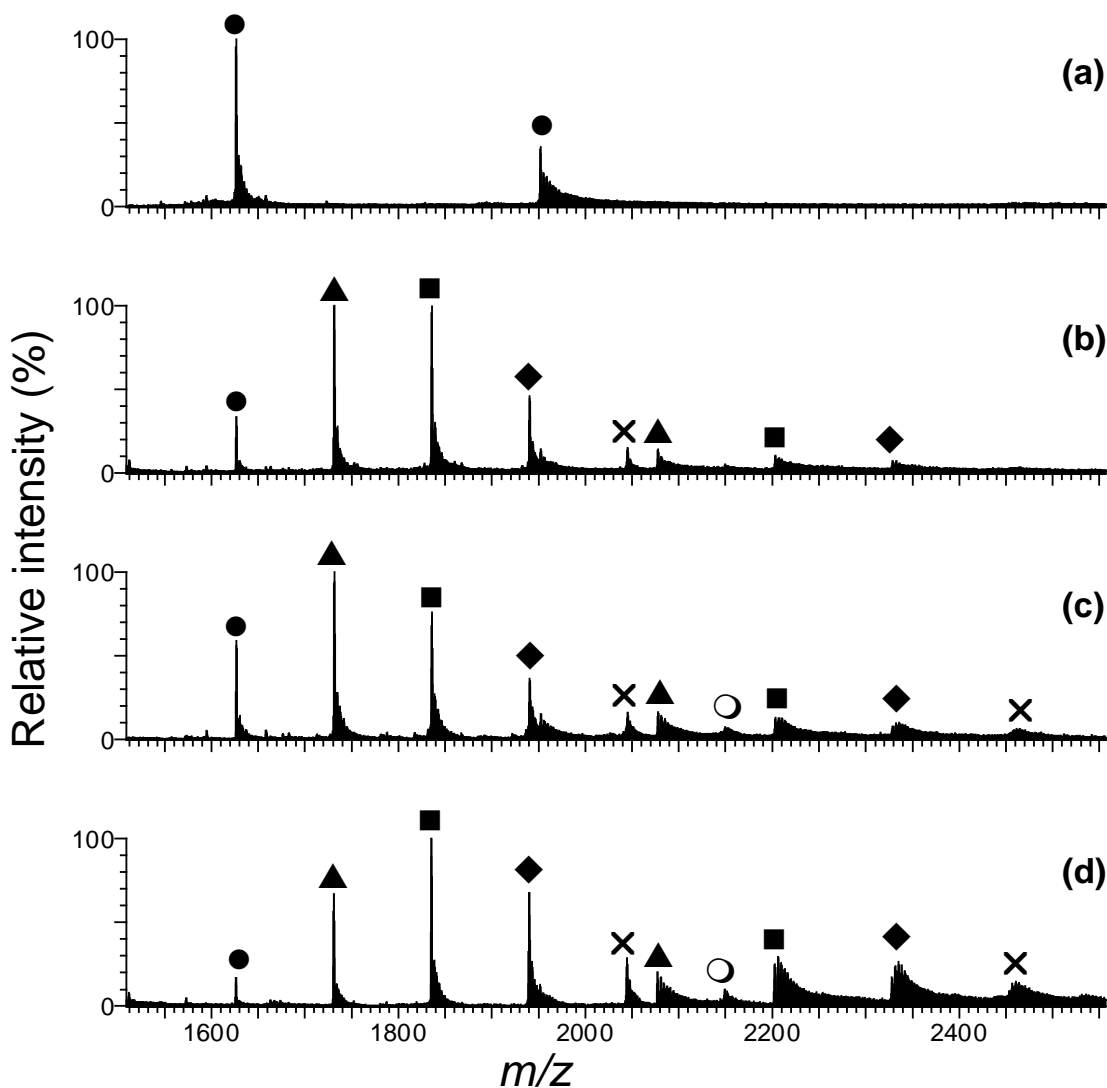


Figure 4.3: Negative ion ESI mass spectra of solutions containing D2 and different nickel Schiff base complexes at a 1:6 ratio. (a) Free D2; (b) D2 + (**8**);

(c) D2 + (11); (d) D2 + (14). ● = free D2; ▲ = [D2 + (Ni)]; ■ = [D2 + 2(Ni)]; ◆ = [D2 + 3(Ni)]; ✕ = [D2 + 4(Ni)]; ○ = [D2 + 5(Ni)].

The spectra in Figure 4.3b and c also show ions of medium or high abundance from non-covalent complexes consisting of two or three nickel complexes bound to D2, as well as ions of lower abundance from non-covalent complexes containing greater numbers of bound nickel molecules. Therefore it appears that changing the location of the ethyl piperidine groups on the Schiff base complexes had little effect on the ability of (14) to bind to and form non-covalent complexes with D2.

Inspection of Figure 4.3 suggests that the order of binding affinity of these three nickel complexes for D2 is: (14) > (8) > (11). However, in order to confirm this conclusion, it was necessary to calculate and compare the relative abundances of ions from free D2 and different types of non-covalent complexes seen in all three spectra. Therefore the relative abundances were calculated by adding the individual abundances of all ions assigned to free DNA or a specific non-covalent complex in a given spectrum, and dividing the result by the sum of the abundances of all ions present in that spectrum. Figure 4.4 shows how the relative abundances of ions varied from the spectrum of one solution to another. The figure shows that complex (14) binds the most extensively to D2, as the relative abundances of ions from non-covalent complexes consisting of two, three or four molecules of (14) bound to D2 are greater than for the corresponding ions containing either of the two other nickel complexes.

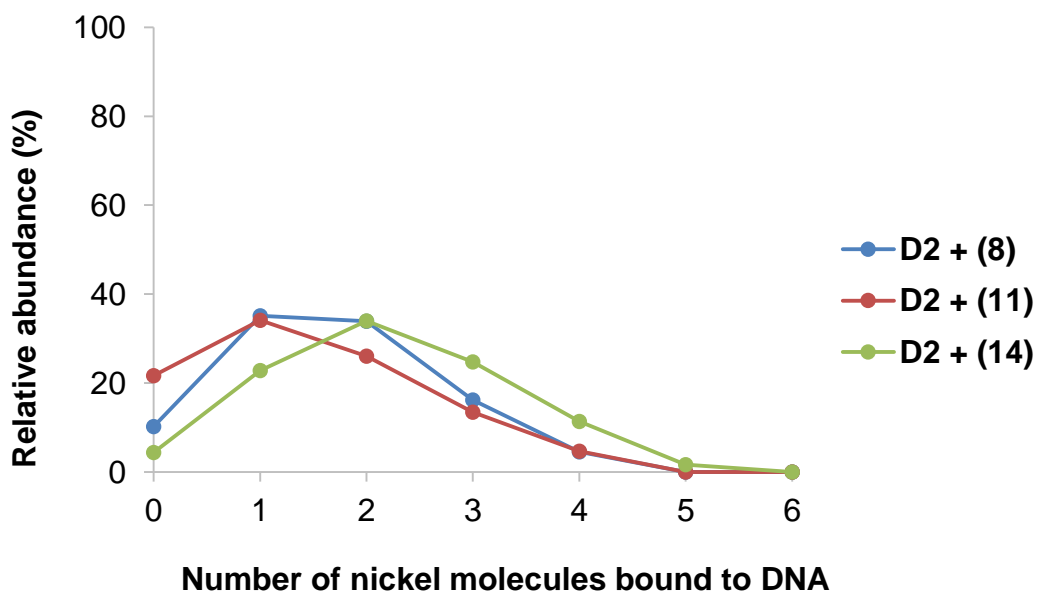


Figure 4.4: Relative abundances of ions in spectra of solutions containing D2 and different nickel Schiff base complexes at a 1:6 ratio.

In addition, Figure 4.4 also shows that the relative abundances of ions from non-covalent complexes consisting of one or four molecules of **(8)** or **(11)** bound to DNA is essentially identical. However, the relative abundances of ions from non-covalent complexes containing two molecules of **(8)** bound to D2 is greater than that for the corresponding non-covalent complexes containing **(11)**. This observation, along with a lower relative abundance of ions from D2, suggests that the affinity of **(8)** is slightly greater than that of **(11)**. Therefore the results illustrated in Figure 4.4 support the order of binding affinity proposed earlier for these three complexes: **(14)** > **(8)** > **(11)**. Overall the extent of non-covalent complex formation with D2 did not vary greatly between the three nickel complexes, suggesting that the position of the ethyl piperidine moiety does not have a major impact on affinity towards dsDNA for this subset of nickel Schiff base complexes. In order to test this

hypothesis further, CD spectra were obtained of solutions containing different ratios of the three nickel Schiff base complexes and D2, and are presented in Figure 4.5.

Circular dichroism (CD) spectroscopy is routinely used along with other techniques such as FTIR difference spectroscopy, ESI-MS and UV-visible absorption spectrophotometry, to study conformational changes of DNA.¹⁶⁵⁻¹⁶⁸ The CD signal of normal (B-form) DNA arises from the asymmetric carbon atoms present in the sugar residues, and its helical structure. Changes to the CD spectrum of DNA may be brought about as a result of conformational changes resulting from the binding of different compounds, or a change in the surrounding solution conditions. Depending on the mode or extent of binding of a small molecule, DNA can either remain in its original structure, or may transform into another secondary structure such as A-form or Z-form DNA. Each of these secondary structures gives rise to a distinct spectrum featuring CD bands at different wavelengths.^{166,169,170} In addition, it is possible to provide evidence in support of the binding modes used by small molecules to bind to DNA, such as intercalation, groove binding and electrostatic interaction, by monitoring the changes in intensity and position of CD bands.¹⁷¹⁻¹⁷⁴ Therefore, CD spectroscopy is considered to be one of the most powerful techniques for providing information about the nature of interactions between metal complexes and dsDNA.

The CD spectra presented in Figure 4.5 show the effect of addition of increasing amounts of each of the three nickel complexes upon the CD spectrum of D2. The spectrum of a solution containing only free D2 shows

large positive and negative CD bands centred at 282 nm and 249 nm, respectively. These values are characteristic for B-form DNA.¹⁶⁶ The addition of the metal complexes to the DNA resulted in changes to the ellipticity and positions of the CD bands, which are summarised in Table 4.1.

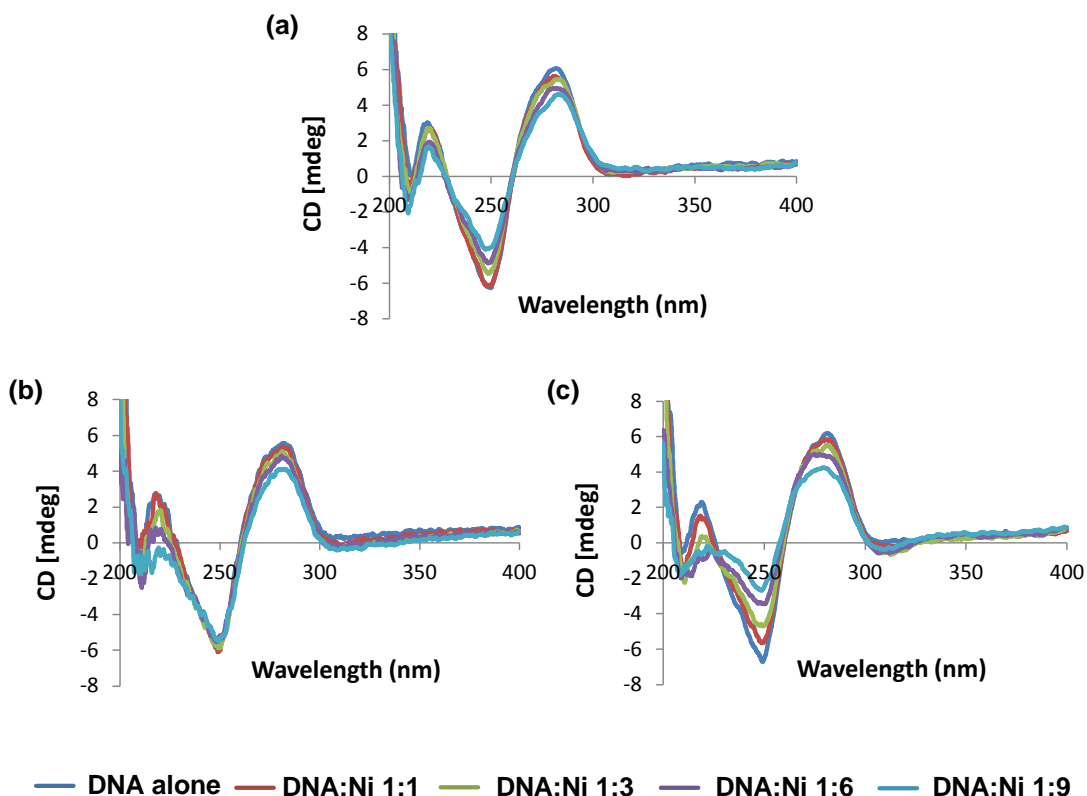


Figure 4.5: Circular dichroism spectra (200-400 nm) of solutions containing D2 and different ratios of nickel Schiff base complexes. (a) D2 + (8); (b) D2 + (11); (c) D2 + (14).

Table 4.1: Effect of addition of nickel Schiff base complexes on the CD spectrum of D2.*

Nickel complex	Positive CD band at 282 nm		Negative CD band at 249 nm	
	$\Delta\lambda$ (nm)	$\Delta\varepsilon$ (mdeg)	$\Delta\lambda$ (nm)	$\Delta\varepsilon$ (mdeg)
(8)	1.9	-1.5	-2.6	2.2
(11)	0.7	-1.5	1.5	0.4
(14)	-2.0	-1.9	-0.5	4.0

* All $\Delta\lambda$ and $\Delta\varepsilon$ values are the difference between the values for free DNA and those for a solution containing a DNA:nickel complex ratio of 1:9. Negative $\Delta\lambda$ values indicate a blue shift; positive values indicate a red shift. $\Delta\varepsilon$ values are the difference between ε_{\max} for this CD band for the solution

containing no metal complex, and ϵ_{\max} for the same CD band for the solution with the highest DNA:nickel complex ratio.

Inspection of Figure 4.5c suggests that overall the addition of **(14)** to D2 caused the largest changes to the CD spectrum of D2, whereas the addition of **(11)** resulted in the smallest changes (Figure 4.5b). These conclusions are reinforced by the results presented in Table 4.1. The most notable effect caused by addition of a nickel complex was the change in ellipticity of the negative CD band upon addition of **(14)**. Addition of 9 equivalents of this nickel complex more than doubled the initial ellipticity of this CD signal. Furthermore, the change in ellipticity caused by addition of **(14)** was almost double that observed upon addition of the same amount of **(8)**, and 10 times larger than that seen with complex **(11)**. Addition of **(14)** also resulted in a slightly larger change to the ellipticity of the positive CD band than that caused by either **(8)** or **(11)**. It is also worthwhile noting that addition of **(14)** resulted in a small blue shift for the positive CD band of D2, whereas the other two nickel complexes had the opposite effect, possibly indicating subtle differences in their modes of interaction. Inspection of Table 4.1 shows that the magnitude of changes to the position and ellipticity of both CD bands generally increased in the order: **(14)** > **(8)** > **(11)**, which is the same as the order of increasing binding affinities derived from the ESI-MS studies presented earlier.

In order to investigate the binding of **(8)**, **(11)** and **(14)** to tetramolecular quadruplex DNA, a similar series of ESI-MS and CD experiments to those described above, was also performed with Q4 (Table 2.1). Figure 4.6 shows the ESI mass spectra of solutions containing a 1:6 ratio of Q4 and **(8)**, **(11)** or

(14). The spectrum of a solution containing Q4 alone (Figure 4.6a), contains ions of low and high abundance at m/z 1675.1 and 2010.4, which are assigned to $[Q4 + 4NH_4^+ - 10H]^{6-}$ and $[Q4 + 4NH_4^+ - 9H]^{5-}$, respectively. The presence of four ammonium ions in these ions is not surprising, and provides support for the conclusion that the tetramolecular quadruplex structure initially formed in solution has been successfully transferred to the gas phase. This is because Q4 contains five G-tetrads, and would therefore be expected to trap four unimolecular cations in between each quartet. Since the mass spectra were obtained using solutions of Q4 in ammonium acetate, it is not surprising that those four unimolecular cations were all ammonium ions.

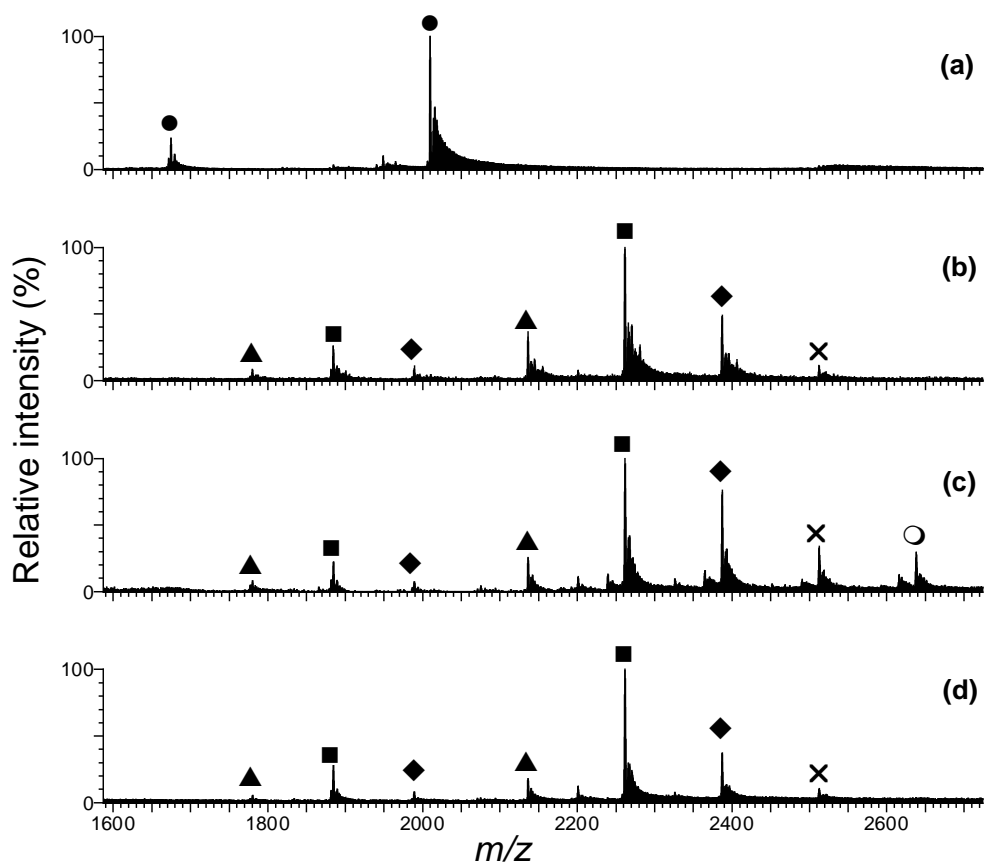


Figure 4.6: Negative ion ESI mass spectra of solutions containing Q4 and different nickel Schiff base complexes at a 1:6 ratio. (a) Free Q4; (b) Q4 +

(**8**); (c) Q4 + (**11**); (d) Q4 + (**14**). ● = free Q4; ▲ = [Q4 + (Ni)]; ■ = [Q4 + 2(Ni)]; ◆ = [Q4 + 3(Ni)]; ✕ = [Q4 + 4(Ni)]; ○ = [Q4 + 5(Ni)].

After addition of the nickel Schiff base complexes, none of the spectra showed ions from free DNA. This observation suggests that each of the three complexes has a significant affinity towards Q4, and is in contrast with what was observed for D2 (Figure 4.3). Further examination of Figure 4.6b-d reinforces this view. For example, each of the spectra in Figure 4.6b and d contain ions of high abundance at m/z 2261.7, which correspond to [Q4 + 2(Ni) + 4NH₄⁺ - 13H]⁵⁻, which may be more simply stated as [Q4 + 2(Ni)]. In addition, ions of low to medium abundance are present at m/z 2387.3, which are attributable to [Q4 + 3(Ni)]. These observations confirm that each of the isomeric nickel complexes exhibits a significant and similar degree of affinity towards Q4. In order to determine the order of binding affinities towards this qDNA molecule, the relative abundances of each of the ions observed was calculated, and is presented in Figure 4.7. Inspection of the figure shows that the only nickel complex to form non-covalent complexes with Q4 that involved five bound nickel molecules was (**11**). This observation, combined with the slightly higher abundances of ions from [Q4 + 3(**11**)] and [Q4 + 4(**11**)], compared to the corresponding ions containing either (**8**) or (**14**), suggests that (**11**) may have the highest overall affinity of the nickel complexes for this tetramolecular quadruplex. Examination of Figure 4.7 also reveals that while the relative abundances of ions from [Q4 + 2(Ni)] is greater for (**14**) than for (**8**), the converse is true in the case of ions arising from [Q4 + 3(Ni)]. This suggests that (**8**) and (**14**) have very similar affinities for Q4, and therefore the overall order of binding affinity of these three complexes is:

(11) > (8) \approx (14). This order is essentially the reverse of what was obtained from studies involving the dsDNA molecule D2. It therefore appears that the nature and extent of binding modes used by the nickel complexes with the G-quadruplex DNA molecule may be slightly different to those used in interactions with dsDNA.

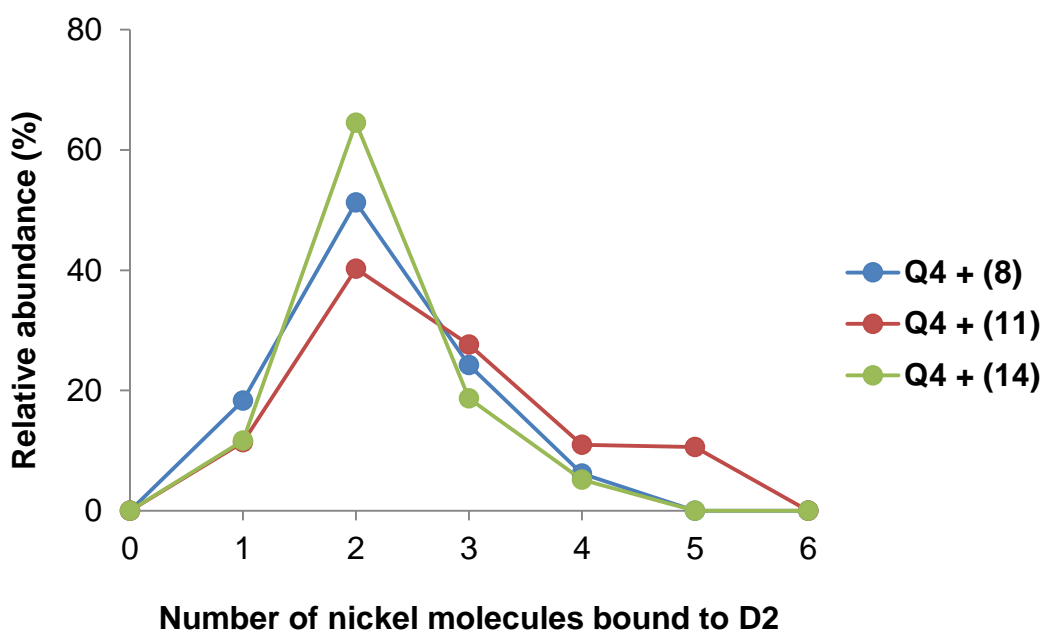


Figure 4.7: Relative abundances of ions in ESI mass spectra of solutions containing Q4 and different nickel Schiff base complexes at a 1:6 ratio.

Comparison of Figure 4.4 and Figure 4.7 shows that the abundances of ions from free D2 in the spectra of solutions containing a nickel complex and this DNA molecule were between 4 and 22 %, while ions from free Q4 were absent in the spectra of solutions containing a nickel complex and this tetramolecular G-quadruplex. This indicates that while complexes (8), (11) and (14) interact with both types of DNA, the extent of binding is greater in all

cases with Q4. It is also worth reflecting on the observation that although 6 equivalents of nickel complexes were added to the solutions used to obtain the spectra shown in Figure 4.6, the most abundant ions in each case were from non-covalent complexes consisting of just two nickel molecules bound to the quadruplex. It therefore appears that after two nickel molecules are bound to Q4, further binding events occur less readily. This may be because the preferred binding sites for the nickel molecules are the two G-quartets at either end of the quadruplex. Once these sites become occupied, further binding interactions with lower affinity sites in this relatively small qDNA molecule are inhibited because of steric hindrance and electronic factors.

Circular dichroism spectroscopy was then used to provide support for or against the above order of nickel binding affinities towards Q4, determined using ESI-MS. Circular dichroism spectroscopy has also been used previously to characterise the different topologies of quadruplex DNA, and monitor changes in its conformation upon interaction with different DNA-binding ligands.^{166,175-178} Each qDNA conformation gives a characteristic CD spectrum.^{166,175,178,179} For example, a parallel G-quadruplex displays a positive CD band at 260 nm, whereas an anti-parallel G-quadruplex displays a negative CD band at this wavelength. In addition both types of quadruplex DNA conformations give an additional positive CD band around 210 nm. The CD spectra illustrated in Figure 4.8 show the effect of adding increasing amounts of each of the three nickel complexes on the CD spectrum of Q4. The spectrum of a solution containing only free Q4 exhibited major positive

and negative CD peaks centred at 264 nm and 243 nm, respectively, which are characteristic for parallel DNA quadruplexes.¹⁶⁶

Inspection of Figure 4.8 shows that the addition of **(8)** or **(14)** to Q4 caused larger changes to the ellipticity of the positive CD band, compared to that which resulted from the addition of **(11)**. Table 4.2 summarises the changes to the position and ellipticity of both CD bands caused by addition of the three nickel complexes.

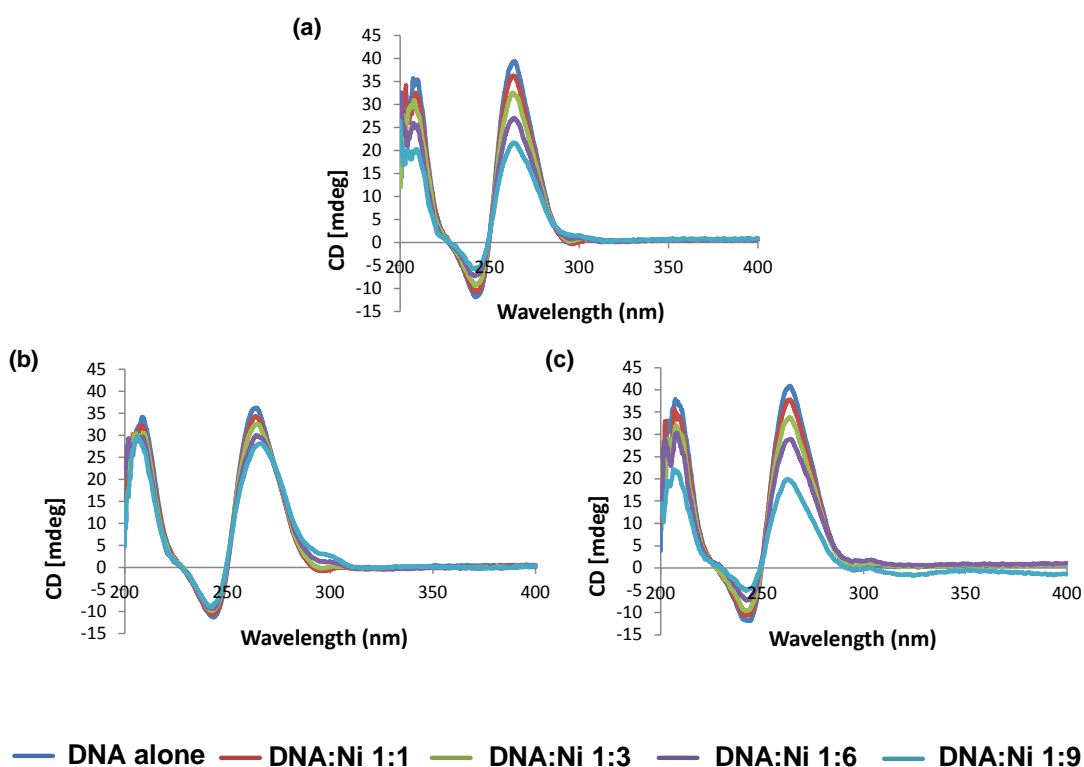


Figure 4.8: Circular dichroism spectra (200-400 nm) of solutions containing Q4 and different ratios of nickel Schiff base complexes. (a) Q4 + **(8)**; (b) Q4 + **(11)**; (c) Q4 + **(14)**.

Table 4.2: Effect of addition of nickel Schiff base complexes on the CD spectrum of Q4.*

Nickel complex	Positive CD band at 264 nm		Negative CD band at 243 nm	
	$\Delta\lambda$ (nm)	$\Delta\epsilon$ (mdeg)	$\Delta\lambda$ (nm)	$\Delta\epsilon$ (mdeg)
(8)	-0.5	-17.6	-0.9	6.1
(11)	2.9	-8.1	-1.7	2.3
(14)	-0.8	-21.0	-1.4	6.9

* All $\Delta\lambda$ and $\Delta\epsilon$ values are the difference between the values for free DNA and those for a solution containing a DNA: nickel complex ratio of 1:9. Negative $\Delta\lambda$ values indicate a blue shift; positive values indicate a red shift. $\Delta\epsilon$ values are the difference between ϵ_{\max} for this CD band for the solution containing no metal complex, and ϵ_{\max} for the same CD band for the solution with the highest DNA: nickel complex ratio.

Inspection of Table 4.2 shows that addition of 9 equivalents of (14) and (8) decreased the ellipticity of the positive CD band by 21.0 and 17.6 mdeg, respectively. In contrast, the change resulting from the addition of (11) was only 8.1 mdeg. Although this smaller change in ellipticity is consistent with the notion that (11) has a lower affinity towards Q4 than either of the other nickel complexes, its addition did result in a red shift to the position of this CD band that was greater than the blue shifts caused by (8) or (14). This highlights the sensitivity of CD spectroscopy to subtle changes in DNA conformation caused by the addition of isomeric complexes such as those investigated in this thesis. The larger changes to the ellipticity of the positive CD band caused by addition of (8) and (14) were mirrored by proportionately larger changes also to the ellipticity of the negative CD signal. If it is assumed that changes in ellipticity are more indicative of the overall strength of the metal/DNA binding interactions than alterations to the positions of the CD signals, then the order of binding affinity for the three complexes is: (14) > (8) > (11). This sequence is very different to the overall order obtained from the

ESI-MS experiments, with the positions of complexes (11) and (14) being reversed. If instead the shift in position of the more intense, positive CD band is used as a measure of the binding ability of the nickel complexes, then the overall order of binding affinity is: (11) > (14) \approx (8). This sequence is essentially the same as that derived from the ESI-MS study, suggesting that changes in position of the positive CD band, although they may be typically small in magnitude, may more accurately reflect the extent of metal/DNA interactions.

The significant difference in binding affinity series based on changes to the ellipticity of the positive CD band, and the extent of non-covalent complex formation revealed in the ESI-MS study, is perhaps not surprising as the methods exhibit varying sensitivities to different aspects of the binding interaction. In the case of ESI-MS, the results reflect stability of non-covalent complexes in the gas phase, whilst the changes to the CD spectrum are the result of changes to DNA conformation in the solution. In the absence of qualitative or quantitative binding data obtained by applying other techniques, it is therefore impossible to know whether ESI-MS or CD spectroscopy provides the best overall picture of the relative DNA-binding affinity of a group of related metal complexes.

4.2.2 DNA binding experiments performed using nickel complexes containing the 1,2-ethylenediamine moiety

This section explores the effect of changing the position of the appended ethyl piperidine moieties in nickel Schiff base complex (13), on the binding

affinity of the resulting nickel complexes ((**7**) and (**10**)) towards D2 and Q4. The structures of these three complexes are shown in Figure 4.9.

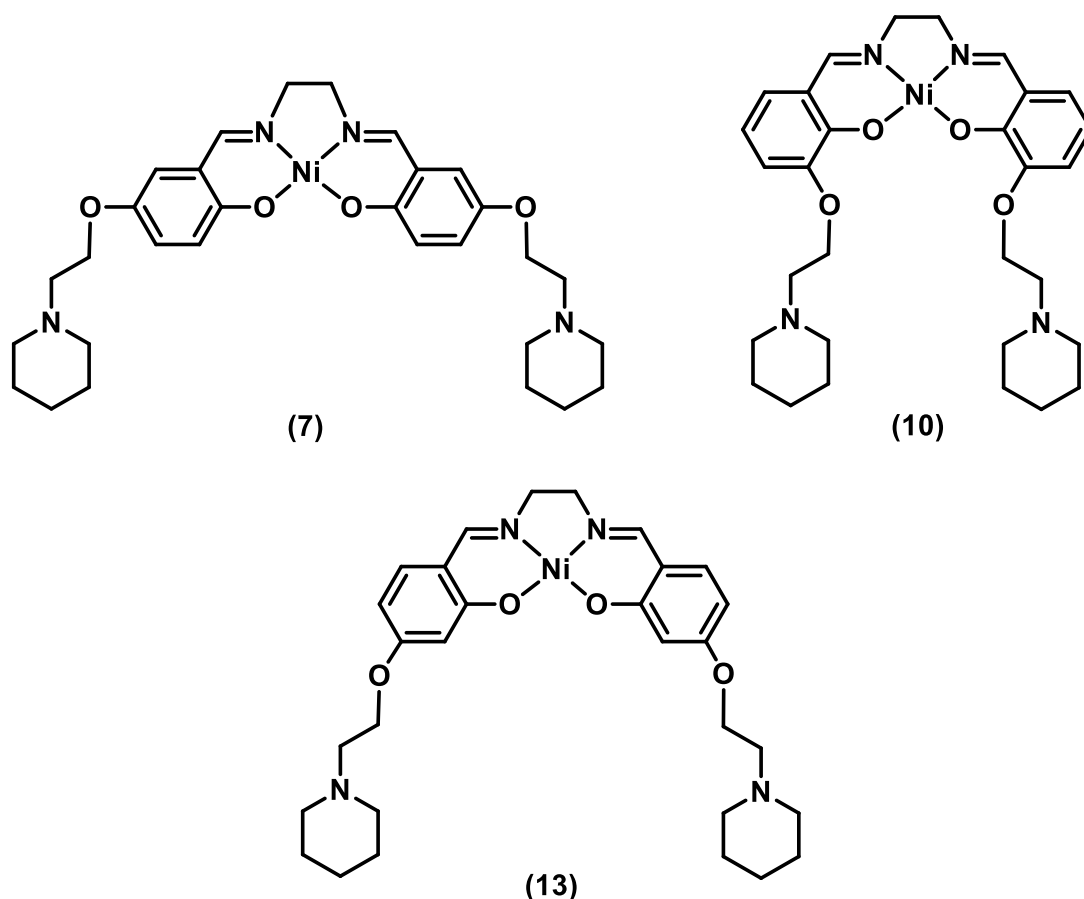


Figure 4.9: Structures of nickel Schiff base complexes containing the 1,2-ethylenediamine moiety, whose binding to dsDNA and qDNA are explored in this section.

The binding affinity of complex (**13**) has been examined previously,^{155,157} and was found to exhibit a lower binding affinity towards both of the above DNA molecules than the corresponding salphen complex (**14**). This was attributed to the former complex having one less aromatic ring able to contribute to interactions with the base pair stack of the double-stranded D2, or

alternatively interact with a terminal G-quartet of Q4. It was hoped that altering the points of attachment of the ethyl piperidine groups might facilitate additional favourable binding interactions that compensate for these issues, and thereby endow complexes **(7)** and **(10)** with superior DNA affinity and/or selectivity to the complexes discussed in the previous section.

A series of ESI-MS experiments was performed using solutions containing a 1:6 ratio of each of the three nickel complexes and the dsDNA molecule D2. Figure 4.10 shows the ESI mass spectra of these solutions. The relative abundances of all the ions observed were then calculated and are presented in Figure 4.11. Each of the spectra in Figure 4.10b-d shows ions at m/z 1626.2 and 1952.5, which correspond to $[D2 - 6H]^{6-}$ and $[D2 - 5H]^{5-}$, respectively. These ions are present in medium to high abundance in Figure 4.10c, and with low to medium abundance in Figure 4.10b and d. This suggests that the binding affinity of these nickel complexes toward D2 is generally less than that of nickel complexes with the 1,2-phenylenediamine moiety at the “top” of the molecule, namely **(8)**, **(11)** and **(14)**. This is because the relative abundances of ions from free D2 in ESI-mass spectra of solutions containing a 1:6 ratio of D2 and the latter complexes were always very low (<22%)

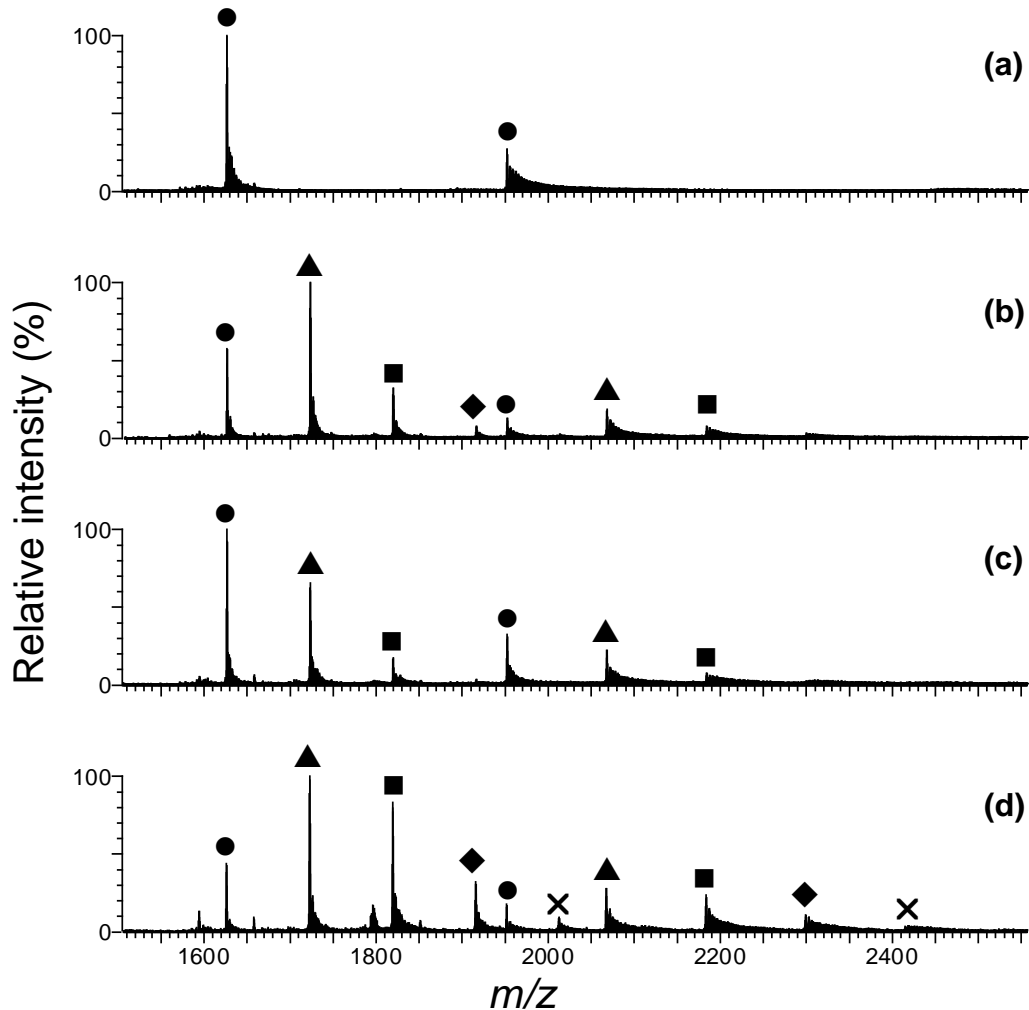


Figure 4.10: Negative ion ESI mass spectra of solutions containing D2 and different nickel Schiff base complexes at a 1:6 ratio. (a) Free D2; (b) D2 + (**7**); (c) D2 + (**10**); (d) D2 + (**13**). ● = free D2; ▲ = [D2 + (Ni)]; ■ = [D2 + 2(Ni)]; ◆ = [D2 + 3(Ni)]; X = [D2 + 4(Ni)].

Inspection of Figure 4.10 shows that the abundances of ions from free DNA followed the order: (**13**) < (**7**) < (**10**). This suggests that the order of relative DNA binding affinities is the opposite sequence; namely (**10**) < (**7**) < (**13**). Further evidence for the conclusion that (**13**) has the highest affinity towards D2 of these complexes is provided by Figure 4.11, which shows that the relative abundances of ions from [D2 + 2(Ni)] were highest for this nickel complex. Furthermore, (**13**) was the only nickel complex to give rise to ions of

significant abundance from non-covalent complexes containing three bound nickel molecules.

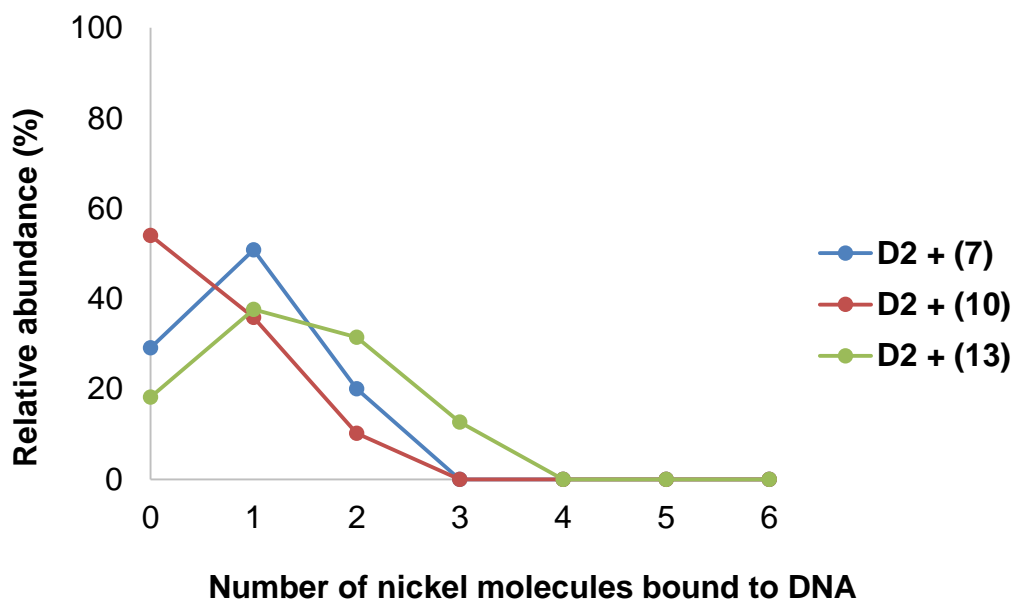


Figure 4.11: Relative abundances of ions from free DNA and different non-covalent complexes in spectra of solutions containing D2 and different nickel Schiff base complexes at a 1:6 ratio.

Examination of Figure 4.11 also provides evidence that **(10)** has the lowest affinity towards D2 of the three nickel complexes. Foremost amongst this is the observation that the relative abundance of ions from free D2 is greater than that of any of the non-covalent complexes present, only in the case of the spectrum obtained from the solution containing **(10)**. In addition, the relative abundances of ions from [D2 + **(10)**] and [D2 + 2**(10)**] were both significantly less than that for the corresponding ions arising from non-covalent complexes containing **(7)**. Confirmation of the lower affinity of complex **(10)** towards D2, compared to that exhibited by **(13)**, is also provided by the data in Figure 4.11. In particular, the relative abundance of

ions from [D2 + 2(**10**)] is much lower than that of ions from [D2 + 2(**13**)]. Furthermore, the absence of ions from non-covalent complexes of the type [D2 + 3(**10**)] also supports this conclusion.

The results presented in Figure 4.10 and Figure 4.11 show that binding affinity towards D2 was not enhanced by changing the position of the ethyl piperidine groups from those they occupy in complex (**13**). This is the same conclusion as that reached previously for complexes containing the phenylenediamine moiety in the top region of the Schiff base ligand, suggesting that the 4-position may be generally the optimal location for these substituents.

In order to provide further support for the above conclusions, CD spectra were obtained of solutions containing different ratios of (**7**), (**10**) or (**13**), and D2, and are presented in Figure 4.12. Inspection of Figure 4.12b and c shows that the addition of either (**10**) or (**13**) to D2 caused no significant changes to the CD spectrum of D2. These observations suggest that (**10**) and (**13**) do not interact to a notable extent with this dsDNA molecule. This conclusion contrasts markedly with that based on the results of the ESI-MS study presented earlier, which suggests that (**13**) had the greatest ability of the three nickel complexes to form non-covalent complexes with dsDNA. This apparent dichotomy in the results may be a reflection of the two experimental techniques used being more sensitive to different aspects of the metal complex/DNA interaction, as outlined earlier in this chapter, and commented on by others. For example, Davis *et al.* found that CD experiments sometimes suggest different trends in DNA-binding affinity for nickel

complexes, to those indicated by ESI-MS studies.¹⁵⁶ These researchers reported that mass spectral studies suggested that nickel salphen complex (**14**) binds to D2 to a significant extent, however, the addition of this complex to D2 caused no significant changes to the CD spectrum of the nucleic acid. This may be because electrostatic interactions are well-maintained in the gas phase relative to hydrophobic interactions, and binding modes in which one type of interaction predominates over others may result in a bias in ESI-MS experiments.¹⁸⁰ CD spectra show only bulk effects and give no information about the different complexes that may be present in a mixture.

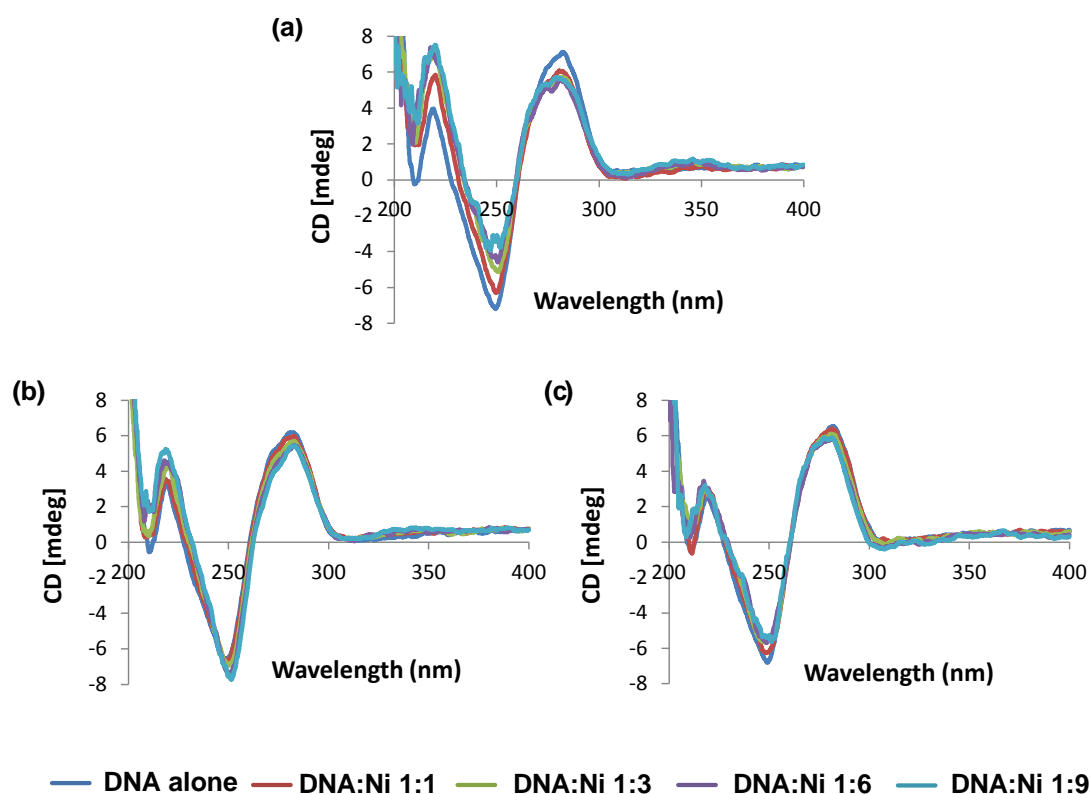


Figure 4.12: Circular dichroism spectra (200-400 nm) of solutions containing D2 and different ratios of nickel Schiff base complexes. (a) D2 + (**7**); (b) D2 + (**10**); (c) D2 + (**13**).

Figure 4.12a shows that addition of complex (7) had the greatest effect on the ellipticity of three major CD bands. For example, addition of 9 equivalents of (7) increased the ellipticity of the negative CD band by 3.3 mdeg. The contrast been the effect of addition of complex (7) on the CD spectrum of D2, and that caused by addition of either (10) or (13), is summarised by Table 4.3, which presents the changes in wavelength and ellipticity of the two principal CD bands caused by addition of the three nickel complexes.

Table 4.3: Effect of addition of nickel Schiff base complexes on the CD spectrum of D2.*

Nickel complex	Positive CD band at 282 nm		Negative CD band at 252 nm	
	$\Delta\lambda$ (nm)	$\Delta\varepsilon$ (mdeg)	$\Delta\lambda$ (nm)	$\Delta\varepsilon$ (mdeg)
(7)	-2.8	-1.4	-2.6	3.3
(10)	1.1	-0.8	2.2	-1.2
(13)	-0.6	-0.7	2.1	1.2

* All $\Delta\lambda$ and $\Delta\varepsilon$ values are the difference between the values for free DNA and those for a solution containing a DNA:nickel complex ratio of 1:9. Negative $\Delta\lambda$ values indicate a blue shift; positive values indicate a red shift. $\Delta\varepsilon$ values are the difference between ε_{\max} for this CD band for the solution containing no metal complex, and ε_{\max} for the same CD band for the solution with the highest DNA:nickel complex ratio.

The variation in the magnitude of the changes in ellipticity of the CD bands at 252 and 282 nm suggests the following binding affinity order: (7) > (13) \approx (10). The difference between this binding affinity sequence, and that derived by ESI-MS, can be explained by proposing that the location of the ethyl piperidine moieties in complex (7) enables it to participate in slightly different modes of DNA binding to that employed by (13) and (10). Furthermore, the binding mode used by (7) results in larger changes to the overall DNA

conformation and therefore the CD spectrum, but does not afford non-covalent complexes sufficient stability to withstand the environment of the mass spectrometer. Despite the apparent differences in binding affinity order that the two techniques suggest for complexes (7) and (13), both methods give results consistent with the conclusion that complex (10) has the lowest affinity towards D2 of the three nickel complexes.

A series of ESI-MS experiments was also performed using solutions containing a 1:6 ratio of the tetramolecular quadruplex Q4, and either (7), (10) or (13). These experiments were performed to provide the information required to make an assessment of whether altering the position of the ethyl piperidine groups favourably affects the selectivity of the nickel complexes for qDNA over dsDNA. Figure 4.13 shows the mass spectra obtained of the above solutions.

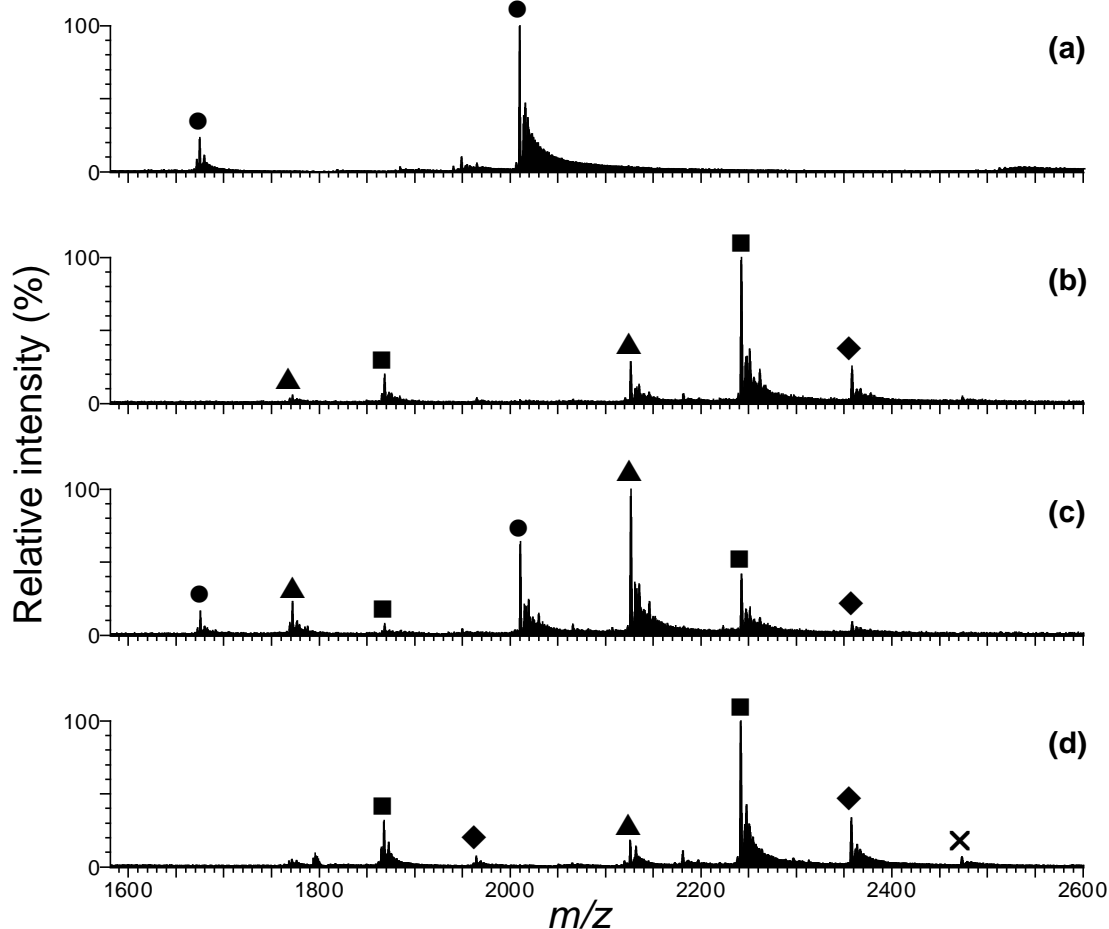


Figure 4.13: Negative ion ESI mass spectra of solutions containing Q4 and different nickel Schiff base complexes at a 1:6 ratio. (a) Free Q4; (b) Q4 + (**7**); (c) Q4 + (**10**); (d) Q4 + (**13**). ● = free Q4; ▲ = [Q4 + (Ni)]; ■ = [Q4 + 2(Ni)]; ◆ = [Q4 + 3(Ni)]; X = [Q4 + 4(Ni)].

After addition of the nickel Schiff base complexes, the only spectrum to show ions from free DNA was that presented in Figure 4.13c, which was of a solution containing a 1:6 ratio of Q4 and (**10**). This observation, combined with the much lower abundance of ions from non-covalent complexes consisting of [Q4 + 2(**10**)], compared to that of analogous ions in the spectra shown in Figure 4.13b and d, indicates that (**10**) has the lowest affinity of these three nickel complexes for this particular tetramolecular quadruplex. Reinforcing this conclusion is the observation that the most abundant ions in

Figure 4.13c are from [Q4 + (10)]. In contrast, the most abundant ions in Figure 4.13b and d are from [Q4 + 2(7)] and [Q4 + 2(13)], respectively. Furthermore, Figure 4.13b and d both show ions of low to medium abundance at m/z 2358.1, from [Q4 + 3(Ni)], which are of greater abundance than the corresponding ions in the spectrum of the solution containing (10). Comparison of Figure 4.13b and d does not, however, enable a determination as to which of complexes (7) and (13) has the highest affinity towards Q4 to be readily made. Therefore in order to address this question the relative abundances of each of the ions present in Figure 4.13b-d were calculated, and are presented in Figure 4.14.

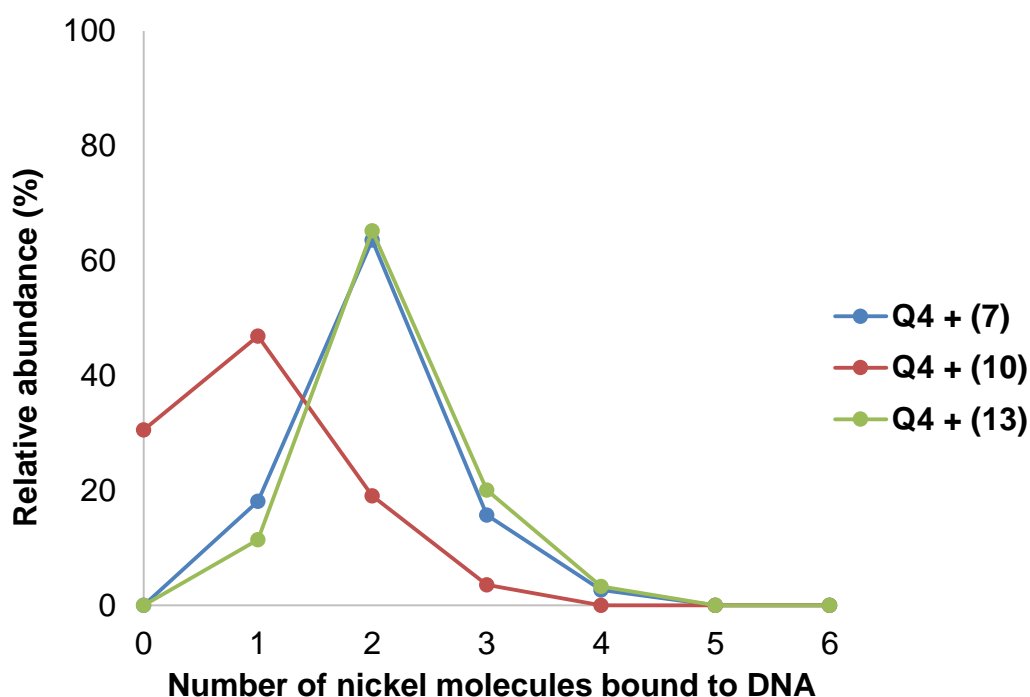


Figure 4.14: Relative abundances of ions in ESI mass spectra of solutions containing Q4 and different nickel Schiff base complexes at a 1:6 ratio.

Examination of Figure 4.14 shows that while the abundance of ions from [Q4 + (Ni)] is perhaps slightly greater for (7) than (13), the opposite was true for ions arising from non-covalent complexes of the type [Q4 + 3(Ni)]. These observations, together with the very similar relative abundances of ions from [Q4 + 2 (Ni)], for complex (7) and (13), suggests that the affinity of these two nickel complexes towards Q4 are very similar. The preference of Q4 to bind two molecules of (7) and (13) is striking, and was also evident in Figure 4.6 based on the results presented in Figure 4.14, the overall order of binding affinity for these three complexes is: (13) \approx (7) > (10). This is very similar to the order of DNA affinities obtained for these nickel complexes from ESI-MS binding studies involving the dsDNA molecule D2.

It is possible to gain insight into the DNA-binding selectivity of the three nickel complexes by comparing the relative abundance data present in Figure 4.11 and Figure 4.14. This reveals that the most abundant non-covalent complexes present in the spectra of solutions containing a 1:6 ratio of either D2 or Q4, and (10) are from [D2 + (10)] and [Q4 + (10)], respectively. This suggests that the binding affinity of (10) towards Q4 and D2 is quite similar. In contrast, complexes (7) and (13) appear to have a preference for binding to Q4 over D2, as the relative abundances of ions attributable to non-covalent complexes containing one or more molecules of (7) or (13) bound to Q4 are higher than for the analogous non-covalent complexes involving D2. This indicates that both (7) and (13) display a degree of binding selectivity in favour of Q4, which is greater than that exhibited by (10). Furthermore, the results obtained from the ESI-MS studies performed with both types of DNA

indicate that moving the ethyl piperidine groups from their locations in complex (13), to their positions in (7) did not improve selectivity towards Q4.

In order to further explore the effects of changing the location of the ethyl piperidine groups on DNA selectivity, CD spectra were obtained of solutions containing different ratios of Q4 and either (7), (10) or (13). These spectra are presented in Figure 4.15, while the changes in position and ellipticity of the CD bands are compiled in Table 4.4.

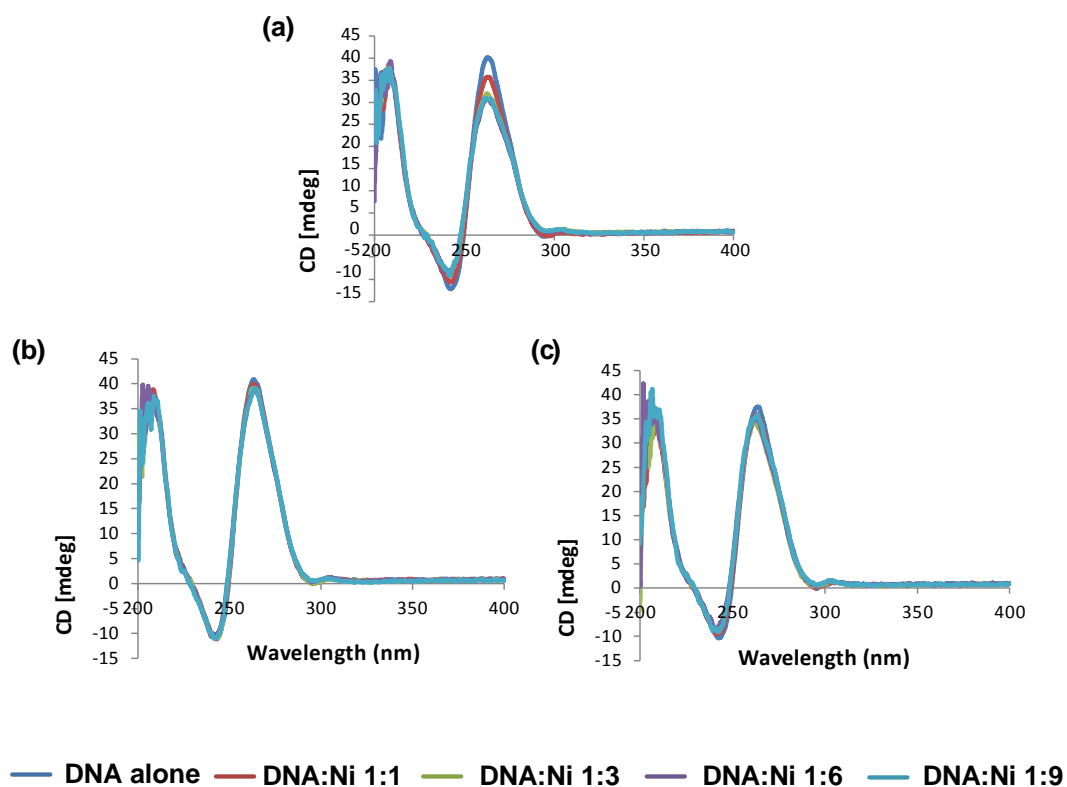


Figure 4.15: Circular dichroism spectra (200-400 nm) of solutions containing Q4 and different ratios of nickel Schiff base complexes. (a) Q4 + (7); (b) Q4 + (10); (c) Q4 + (13).

Table 4.4: Effect of addition of nickel Schiff base complexes on the CD spectrum of Q4.*

Nickel complex	Positive CD band at 264 nm		Negative CD band at 243 nm	
	$\Delta\lambda$ (nm)	$\Delta\epsilon$ (mdeg)	$\Delta\lambda$ (nm)	$\Delta\epsilon$ (mdeg)
(7)	-1.2	-9.2	-0.4	3.0
(10)	0.9	-1.7	-0.8	0.0
(13)	-0.1	-1.6	-0.3	1.3

* All $\Delta\lambda$ and $\Delta\epsilon$ values are the difference between the values for free DNA and those for a solution containing a DNA:nickel complex ratio of 1:9. Negative $\Delta\lambda$ values indicate a blue shift; positive values indicate a red shift. $\Delta\epsilon$ values are the difference between ϵ_{\max} for this CD band for the solution containing no metal complex, and ϵ_{\max} for the same CD band for the solution with the highest DNA:nickel complex ratio.

Inspection of the results shows that the addition of either (10) or (13) to Q4 had essentially no effect on the CD spectrum of the DNA. The absence of notable changes to the CD spectrum is perhaps not too surprising in the case of complex (10), as it showed the poorest ability to form non-covalent complexes with this quadruplex molecule in ESI-MS experiments. In contrast, complex (13) was shown to exhibit the highest affinity towards Q4, thereby making the absence of any effect it has on the CD spectrum of this quadruplex another example of a surprising result that can best be explained by reflecting on the differing abilities of the two analytical methods to differentiate complexes employing different binding modes.

Figure 4.15a shows that the effect of addition of (7) on the CD spectrum of Q4 is greater than that elicited by the other two complexes. Most notably, the ellipticity of the positive CD band decreased by 9.2 mdeg, which was by far the largest change observed. Complex (7) also had the largest effect on the CD spectrum of D2 (Figure 4.12). This suggests that complex (7) is able to interact in one or more ways with both Q4 and D2 that are different to that

used by other nickel complexes, and which results in the largest changes to the conformation of these DNA molecules.

4.2.3 DNA binding experiments performed using nickel complexes containing the *meso*-1,2-diphenylethylenediamine moiety

Previous work showed that nickel complex (**15**), containing the *meso*-1,2-diphenylethylenediamine moiety, exhibited a significant degree of DNA selectivity as a consequence of exhibiting a comparable ability to most other complexes of this type to bind to Q4, but essentially no ability to interact with D2.¹⁵⁶ It was therefore decided to synthesise complex (**12**), in which the two ethyl piperidine groups are located in different positions to those they occupy in (**15**), to see if this complex might retain the ability to bind to dsDNA conferred by the diamine moiety in the “top” of the Schiff base ligand, but more avidly bind to Q4. This section compares the DNA-binding properties of (**12**) and (**15**), whose structures are shown in Figure 4.16. It was initially hoped to also be able to extend this investigation to the third isomer, complex (**9**). However, the latter complex could not be obtained in sufficient purity to facilitate these additional studies.

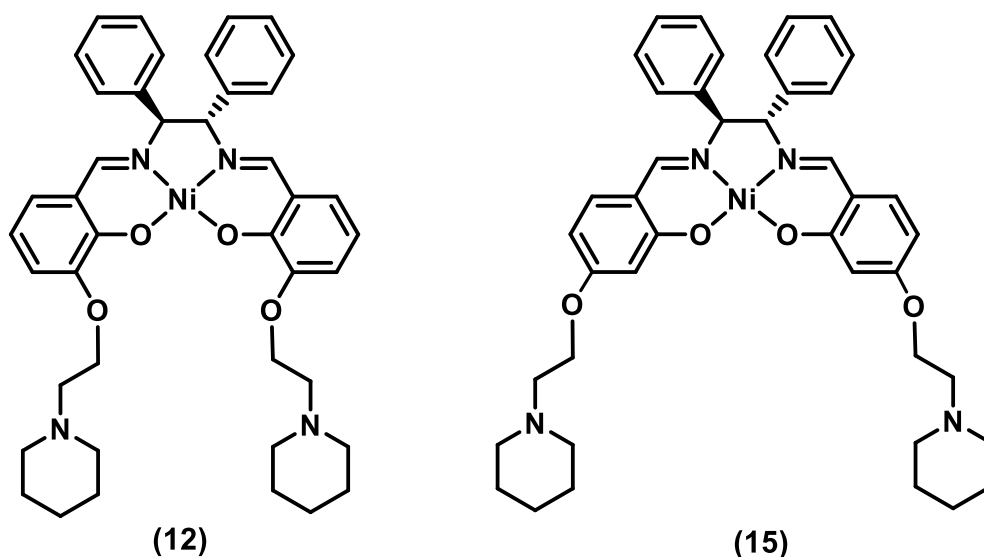


Figure 4.16: Structures of nickel Schiff base complexes containing the *meso*-1,2-diphenylethylenediamine moiety, whose binding to dsDNA and qDNA are explored in this section.

Initially ESI mass spectra were obtained of solutions containing a 1:6 ratio of D2 and the two different nickel complexes (Figure 4.17). Both spectra showed ions with high abundance at m/z 1626.6 from $[D2 - 6H]^{6-}$, as well as ions of low to medium abundance at 1952.0 from $[D2 - 5H]^{5-}$. In fact the spectra in Figure 4.17b and c are very similar to each other, and to the spectrum of the solution containing only D2, which is shown in Figure 4.17a. These observations support the view that neither (12) or (15) have significant affinity towards D2. This view is reinforced by the observation of ions of only low to very low abundance which can be attributed to the formation of non-covalent complexes between the nickel molecules and D2, and is consistent with the results of a published investigation into the affinity of complex (15) towards this dsDNA sequence.¹⁵⁶

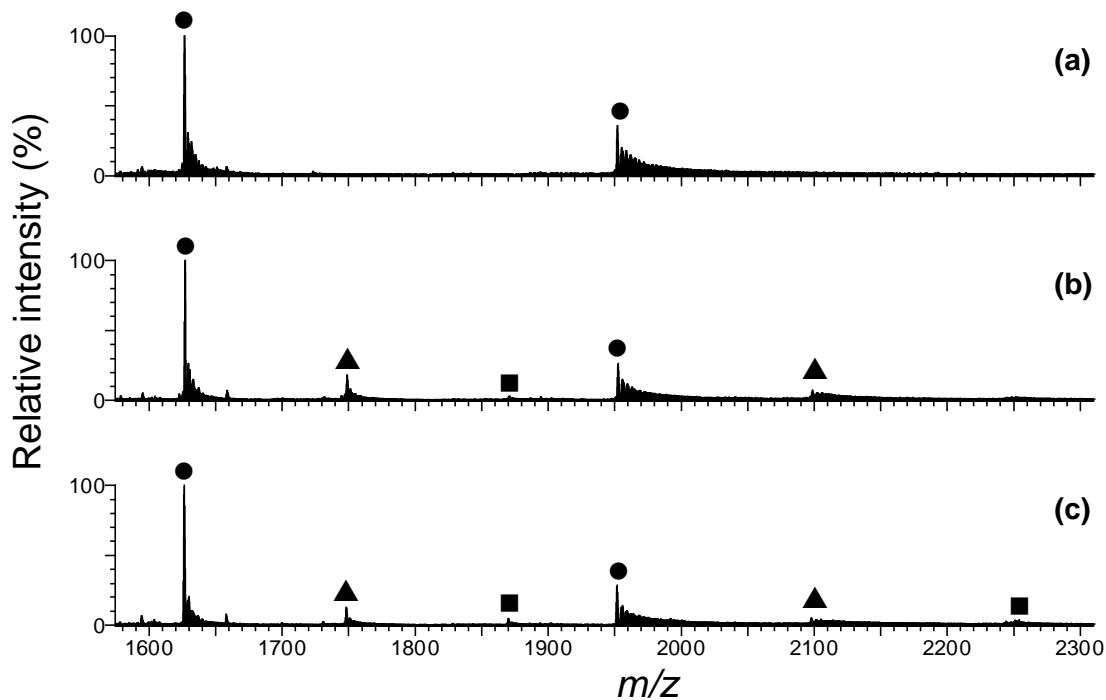


Figure 4.17: Negative ion ESI mass spectra of solutions containing D2 and different nickel Schiff base complexes at a 1:6 ratio. (a) Free D2; (b) D2 + (12); (c) D2 + (15). ● = free D2; ▲ = [D2 + (Ni)]; ■ = [D2 + 2(Ni)].

The results of the present study therefore both confirm the results of the previous study which showed that (15) exhibits very low affinity towards D2,¹⁵⁶ and also suggests that changing the position of the ethyl piperidine groups on the Schiff base ligand has little impact on the ability to bind to this type of nucleic acid molecule. Instead the results reaffirm the view that the presence of the non-planar *meso*-1,2-diphenylethylenediamine moiety prohibits strong interactions with D2, perhaps by hindering the approach of these molecule to the dsDNA to bind via partial intercalation or groove binding.

In order to provide further evidence that changing the position of the ethyl piperidine groups in (15) does not significantly affect affinity of the nickel molecule towards D2, CD spectra were obtained of solutions containing

different ratios of D2 and either (12) or (15). Figure 4.18 shows the CD spectra obtained of these solutions, while Table 4.5 present the changes in position and ellipticity of the individual CD bands of the nucleic acid caused by addition of 9 equivalents of the nickel complexes.

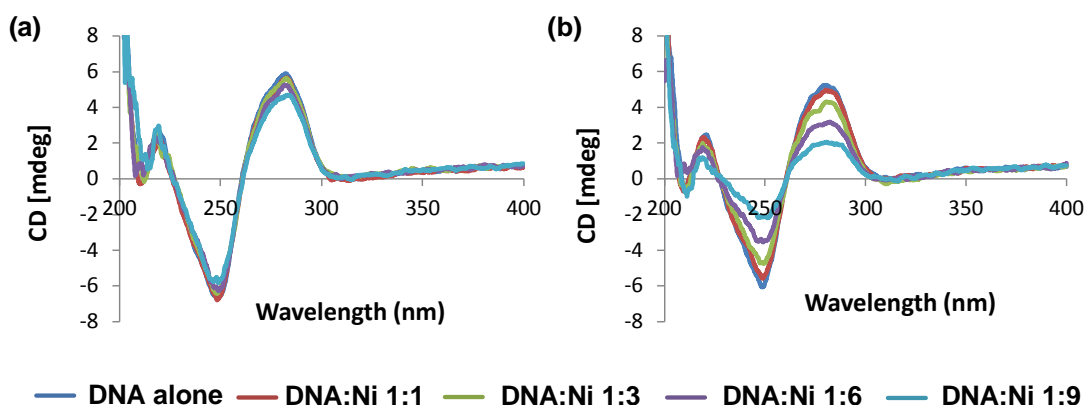


Figure 4.18: Circular dichroism spectra (200-400 nm) of solutions containing D2 and different ratios of nickel Schiff base complexes. (a) D2 + (12); (b) D2 + (15).

Table 4.5: Effect of addition of nickel Schiff base complexes on the CD spectrum of D2.*

<i>Nickel complex</i>	<i>Positive CD band at 282 nm</i>		<i>Negative CD band at 252 nm</i>	
	$\Delta\lambda$ (nm)	$\Delta\varepsilon$ (mdeg)	$\Delta\lambda$ (nm)	$\Delta\varepsilon$ (mdeg)
(12)	0.7	-1.2	0.6	0.9
(15)	1.4	-3.2	2.4	3.9

* All $\Delta\lambda$ and $\Delta\varepsilon$ values are the difference between the values for free DNA and those for a solution containing a DNA:nickel complex ratio of 1:9. Negative $\Delta\lambda$ values indicate a blue shift; positive values indicate a red shift. $\Delta\varepsilon$ values are the difference between ε_{\max} for this CD band for the solution containing no metal complex, and ε_{\max} for the same CD band for the solution with the highest DNA:nickel complex ratio.

Addition of complex (12) had only a minor effect on the CD spectrum of D2, as expected, since this complex showed little ability to bind to D2 in the ESI-

MS experiments. In contrast, the addition of **(15)** did have a significant effect on both major CD bands of the nucleic acid. This was a surprising result, as **(15)** also showed a very poor ability to form non-covalent complexes in the solutions used to obtain ESI mass spectra. The observation that complex **(15)** did cause significant changes to the CD spectrum of D2, whereas addition of **(12)** did not, again highlights the high degree of sensitivity of CD spectroscopy to what are perhaps small differences in how different metal complexes affect the conformation of nucleic acids. It is worthwhile noting that the change in ellipticity of the positive band of D2 caused by addition of **(15)** was greater than that caused by addition of any of the other nickel complexes investigated in this study. For example, the decrease in ellipticity of the positive CD band of D2 caused by addition of **(15)** (3.2 mdeg) was almost double that observed upon addition of the same amount of either **(7)**, **(8)**, **(11)** or **(14)**. Addition of **(15)** also resulted in a larger change to the ellipticity of the negative CD band of D2 than that caused by any of the other nickel complexes investigated in this thesis, with the exception of complex **(14)**, which resulted in an equivalent change.

The results in the previous section indicate that changing the location of the ethyl piperidine groups from where they are situated in complex **(15)**, to their positions in **(12)**, did not change the very low affinity exhibited by the former complex towards a typical dsDNA molecule. This meant that if this change in structure resulted in an increase in affinity towards Q4, compared to that exhibited by **(15)**, then complex **(12)** could be considered to display a greater degree of DNA-binding selectivity.

To investigate this possibility, ESI mass spectra were obtained of solutions containing Q4 and either (12) or (15) at a DNA:nickel complex ratio of 1:6. The spectrum of the solution containing Q4 and (12) (Figure 4.19b), shows ions from free DNA with low and medium abundance at m/z 1675.4 and 2010.7, respectively. These ions do not, however, appear in the spectrum of the solution containing Q4 and (15). This observation, combined with the lower abundance of ions from $[Q4 + 2(Ni)]$ in Figure 4.19b, compared to that of analogous ions in Figure 4.19c, indicates that (12) has a slightly lower affinity towards Q4 than (15).

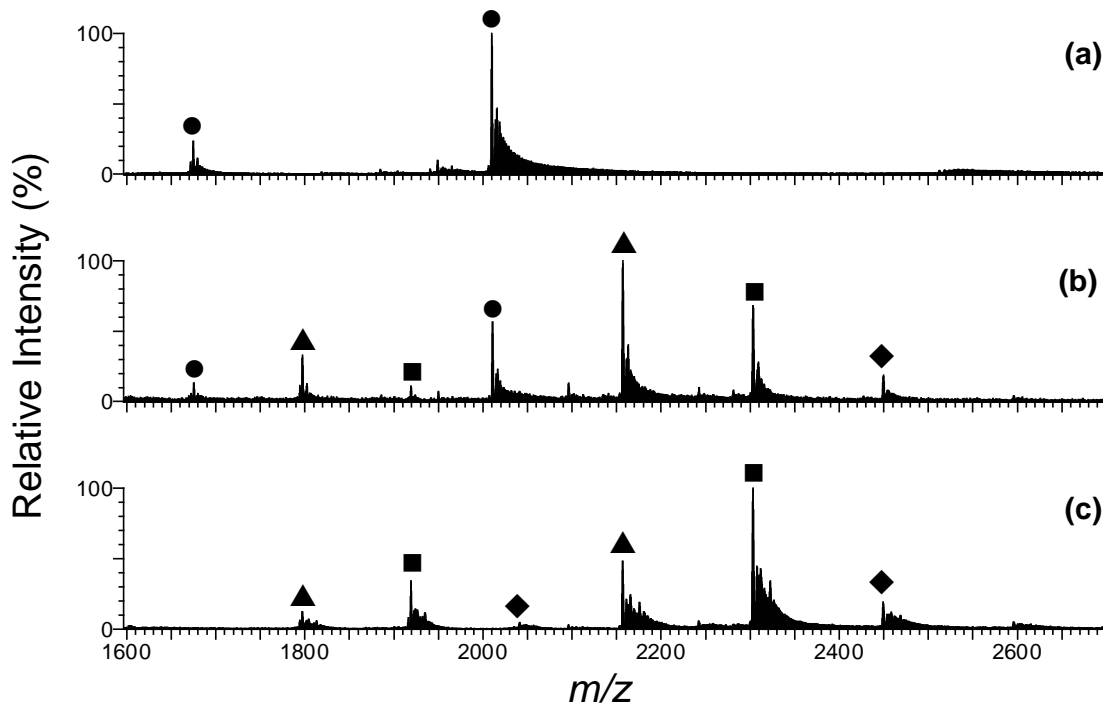


Figure 4.19: Negative ion ESI mass spectra of solutions containing Q4 and different nickel Schiff base complexes at a 1:6 ratio. (a) Free Q4; (b) Q4 + (12); (c) Q4 + (15). ● = free Q4; ▲ = $[Q4 + (Ni)]$; ■ = $[Q4 + 2(Ni)]$; ◆ = $[Q4 + 3(Ni)]$.

The results presented in Figure 4.17 and Figure 4.19 therefore suggest that changing the location of the ethyl piperidine groups, from where they are in complex (12), to where they are in (15), did have a small, but favourable effect on selectivity for Q4. In order to test this conclusion, CD spectra were obtained of solutions containing different ratios of either (12) or (15) and Q4, and are presented in Figure 4.20. Table 4.6 summarises the changes to the position and ellipticity of both CD bands caused by addition of the two nickel complexes.

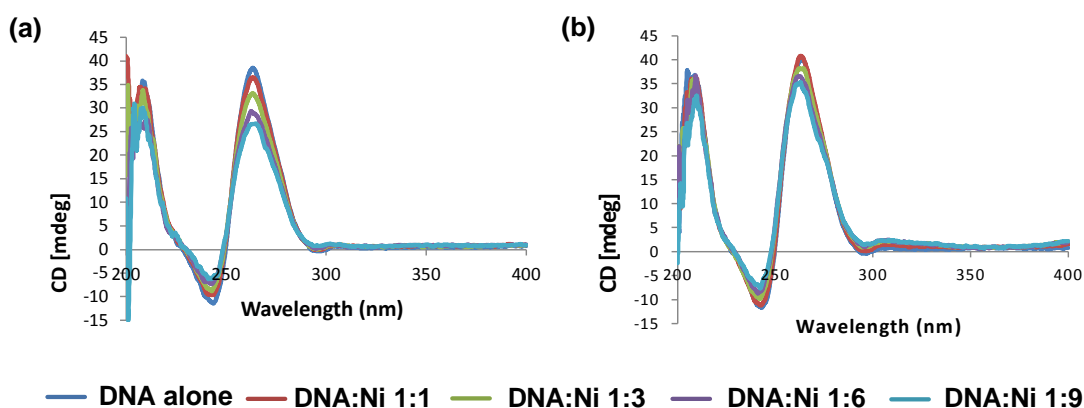


Figure 4.20: Circular dichroism spectra (200-400 nm) of solutions containing different ratios of Q4 and nickel Schiff base complexes. (a) Q4 + (12); (b) Q4 + (15).

Table 4.6: Effect of addition of nickel Schiff base complexes on the CD spectrum of Q4.*

<i>Nickel complex</i>	<i>Positive CD band at 264 nm</i>		<i>Negative CD band at 243 nm</i>	
	$\Delta\lambda$ (nm)	$\Delta\epsilon$ (mdeg)	$\Delta\lambda$ (nm)	$\Delta\epsilon$ (mdeg)
(12)	1.5	-11.8	-1.2	5.1
(15)	-1.0	-4.8	-0.7	4.1

* All $\Delta\lambda$ and $\Delta\epsilon$ values are the difference between the values for free DNA and those for a solution containing a DNA:nickel complex ratio of 1:9. Negative $\Delta\lambda$ values indicate a blue shift; positive values indicate a red shift. $\Delta\epsilon$ values are the difference between ϵ_{\max} for this CD band for the solution containing no metal complex, and ϵ_{\max} for the same CD band for the solution with the highest DNA:nickel complex ratio.

Figure 4.20 reveals that the addition of increasing amounts of either **(12)** or **(15)** to a solution of Q4 resulted in small changes to the CD spectrum of the nucleic acid. Surprisingly, it was found that the changes to the position of the CD bands caused by addition of **(12)** were greater than that caused by addition of **(15)** (Table 4.6). This suggests that **(12)** may exhibit a higher binding affinity than **(15)** toward Q4, which contrasts with the conclusion reached on the basis of the results obtained from the ESI-MS study. Most notable was the significant decrease in ellipticity of the positive CD band of 11.8 mdeg caused by addition of 9 equivalents of **(12)** (Table 4.6). In contrast, addition of **(15)** only changed the ellipticity of this CD band by 4.8 mdeg. This therefore represents one final example where the results obtained from DNA-binding studies performed using the two different instrumental methods must be interpreted with caution, as they most likely provide information about different aspects of the metal complex/DNA interaction.

CHAPTER 5 CONCLUSIONS

The ability of nickel Schiff base complexes to bind selectively to quadruplex DNA has attracted significant attention in recent years. This is a consequence of their ease of synthesis, and the combination of structural and electronic properties that endow upon them the ability to bind effectively to these nucleic acid secondary structures. Previous investigations in this area have focussed on the DNA-binding interactions of complexes such as (13), (14) and (15), which were prepared via a two-step procedure that involved initially the reaction between different diamines and 2,4-dihydroxybenzaldehyde, in the presence of nickel(II).^{156,157} Subsequently the hydroxyl groups present in the resulting compounds were derivatised using 1-(2-chloroethyl) piperidine hydrochloride to afford nickel complexes with sufficient water solubility for studying their DNA-binding behaviour in aqueous solution. It was shown that changing the diamine used in the initial step of the synthetic procedure can have a significant effect on affinity towards either or both dsDNA and qDNA.¹⁵⁶

One aspect of the structure of the above complexes, whose effect on DNA-binding properties had not been examined previously, was the location of the ethyl piperidine moieties on the Schiff base ligand. The current investigation into the effect of such alterations was prompted by both the absence of information concerning the effects of such changes, and the knowledge that the ethyl piperidine groups have been shown to play a significant role in interactions with quadruplex DNA structures.¹⁵⁴ Therefore, the overall aim of

this thesis was to use a combination of two different techniques, ESI-MS and CD spectroscopy, to investigate the effects of varying the position of the ethyl piperidine groups in the nickel Schiff base complexes, on their abilities to bind to a duplex 16mer DNA molecule and a tetramolecular DNA quadruplex. Over the course of this project five novel alkylated nickel Schiff base complexes were prepared, which featured ethyl piperidine moieties in different locations to those in previously studied compounds. All new compounds were synthesised in high purity, and characterised using NMR spectroscopy, ESI-MS and microanalysis. In addition, the solid-state structures of two of these nickel complexes, as well as one of the precursor complexes, were determined by single crystal X-ray diffraction methods.

ESI-MS and CD spectroscopy were both used to assess the extent of binding interactions between the nickel complexes and DNA. In the case of ESI-MS, it was assumed that the abundance of ions from non-covalent complexes containing different numbers of nickel molecules bound to DNA would reflect the extent of the binding interactions, and could be used to determine relative orders of binding affinity. Addition of the nickel complexes in some instances produced changes to the position and, in particular the ellipticity, of the principal features in the CD spectra of D2 and Q4. The magnitudes of these changes were also used to determine relative orders of binding affinity, that were then compared to those determined from ESI mass spectra.

On some occasions both the ESI-MS and CD spectroscopic results gave essentially the same conclusions regarding the impact of changing the location of the ethyl piperidine moieties on DNA-binding properties. For

example, variations in the relative abundances of ions from non-covalent complexes observed in ESI mass spectra, and changes to the ellipticity of the positive CD band of D2, both suggested that the affinity of complex (14) for this DNA molecule was at least as great as, if not greater than, that of the two isomeric molecules (8) and (11). Addition of (14) did produce a small blue shift for this CD signal, in contrast to the red shifts observed upon addition of the other two nickel complexes, perhaps suggesting some subtle differences in their modes of DNA binding. Overall, however, it appeared that changing the position of the ethyl piperidine groups from their positions in the previously studied complex (14) had only a small effect on affinity towards the dsDNA molecule D2.

The results of ESI-MS studies into the binding of the other two series of nickel complexes to D2 also suggested that changing the position of the ethyl piperidine moieties from where they are located in the two lead complexes, ((13) and (15)) did not enhance affinity towards this dsDNA molecule. For the complexes prepared using ethylenediamine as one of the starting materials, the relative abundances of ions from non-covalent complexes containing one or more molecules of (13) bound to D2 was greater than that for analogous ions containing either (7) or (10). This suggests that changing the location of the ethyl piperidine moieties from their location in (13) was in fact detrimental to the ability of the complex to bind to dsDNA. A different conclusion was reached upon analysis of the changes observed to the CD spectrum of D2 when (7), (10) or (13) was added, as it was the former nickel complex which had the greatest effect. As expected complexes (12) and (15), which were

both prepared via synthetic routes involving *meso*-1,2-diphenylethylenediamine as one of the starting materials, exhibited essentially no ability to form non-covalent complexes with D2 in ESI mass spectral experiments. This suggests that neither complex exhibits a significant ability to bind to dsDNA. Surprisingly, however, addition of **(15)** resulted in the biggest changes to the CD spectrum of D2 of any of the nickel complexes examined.

In order to develop an understanding of the origin of variations in binding affinities derived by the two techniques, such as those discussed above, it is important to reflect upon differences between the two instrumental techniques used. In the case of mass spectrometry, the spectra obtained show ions from non-covalent complexes which have sufficient stability to pass from the solution to the gas phase. It has been proposed that electrostatic interactions may play an important role in maintaining non-covalent complexes during the ESI process and in the gas phase, and therefore be a contributing factor to the differences with the DNA-binding results obtained via the two methods.¹⁸⁰ Essentially, two different non-covalent complexes with the same stability as reflected in an overall binding constant, may exhibit different relative abundances of ions in ESI mass spectra, if the contributions of electrostatic interactions to their overall stability vary. In contrast, CD spectroscopy is uniquely sensitive to the effects that binding of small molecules can have on the chirality of DNA molecules. Therefore even a relatively minor component of the overall binding interaction between a nickel molecule and D2 can result in large changes to the CD

spectrum of the latter, or another type of DNA molecule, if the interaction alters the helicity of the nucleic acid. It is not a requirement for such binding interactions to survive on being transferred from solution to the gas phase, in order for its effects to become apparent in a CD spectrum.

Differences between orders of binding affinity determined on the basis of ESI-MS and CD experiments were even more prevalent amongst studies conducted using the tetramolecular quadruplex Q4. The results of binding studies performed using mass spectrometry suggested that for two of the three series of complexes studied it was the lead nickel complex, prepared using a synthetic pathway that employed 2,4-dihydroxybenzaldehyde, which exhibited the highest binding affinity. For the complexes containing an ethylenediamine moiety, complex (13) showed a greater ability to form non-covalent complexes with Q4 than either (7) or (10), while for those featuring the 1,2-*meso*-diphenylethylenediamine moiety in the “top” of the molecule, complex (15) proved to have a higher affinity than (12). The results of the binding experiments performed using CD spectroscopy yielded a different perspective for both series of complexes. Complex (7), prepared via a pathway that involved 2,5-dihydroxybenzaldehyde, had a bigger impact on the CD spectrum of Q4 than either (10) or (13), mimicking the results obtained in binding studies involving D2. Addition of (15) to a solution of Q4 did not affect the CD spectrum of the latter as much as the introduction of (12), which was prepared using 2,3-dihydroxybenzaldehyde as one of the initial reactants. This result is in direct contrast to what was expected on the basis of the ESI-MS studies of these systems. The series of complexes

containing the phenylenediamine moiety in the “top” of the Schiff base ligand also produced different results in ESI-MS and CD experiments involving Q4. On this occasion, the results of the CD investigation showed that the isomer prepared using 2,4-dihydroxybenzaldehyde, complex **(14)**, had the biggest impact, thereby suggesting it may have the greatest binding affinity. In contrast, the results of the ESI-MS study performed using this series of three nickel complexes indicated that **(11)** was more capable of forming non-covalent complexes with Q4, than either **(8)** or **(14)**. The results of ESI-MS experiments performed using this triad of nickel complexes, and both types of DNA molecules, suggest that **(11)** may have a greater degree of binding selectivity in favour of Q4 over D2, than either of the other complexes. However, the changes observed to the CD spectra of Q4, in particular, cast doubt over this assessment. It should be noted that where binding is predominantly stabilised by hydrophobic interactions, such as end-stacking on a tetramolecular qDNA, it is thought that such interactions are either unchanged in strength or weakened relative to electrostatic interactions.¹⁸⁰ End-stacking has been observed for the binding of the anthracycline, daunomycin, to a molecule similar to Q4.¹¹⁵

The results of the ESI-MS investigations carried out as part of this study suggest that, in general, changing the location of the ethyl piperidine moieties on the Schiff base ligand did not have a great effect on affinity for either type of DNA molecule. Most of the new nickel complexes, with the exception of **(12)**, showed a significant ability to form non-covalent complexes with D2 and Q4, indicating a notable degree of binding affinity. In the case of **(12)**, ESI

mass spectra of solutions containing this nickel complex and D2 were almost completely devoid of ions arising from non-covalent complexes formed between the metal complex and dsDNA molecule. This was not unexpected as complex (**15**), which also features the 1,2-*meso*-diphenylethylenediamine moiety in the “top” of the Schiff base ligand, was shown previously by a variety of methods to have a very low affinity towards dsDNA molecules.¹⁵⁶ Incorporation of this structural unit into the Schiff base ligand therefore appears to consistently have a far more significant impact upon DNA binding, at least in the case of the dsDNA molecule D2, than changing the location of the ethyl piperidine moieties.

In some instances the magnitude of changes to the CD spectrum of D2 and Q4 were generally consistent with what would be predicted using DNA affinities based on ESI-MS studies of the same systems. However, on many occasions there were significant discrepancies between DNA binding affinities based on relative ion abundances on the one hand, and the magnitude of changes to the ellipticity of CD signals arising from DNA, on the other. It should be noted that addition of nickel complexes resulted in changes to both the position and ellipticity of the CD signals arising from D2 and Q4. However, the magnitude of the red and blue shifts of the CD bands was always very small, suggesting that the strength of the overall binding interactions may not be that great, and that this parameter is unlikely to be an accurate measure of subtle changes in binding affinities. In contrast, on some occasions very large changes to the ellipticity of the CD bands were

observed, including where the results of ESI-MS investigations into the same system did not suggest a strong overall binding interaction.

The above observations highlight that care must be taken when interpreting in isolation the results of DNA-binding studies performed using different techniques. ESI-MS and CD spectroscopy may be uniquely suited to providing information about different aspects of the metal complex/DNA interaction. CD spectroscopy can probe subtle changes in binding mode but offers a view of only bulk solution effects. ESI-MS allows for high-throughput screening, and is suitable for small sample sizes and allows observation of all species present in the sample. Under some conditions, the disadvantage of ESI-MS may be in comparing the abundances of complexes where the relative contributions of hydrophobic versus electrostatic interactions are vastly different, and one type predominates to a great extent over the other. The fact that different techniques for observing snapshots of equilibria have different advantages and disadvantages is not surprising.

It is therefore recommended that other spectroscopic techniques commonly applied to examining metal complex/DNA interactions be used to explore the systems presented in this thesis. Absorption spectrophotometry, which can be used to provide a measure of the overall strength of binding interactions in the form of a binding constant, and fluorescence resonance energy transfer (FRET) spectroscopy, which affords this information in the form of changes to the melting temperature of a DNA molecule, are two such methods widely used by the bio-inorganic chemistry community for this purpose. It would be particularly interesting to see if these methods afforded orders of binding

affinity that match more closely those derived here using ESI-MS or CD spectroscopy. If this were to prove to be the case, it would not necessarily follow that the other technique should be abandoned for examining these binding interactions. In contrast, it may allow a stronger focus to be turned to those aspects of the overall interaction that are highlighted by different spectroscopic methods.

CHAPTER 6 REFERENCES

- (1) Hurley, L. H.; Boyd, F. L. *Trends in Pharmacological Sciences* **1988**, *9*, 402-407.
- (2) O'Connor, C. J.; Denny, W. A.; Fan, J. Y.; Gravatt, G. L.; Grigor, B. A.; McLennan, D. J. *J. Chem. Soc., Perkin Trans. 2*. **1991**, 1933-1939.
- (3) Noll, D. M.; McGregor Mason, T.; Miller, P. S. *Chem. Rev.* **2006**, *106*, 277-301.
- (4) Rajski, S. R.; Williams, R. M. *Chem. Rev.* **1998**, *98*, 2723-2795.
- (5) Osborn, M. J.; Freeman, M.; Huennekens, F. M. *Proceedings of the Society for Experimental Biology and Medicine* **1958**, *97*, 429-431.
- (6) Osborn, M. J.; Huennekens, F. M. *The Journal of biological chemistry* **1958**, *233*, 969-974.
- (7) Nygren, P. *Acta oncologica (Stockholm, Sweden)* **2001**, *40*, 166-174.
- (8) Berenblum, I. *Journal of Pathology and Bacteriology* **1935**, *40*, 549-558.
- (9) Goodman, L. S.; Wintrobe, M. M.; Dameshek, W.; Goodman, M. J.; Gilman, A.; McLennan, M. T. *J. Am. Med. Assoc.* **1946**, *132*, 126-132.
- (10) Marshall, E. K., Jr. *Advan. Chemotherapy* **1964**, *1*, 1-8.
- (11) Krumbhaar, E. B.; Krumbhaar, H. D. *The Journal of medical research* **1919**, *40*, 497-508 493.
- (12) Gilman, A. *Federation Proceedings* **1946**, *5*, 285-292.
- (13) Gilman, A.; Philips, F. S. *Science (New York, N.Y.)* **1946**, *103*, 409-415.
- (14) Kitta, K.; Ohnishi-Kameyama, M.; Moriyama, T.; Ogawa, T.; Kawamoto, S. *Analytical Biochemistry* **2006**, *351*, 290-297.
- (15) Watson, J. D.; Crick, F. H. *Nature* **1953**, *171*, 737-738.
- (16) Watson, J. D.; Crick, F. H. C. *Nature* **1953**, *171*, 964-967.
- (17) Kowalczyk, A.; Carmical, J. R.; Zou, Y.; Van Houten, B.; Lloyd, R. S.; Harris, C. M.; Harris, T. M. *Biochemistry* **2002**, *41*, 3109-3118.

- (18) Farber, S.; Diamond, L. K.; Mercer, R. D.; Sylvester, R. F., Jr.; Wolff, J. A. *New England Journal of Medicine* **1948**, *238*, 787-793.
- (19) Bertino, J. R. *Cancer* **1979**, *43*, 2137-2142.
- (20) Hertz, R.; Li, M. C.; Spencer, D. B. *Proceedings of the Society for Experimental Biology and Medicine* **1956**, *93*, 361-366.
- (21) Rosenberg, B.; VanCamp, L.; Trosko, J. E.; Mansour, V. H. *Nature* **1969**, *222*, 385-386.
- (22) Rosenberg, B.; Van Camp, L.; Krigas, T. *Nature* **1965**, *205*, 698-699.
- (23) Rosenberg, B. *Platinum Metals Review* **1971**, *15*, 42-51.
- (24) Pinto, A. L.; Lippard, S. J. *Biochimica et Biophysica Acta, Reviews on Cancer* **1985**, *780*, 167-180.
- (25) Van der Veer, J. L.; Reedijk, J. *Chemistry in Britain* **1988**, *24*, 775-780.
- (26) Johnson, N. P.; Butour, J. L.; Villani, G.; Wimmer, F. L.; Defais, M.; Pierson, V.; Brabec, V. *Progress in Clinical Biochemistry and Medicine* **1989**, *10*, 1-24.
- (27) Takahara, P. M.; Frederick, C. A.; Lippard, S. J. *Journal of the American Chemical Society* **1996**, *118*, 12309-12321.
- (28) Hambley, T. W. *Journal of the Chemical Society, Dalton Transactions* **2001**, 2711-2718.
- (29) Bose, R. N. *Mini-Reviews in Medicinal Chemistry* **2002**, *2*, 103-111.
- (30) Reedijk, J. *Proc. Natl. Acad. Sci.* **2003**, *100*, 3611-3616.
- (31) Wang, D.; Lippard, S. J. *Nature Reviews Drug Discovery* **2005**, *4*, 307-320.
- (32) Jung, Y.; Lippard, S. J. *Chem. Rev.* **2007**, *107*, 1387-1407.
- (33) Pizarro, A. M.; Sadler, P. J. *Biochimie* **2009**, *91*, 1198-1211.
- (34) Heby, O.; Persson, L. *Trends in Biochemical Sciences* **1990**, *15*, 153-158.
- (35) Tamori, A.; Nishiguchi, S.; Kuroki, T.; Koh, N.; Kobayashi, K.; Yano, Y.; Otani, S. *Cancer Research* **1995**, *55*, 3500-3503.
- (36) Auvinen, M.; Paasinen, A.; Andersson, L. C.; Holtta, E. *Nature* **1992**, *360*, 355-358.
- (37) Janne, J.; Alhonen, L.; Leinonen, P. *Ann. Med.* **1991**, *23*, 241-259.

- (38) Bonetti, A.; Franceschi, T.; Apostoli, P.; Messori, A.; Sperotto, L.; Cetto, G. L.; Molino, A.; Leone, R. *Therapeutic Drug Monitoring* **1995**, *17*, 25-32.
- (39) Lehman, M.; Thomas, G. *Int J. Gynecol. Cancer* **2001**, *11*, 87-99.
- (40) Loehrer, P. J.; Einhorn, L. H. *Ann. Intern Med.* **1984**, *100*, 704-713.
- (41) Ozols, R. F. *Seminars in Oncology* **1995**, *22*, 61-66.
- (42) Rabik, C. A.; Dolan, M. E. *Cancer Treatment Reviews* **2007**, *33*, 9-23.
- (43) Reedijk, J. *ACS Symposium Series* **2005**, *903*, 80-109.
- (44) Wong, E.; Giandomenico, C. M. *Chem. Rev.* **1999**, *99*, 2451-2466.
- (45) Hamilton, A.; Gallipoli, P.; Nicholson, E.; Holyoake, T. L. *Journal of Pathology* **2010**, *220*, 404-418.
- (46) Dervan, P. B. *Bioorganic & Medicinal Chemistry* **2001**, *9*, 2215-2235.
- (47) Richards, A. D.; Rodger, A. *Chemical Society Reviews* **2007**, *36*, 471-483.
- (48) Martinez, R.; Chacon-Garcia, L. *Current Medicinal Chemistry* **2005**, *12*, 127-151.
- (49) Franklin, R. E.; Gosling, R. G. *Nature* **1953**, *172*, 156-157.
- (50) Behe, M.; Felsenfeld, G. *Proc. Natl. Acad. Sci.* **1981**, *78*, 1619-1623.
- (51) Ramstein, J.; Leng, M. *Nature* **1980**, *288*, 413-414.
- (52) Keene, F. R.; Smith, J. A.; Collins, J. G. *Coordination Chemistry Reviews* **2009**, *253*, 2021-2035.
- (53) Biver, T. *Coordination Chemistry Reviews* **2013**, *257*, 2765-2783.
- (54) Nucleic acid structure. https://www.wikipedia.org/wiki/Nucleic_acid_structure (accessed 26/08/2014).
- (55) Suram, A.; Rao, J. K. S.; Latha, K. S.; Viswamitra, M. A. *NeuroMolecular Medicine* **2002**, *2*, 289-297.
- (56) Zeglis, B. M.; Pierre, V. C.; Barton, J. K. *Chem. Commun.* **2007**, 4565-4579.
- (57) Bischoff, G.; Hoffmann, S. *Current Medicinal Chemistry* **2002**, *9*, 321-348.

- (58) Gupta, R.; Beck, J. L.; Ralph, S. F.; Sheil, M. M.; Aldrich-Wright, J. R. *Journal of the American Society for Mass Spectrometry* **2004**, *15*, 1382-1391.
- (59) Blackburn, G. M.; Gait, M. J.; Editors: *Nucleic Acids in Chemistry and Biology*, Oxford University Press, Oxford: UK, 1990.
- (60) Ghosh, I.; Stains, C. I.; Ooi, A. T.; Segal, D. J. *Molecular BioSystems* **2006**, *2*, 551-560.
- (61) Nelson, S. M.; Ferguson, L. R.; Denny, W. A. *Mutation Research, Fundamental and Molecular Mechanisms of Mutagenesis* **2007**, *623*, 24-40.
- (62) Wemmer, D. E. *Biopolymers* **2001**, *52*, 197-211.
- (63) Streckowski, L.; Wilson, B. *Mutation Research, Fundamental and Molecular Mechanisms of Mutagenesis* **2007**, *623*, 3-13.
- (64) Lippard, S. J. *Accounts of Chemical Research* **1978**, *11*, 211-217.
- (65) Cashman, D. J.; Scarsdale, J. N.; Kellogg, G. E. *Nucleic Acids Research* **2003**, *31*, 4410-4416.
- (66) Beck, J. L.; Colgrave, M. L.; Ralph, S. F.; Sheil, M. M. *Mass Spectrometry Reviews* **2001**, *20*, 61-87.
- (67) Rabbani, A.; Finn, R. M.; Ausio, J. *BioEssays* **2004**, *27*, 50-56.
- (68) Patel, D. J.; Phan, A. T.; Kuryavyi, V. *Nucleic Acids Research* **2007**, *35*, 7429-7455.
- (69) Neidle, S.; Parkinson, G. N. *Current Opinion in Structural Biology* **2003**, *13*, 275-283.
- (70) Wang, Y.; Patel, D. J. *Biochemistry* **1992**, *31*, 8112-8119.
- (71) Wang, Y.; Patel, D. J. *Journal of Molecular Biology* **1993**, *234*, 1171-1183.
- (72) Laughlan, G.; Murchie, A. I. H.; Norman, D. G.; Moore, M. H.; Moody, P. C. E.; Lilley, D. M.; Luisi, B. *Science (New York, N.Y.)* **1994**, *265*, 520-524.
- (73) Wheelhouse, R. T.; Sun, D.; Han, H.; Han, F. X.; Hurley, L. H. *Journal of the American Chemical Society* **1998**, *120*, 3261-3262.
- (74) Sun, D.; Thompson, B.; Cathers, B. E.; Salazar, M.; Kerwin, S. M.; Trent, J. O.; Jenkins, T. C.; Neidle, S.; Hurley, L. H. *Journal of Medicinal Chemistry* **1997**, *40*, 2113-2116.

- (75) Fedoroff, O. Y.; Salazar, M.; Han, H.; Chemeris, V. V.; Kerwin, S. M.; Hurley, L. H. *Biochemistry* **1998**, *37*, 12367-12374.
- (76) Bryan, T. M.; Cech, T. R. *Current Opinion in Cell Biology* **1999**, *11*, 318-324.
- (77) McEachern, M. J.; Krauskopf, A.; Blackburn, E. H. *Annual Review of Genetics* **2000**, *34*, 331-358.
- (78) Schaffitzel, C.; Berger, I.; Postberg, J.; Hanes, J.; Lipps, H. J.; Plueckthun, A. *Proc. Natl. Acad. Sci.* **2001**, *98*, 8572-8577.
- (79) Smolikov, S.; Mazor, Y.; Krauskopf, A. *Proc. Natl. Acad. Sci.* **2004**, *101*, 1656-1661.
- (80) Shay, J. W.; Bacchetti, S. *European journal of cancer (Oxford, England : 1990)* **1997**, *33*, 787-791.
- (81) Kim, N. W.; Piatyszek, M. A.; Prowse, K. R.; Harley, C. B.; West, M. D.; Ho, P. L. C.; Coviello, G. M.; Wright, W. E.; Weinrich, S. L.; Shay, J. W. *Science (New York, N.Y.)* **1994**, *266*, 2011-2015.
- (82) Zaug, A. J.; Podell, E. R.; Cech, T. R. *Proc. Natl. Acad. Sci. USA.* **2005**, *102*, 10864-10869.
- (83) Neidle, S.; Parkinson, G. *Nat. Rev. Drug Discov.* **2002**, *1*, 383-393.
- (84) Qin, Y.; Hurley, L. H. *Biochimie* **2008**, *90*, 1149-1171.
- (85) Bugaut, A.; Balasubramanian, S. *Biochemistry* **2008**, *47*, 689-697.
- (86) Hazel, P.; Huppert, J.; Balasubramanian, S.; Neidle, S. *Journal of the American Chemical Society* **2004**, *126*, 16405-16415.
- (87) Zhang, A. Y. Q.; Bugaut, A.; Balasubramanian, S. *Biochemistry* **2011**, *50*, 7251-7258.
- (88) Rachwal, P. A.; Brown, T.; Fox, K. R. *Biochemistry* **2007**, *46*, 3036-3044.
- (89) Han, H.; Hurley, L. H. *Trends in Pharmacological Sciences* **2000**, *21*, 136-142.
- (90) Nelson, S. M.; Ferguson, L. R.; Denny, W. A. *Cell & Chromosome* **2004**, *3*, 1-26.
- (91) Catasti, P.; Chen, X.; Moyzis, R. K.; Bradbury, E. M.; Gupta, G. *Journal of Molecular Biology* **1996**, *264*, 534-545.

- (92) Verkerk, A. J. M. H.; Pieretti, M.; Sutcliffe, J. S.; Fu, Y. H.; Kuhl, D. P. A.; Pizzuti, A.; Reiner, O.; Richards, S.; Victoria, M. F.; et al. *Cell* **1991**, *65*, 905-913.
- (93) Kotin, R. M.; Siniscalco, M.; Samulski, R. J.; Zhu, X. D.; Hunter, L.; Laughlin, C. A.; McLaughlin, S.; Muzyczka, N.; Rocchi, M.; Berns, K. I. *Proc Natl Acad Sci* **1990**, *87*, 2211-2215.
- (94) Verma, A.; Halder, K.; Halder, R.; Yadav, V. K.; Rawal, P.; Thakur, R. K.; Mohd, F.; Sharma, A.; Chowdhury, S. *Journal of Medicinal Chemistry* **2008**, *51*, 5641-5649.
- (95) Siddiqui-Jain, A.; Grand, C. L.; Bearss, D. J.; Hurley, L. H. *Proc. Natl. Acad. Sci.* **2002**, *99*, 11593-11598.
- (96) Kumari, S.; Bugaut, A.; Huppert, J. L.; Balasubramanian, S. *Nature Chemical Biology* **2007**, *3*, 218-221.
- (97) Boan, F.; Gomez-Marquez, J. *ChemBioChem* **2010**, *11*, 331-334.
- (98) Mani, P.; Yadav Vinod, K.; Das Swapan, K.; Chowdhury, S. *PloS one* **2009**, *4*, e4399.
- (99) Paeschke, K.; Capra, J. A.; Zakian, V. A. *Cell* **2011**, *145*, 678-691.
- (100) Williamson, J. R. *Annual Review of Biophysics and Biomolecular Structure* **1994**, *23*, 703-730.
- (101) Li, J.; Correia, J. J.; Wang, L.; Trent, J. O.; Chaires, J. B. *Nucleic Acids Research* **2005**, *33*, 4649-4659.
- (102) Tang, J.; Kan, Z.-y.; Yao, Y.; Wang, Q.; Hao, Y.-h.; Tan, Z. *Nucleic Acids Research* **2008**, *36*, 1200-1208.
- (103) Read, M.; Harrison, R. J.; Romagnoli, B.; Tanious, F. A.; Gowan, S. H.; Reszka, A. P.; Wilson, W. D.; Kelland, L. R.; Neidle, S. *Proc. Natl. Acad. Sci.* **2001**, *98*, 4844-4849.
- (104) Kerwin, S. M. *Current Pharmaceutical Design* **2000**, *6*, 441-471.
- (105) Franceschin, M. *European Journal of Organic Chemistry* **2009**, 2225-2238.
- (106) Huang, H.-S.; Chou, C.-L.; Guo, C.-L.; Yuan, C.-L.; Lu, Y.-C.; Shieh, F.-Y.; Lin, J.-J. *Bioorganic & Medicinal Chemistry* **2005**, *13*, 1435-1444.
- (107) Harrison, R. J.; Gowan, S. M.; Kelland, L. R.; Neidle, S. *Bioorganic & Medicinal Chemistry Letters* **1999**, *9*, 2463-2468.

- (108) Seenisamy, J.; Bashyam, S.; Gokhale, V.; Vankayalapati, H.; Sun, D.; Siddiqui-Jain, A.; Streiner, N.; Shinya, K.; White, E.; Wilson, W. D.; Hurley, L. H. *Journal of the American Chemical Society* **2005**, *127*, 2944-2959.
- (109) Han, H.; Cliff, C. L.; Hurley, L. H. *Biochemistry* **1999**, *38*, 6981-6986.
- (110) Arola, A.; Vilar, R. *Curr. Top. Med. Chem.* **2008**, *8*, 1405-1415.
- (111) Anantha, N. V.; Azam, M.; Sheardy, R. D. *Biochemistry* **1998**, *37*, 2709-2714.
- (112) Gowan, S. M.; Harrison, J. R.; Patterson, L.; Valenti, M.; Read, M. A.; Neidle, S.; Kelland, L. R. *Molecular Pharmacology* **2002**, *61*, 1154-1162.
- (113) Kim, M.-Y.; Vankayalapati, H.; Shin-ya, K.; Wierzba, K.; Hurley, L. H. *Journal of the American Chemical Society* **2002**, *124*, 2098-2099.
- (114) Shin-ya, K.; Wierzba, K.; Matsuo, K.-i.; Ohtani, T.; Yamada, Y.; Furihata, K.; Hayakawa, Y.; Seto, H. *Journal of the American Chemical Society* **2001**, *123*, 1262-1263.
- (115) Clark, G. R.; Pytel, P. D.; Squire, C. J.; Neidle, S. *Journal of the American Chemical Society* **2003**, *125*, 4066-4067.
- (116) Guo, Q.; Lu, M.; Marky, L. A.; Kallenbach, N. R. *Biochemistry* **1992**, *31*, 2451-2455.
- (117) McGowan, P. C. *Annual Reports on the Progress of Chemistry, Section A: Inorganic Chemistry* **2005**, *101*, 631-648.
- (118) Chifotides, H. T.; Dunbar, K. R. *Accounts of Chemical Research* **2005**, *38*, 146-156.
- (119) Bergamo, A.; Sava, G. *Dalton Transactions* **2007**, 1267-1272.
- (120) Talib, J.; Beck, J. L.; Ralph, S. F. *JBIC, Journal of Biological Inorganic Chemistry* **2006**, *11*, 559-570.
- (121) Metcalfe, C.; Thomas, J. A. *Chemical Society Reviews* **2003**, *32*, 215-224.
- (122) Erkkila, K. E.; Odom, D. T.; Barton, J. K. *Chem. Rev.* **1999**, *99*, 2777-2795.
- (123) Sigman, D. S.; Bruice, T. W.; Mazumder, A.; Sutton, C. L. *Accounts of Chemical Research* **1993**, *26*, 98-104.
- (124) Liang, Q.; Eason, P. D.; Long, E. C. *Journal of the American Chemical Society* **1995**, *117*, 9625-9631.

- (125) Franklin, C. A.; Fry, J. V.; Collins, J. G. *Inorganic Chemistry* **1996**, *35*, 7541-7545.
- (126) Xu, Q.; Jampani, S. R. B.; Braunlin, W. H. *Biochemistry* **1993**, *32*, 11754-11760.
- (127) Xu, Q.; Jampani, S. R. B.; Deng, H.; Braunlin, W. H. *Biochemistry* **1995**, *34*, 14059-14065.
- (128) Barnes, K. R.; Lippard, S. J. *Metal Ions in Biological Systems* **2004**, *42*, 143-177.
- (129) Cusumano, M.; Di Pietro, M. L.; Giannetto, A.; Nicolo, F.; Rotondo, E. *Inorganic Chemistry* **1998**, *37*, 563-568.
- (130) Jennette, K. W.; Lippard, S. J.; Vassiliades, G. A.; Bauer, W. R. *Proc. Natl. Acad. Sci.* **1974**, *71*, 3839-3843.
- (131) Wang, A. H. J.; Nathans, J.; Van der Marel, G.; Van Boom, J. H.; Rich, A. *Nature* **1978**, *276*, 471-474.
- (132) Bond, P. J.; Langridge, R.; Jennette, K. W.; Lippard, S. J. *Proc. Natl. Acad. Sci.* **1975**, *72*, 4825-4829.
- (133) Barton, J. K.; Lippard, S. J. *Biochemistry* **1979**, *18*, 2661-2668.
- (134) Jennette, K. W.; Gill, J. T.; Sadownik, J. A.; Lippard, S. J. *Journal of the American Chemical Society* **1976**, *98*, 6159-6168.
- (135) Howe-Grant, M.; Wu, K. C.; Bauer, W. R.; Lippard, S. J. *Biochemistry* **1976**, *15*, 4339-4346.
- (136) Lippard, S. J.; Bond, P. J.; Wu, K. C.; Bauer, W. R. *Science (New York, N.Y.)* **1976**, *194*, 726-728.
- (137) Howe-Grant, M.; Lippard, S. J. *Biochemistry* **1979**, *18*, 5762-5769.
- (138) Brodie, C. R.; Collins, J. G.; Aldrich-Wright, J. R. *Dalton Transactions* **2004**, 1145-1152.
- (139) Wheate, N. J.; Taleb, R. I.; Krause-Heuer, A. M.; Cook, R. L.; Wang, S.; Higgins, V. J.; Aldrich-Wright, J. R. *Dalton Transactions* **2007**, 5055-5064.
- (140) Barton, J. K. *Science (New York, N.Y.)* **1986**, *233*, 727-734.
- (141) Elias, B.; Kirsch-De Mesmaeker, A. *Coordination Chemistry Reviews* **2006**, *250*, 1627-1641.
- (142) Luedtke, N. W.; Hwang, J. S.; Nava, E.; Gut, D.; Kol, M.; Tor, Y. *Nucleic Acids Research* **2003**, *31*, 5732-5740.

- (143) Urathamakul, T.; Beck, J. L.; Sheil, M. M.; Aldrich-Wright, J. R.; Ralph, S. F. *Dalton Transactions* **2004**, 2683-2690.
- (144) Talib, J.; Harman, D. G.; Dillon, C. T.; Aldrich-Wright, J.; Beck, J. L.; Ralph, S. F. *Dalton Transactions* **2009**, 504-513.
- (145) Arounaguiri, S.; Easwaramoorthy, D.; Ashokkumar, A.; Dattagupta, A.; Maiya, B. G. *Proceedings - Indian Academy of Sciences, Chemical Sciences* **2000**, *112*, 1-17.
- (146) Rehmann, J. P.; Barton, J. K. *Biochemistry* **1990**, *29*, 1701-1709.
- (147) Rehmann, J. P.; Barton, J. K. *Biochemistry* **1990**, *29*, 1710-1717.
- (148) Dixon, I. M.; Lopez, F.; Tejera, A. M.; Esteve, J.-P.; Blasco, M. A.; Pratviel, G.; Meunier, B. *Journal of the American Chemical Society* **2007**, *129*, 1502-1503.
- (149) Dixon, I. M.; Lopez, F.; Esteve, J.-P.; Tejera, A. M.; Blasco, M. A.; Pratviel, G.; Meunier, B. *ChemBioChem* **2005**, *6*, 123-132.
- (150) Vialas, C.; Pratviel, G.; Meunier, B. *Biochemistry* **2000**, *39*, 9514-9522.
- (151) Arnaud, P.; Zakrzewska, K.; Meunier, B. *Journal of Computational Chemistry* **2003**, *24*, 797-805.
- (152) Maraval, A.; Franco, S.; Vialas, C.; Pratviel, G.; Blasco, M. A.; Meunier, B. *Organic & Biomolecular Chemistry* **2003**, *1*, 921-927.
- (153) Reed, J. E.; Neidle, S.; Vilar, R. *Chem. Commun.* **2007**, 4366-4368.
- (154) Reed, J. E.; Arnal, A. A.; Neidle, S.; Vilar, R. *Journal of the American Chemical Society* **2006**, *128*, 5992-5993.
- (155) Arola-Arnal, A.; Benet-Buchholz, J.; Neidle, S.; Vilar, R. *Inorganic Chemistry* **2008**, *47*, 11910-11919.
- (156) Davis, K. J.; Richardson, C.; Beck, J. L.; Knowles, B. M.; Guedin, A.; Mergny, J.-L.; Willis, A. C.; Ralph, S. F. *Dalton Transactions* **2015**, *44*, 3136-3150.
- (157) Davis, K. J. Binding Interactions between Nickel Schiff Base Complexes and Quadruplex DNA. PhD Thesis, University of Wollongong, 2015.
- (158) Technologies, A.: *CrysAlis PRO*. 1.171.37.35h released 09-02-2015 CrysAlis .NET ed., 2015.
- (159) Altomare, A.; Cascarano, G.; Giacovazzo, C.; Guagliardi, A. *Journal of Applied Crystallography* **1993**, *26*, 343-350.

- (160) Betteridge, P. W.; Carruthers, J. R.; Cooper, R. I.; Prout, K.; Watkin, D. J. *Journal of Applied Crystallography* **2003**, *36*, 1487.
- (161) Spek, A. I.: *PLATON, A Multipurpose Crystallographic Tool*; Utrecht University: Utrecht, The Netherlands, 2008.
- (162) Urathamakul, T. Mass spectrometric studies of non-covalent biomolecular complexes. PhD Thesis, University of Wollongong, 2006.
- (163) Talib, J. Interactions of Metal Complexes with DNA. PhD Thesis, University of Wollongong, 2008.
- (164) Oligo Calc: Oligonucleotide Properties Calculator. <http://www.basic.northwestern.edu/biotools/oligocalc.html>.
- (165) Jangir, D. K.; Dey, S. K.; Kundu, S.; Mehrotra, R. *Journal of Photochemistry and Photobiology, B: Biology* **2012**, *114*, 38-43.
- (166) Kypr, J.; Kejnovska, I.; Renciuik, D.; Vorlickova, M. *Nucleic Acids Research* **2009**, *37*, 1713-1725.
- (167) Gray, D. M.; Ratliff, R. L.; Vaughan, M. R. *Methods in Enzymology* **1992**, *211*, 389-406.
- (168) Holm, A. I. S.; Nielsen, L. M.; Hoffmann, S. V.; Nielsen, S. B. *Physical Chemistry Chemical Physics* **2010**, *12*, 9581-9596.
- (169) Stefl, R.; Trantirek, L.; Vorlickova, M.; Koca, J.; Sklenar, V.; Kypr, J. *Journal of Molecular Biology* **2001**, *307*, 513-524.
- (170) Trantirek, L.; Stefl, R.; Vorlickova, M.; Koca, J.; Sklenar, V.; Kypr, J. *Journal of Molecular Biology* **2000**, *297*, 907-922.
- (171) Chai, J.; Wang, J.; Xu, Q.; Hao, F.; Liu, R. *Molecular BioSystems* **2012**, *8*, 1902-1907.
- (172) Wang, L.; Liu, R.; Teng, Y. *Journal of Luminescence* **2011**, *131*, 705-709.
- (173) Laughton, C. A.; Tanious, F.; Nunn, C. M.; Boykin, D. W.; Wilson, W. D.; Neidle, S. *Biochemistry* **1996**, *35*, 5655-5661.
- (174) Slobodyansky, E.; Stellwagen, J.; Stellwagen, N. C. *Biopolymers* **1988**, *27*, 1107-1126.
- (175) Gray, D. M.; Wen, J.-D.; Gray, C. W.; Regges, R.; Regges, C.; Raabe, G.; Fleischhauer, J. *Chirality* **2008**, *20*, 431-440.
- (176) Paramasivan, S.; Rujan, I.; Bolton, P. H. *Methods* **2007**, *43*, 324-331.

- (177) Chang, C.-C.; Kuo, I. C.; Ling, I. F.; Chen, C.-T.; Chen, H.-C.; Lou, P.-J.; Lin, J.-J.; Chang, T.-C. *Analytical Chemistry* **2004**, *76*, 4490-4494.
- (178) Qi, J.; Shafer, R. H. *Nucleic Acids Research* **2005**, *33*, 3185-3192.
- (179) Vorlickova, M.; Kejnovska, I.; Sagi, J.; Renciuik, D.; Bednarova, K.; Motlova, J.; Kypr, J. *Methods* **2012**, *57*, 64-75.
- (180) Breuker, K.; McLafferty, F. W. *Proceedings of the National Academy of Sciences of the United States of America* **2008**, *105*, 18145-18152.